

**Mechanistic Evaluation of Early Phases of Drug Release from Polymer Microparticles Prepared by  
Atomization Techniques**

by

Richard Schutzman

A dissertation submitted in partial fulfillment  
of the requirements for the degree of  
Doctor of Philosophy  
(Pharmaceutical Sciences)  
in the University of Michigan  
2023

Doctoral Committee:

Professor Steven P. Schwendeman, Chair  
Professor Emeritus Gregory E. Amidon  
Professor Joerg Lahann  
Professor James Moon

Richard Schutzman

rschut@umich.edu

ORCID iD: 0000-0002-0981-2449

© Richard Schutzman 2023

## **Dedication**

To fiancée, Chunyi Zhao, who gave me so much encouragement, and my family who were always supportive.

## Table of Contents

Dedication .....	ii
List of Tables .....	ix
List of Figures .....	x
Abstract .....	xv
Chapter 1 Introduction .....	1
1.1 Introduction to Controlled Release .....	1
1.2 Microencapsulation of Peptides and Steroids .....	3
1.2.1 Solvent Evaporation .....	3
1.2.2 Coacervation .....	4
1.2.3 Spray-drying .....	5
1.2.4 Electrospray .....	6
1.2.5 Remote Loading .....	8
1.2.6 Other Methods .....	9
1.3 Release from PLGA and PLA microparticles and Governing Mechanisms .....	10
1.3.1 Initial Burst Release Phase .....	10
1.3.2 Water Uptake .....	11
1.3.3 Polymer Response to Water Uptake .....	11
1.3.4 Bioerosion .....	13
1.3.5 Hydrolysis .....	13

1.3.6 Drug and Excipient Effects .....	14
1.3.7 Media and Release Conditions .....	14
1.3.8 Diffusion.....	15
1.3.9 Plasticizers and Residual Solvents .....	15
1.4 References .....	16
Chapter 2 Mechanistic Evaluation of the Initial Burst Release of Leuprolide from Poly(Lactic-co-Glycolic Acid) Spray-dried Microspheres.....	26
2.1 Abstract .....	26
2.2 Introduction .....	27
2.3 Materials and Methods .....	31
2.3.1 Materials .....	31
2.3.2 Preparation of poly(lactic-co-glycolic acid) microspheres encapsulating leuprolide by spray-drying.....	31
2.3.3 Drug loading.....	32
2.3.4 In vitro initial burst evaluated by continuous monitoring system .....	33
2.3.5 Single-point monitoring of 24-hr in vitro initial burst.....	33
2.3.6 Dynamic changes of external and internal morphology during initial burst in vitro ...	34
2.3.7 Preparing a bodipy-dextran fluorescent probe .....	34
2.3.8 Dynamic changes of effective diffusion coefficients and characteristic times during in vitro initial burst .....	35
2.3.9 In vivo release study.....	36
2.3.10 Residual drug quantification after administration .....	37
2.3.11 Serum sample analysis of leuprolide.....	37
2.3.12 Non-compartmental pharmacokinetic analysis and numerical deconvolution.....	37
2.3.13 Statistical analysis .....	38
2.4 Results and discussion.....	39

2.4.1 Evaluation of the initial burst by continuous monitoring system.....	40
2.4.2 Extraction of features from dynamic monitoring .....	43
2.4.3 Measurements by single-point sample-and-separate method.....	45
2.4.4 Comparison of initial burst by continuous monitoring and sample-and-separate methods.....	48
2.4.5 Dynamic changes of external and internal morphology during initial burst .....	49
2.4.6 Dynamic changes in effective diffusion of bodipy-dextran probe through aqueous pore networks .....	52
2.4.7 Correlations between in vitro release and probe diffusion.....	57
2.4.8 Pharmacokinetic evaluation of selected spray dried formulations in rats .....	61
2.4.9 Numerical deconvolution of pharmacokinetic data.....	62
2.4.10 In-vitro in-vivo correlations during initial burst.....	63
2.5 Conclusions .....	68
2.6 References .....	70
2.7 Supplementary Data .....	76
Chapter 3 Optimization of a Coaxial Electrospray System for Etonogestrel-loaded Core-Shell Poly(D,L-lactide) Microparticles (ENG csMPs) and Effect of Shell Composition.....	87
3.1 Introduction .....	87
3.2 Materials and Methods .....	88
3.2.1 Materials.....	88
3.2.2 Preparation of ENG-core-shell microparticles by coaxial electrospray .....	88
3.2.3 Determination of ENG drug loading and encapsulation efficiency .....	89
3.2.4 In Vitro Release Studies .....	89
3.2.5 Characterization of thermal properties and etonogestrel solid-state .....	90
3.3 Results and Discussion.....	91
3.3.1 Yields and performance of new system design .....	91

3.3.2 In vitro release of standard formulation .....	92
3.3.3 Effect of PLA molecular weight in shell on release.....	94
3.3.4 Alternative polymers in shell and the effect on release.....	95
3.4 Conclusion.....	98
3.5 References .....	99
3.6 Supplementary Materials.....	101
<b>Chapter 4 Improving the Long-term ENG Release Kinetics of Injectable csMPs by Controlling Particle Morphology and Drug Crystallinity .....</b>	<b>103</b>
4.1 Introduction .....	103
4.2 Materials and Methods .....	104
4.2.1 Materials .....	104
4.2.2 Preparation of ENG-core-shell microparticles by coaxial electrospray .....	104
4.2.3 Ethanol treatment of csMPs during solvent evaporation (Drying).....	105
4.2.4 Resuspension of csMPs with ethanolic solution (Rinse).....	105
4.2.5 Incubation of csMPs with ethanol vapor (Vapor) .....	105
4.2.6 Determination of ENG drug loading and encapsulation efficiency .....	106
4.2.7 Scanning electron microscopy (SEM).....	106
4.2.8 In Vitro Release Studies .....	106
4.2.9 Residual Solvent Quantification.....	107
4.2.10 Characterization of thermal properties and etonogestrel solid-state .....	107
4.3 Results and Discussion.....	108
4.3.1 Encapsulation efficiency and yield of ethanol treatments.....	108
4.3.2 Ethanol treatments effects on residual solvents and crystallinity.....	109
4.3.3 Release from ethanol-treated csMPs .....	112
4.3.4 Morphology of csMPs sprayed in ethanolic solutions .....	114
4.3.5 Effect of spraying into various surfactant solutions on morphology .....	115

4.3.6 Release kinetics of particles spraying into surfactant solutions .....	118
4.4 Conclusion.....	121
4.5 References .....	122
4.6 Supplementary Material .....	126
Chapter 5 Pharmacokinetics and In Vitro-In Vivo Correlation of disc-shaped csMPs .....	127
5.1 Introduction .....	127
5.2 Materials and Methods .....	127
5.2.1 Materials.....	127
5.2.2 Preparation of ENG-core-shell microparticles by coaxial electrospray .....	128
5.2.3 Determination of ENG drug loading and encapsulation efficiency .....	129
5.2.4 In Vitro Release Studies .....	129
5.2.5 Characterization of thermal properties and etonogestrel solid-state .....	130
5.2.6 Pharmacokinetic (PK) assessment of ENG-cs-MPs in rats.....	130
5.2.7 Quantification of ENG in rat serum .....	131
5.2.8 Pharmacokinetic analysis and in vitro-in vivo correlations .....	132
5.3 Results and Discussion.....	133
5.3.1 Pharmacokinetic Profile and Noncompartmental parameters .....	133
5.3.2 Absorption Kinetics.....	134
5.3.3 Unscaled in vitro-in vivo correlation.....	135
5.3.4 Power-based time scaling and scaled IVIVC .....	136
5.3.5 Mixed effects of linearized power law scaling.....	137
5.3.6 Predictive capabilities of IVIVC .....	139
5.4 Conclusions .....	141
5.5 References .....	143
5.6 Supplementary Materials.....	146

Chapter 6 Conclusions, Significance and Future Directions ..... 152

## List of Tables

Table 2-1. Characteristics of Release Profiles.....	47
Table 2-2. Pharmacokinetics parameters for subcutaneous administration (3mg/kg) in rats (n=4) .....	62
Table S2-1. The compositions and formulations of spray-dried leuprolide-PLGA microspheres with altered spray drying parameters including inlet air temperature ( $T_{inlet}$ ), PLGA concentration ( $C_{feed}$ ), airflow in nozzle ( $AF_{nozzle}$ ), ratio between atomization gas flow rate and the liquid mass flow rate ( $Ratio_{A/L}=AF_{inlet}/LF_{nozzle}$ ), nozzle size ( $S_{nozzle}$ ) and initial sample temperature ( $T_{feed}$ )..	76
Table 3-1. Compositions and yields of PLA blend formulations .....	94
Table 3-2. Compositions and yields when using alternative polymer in shell of csMPs .....	96
Table 4-1. Yields and loading of various ethanol-treated formulations .....	109
Table 4-2. Yields and loading of formulations after using different surfactants in collection media and with or without addition of ethanol during solvent evaporation step.....	116
Table 5-1. Predicted values, similarity, and accuracies from leave-one-out analysis of mixed effects power law scaled IVIVC. NS refers to “not statistically significant”, * $p<0.05$ , ** $p<0.01$ , and *** $p<0.001$ . .....	140

## List of Figures

Figure 2-1. Diagram of the spray dryer components (A) including: the atomizing nozzle (I), drying/atomization chamber (II), microparticles (III), inlet air flow (IV), outlet air/exhaust (V), separation cyclone (VI), collection vessel (VII), cooling airflow (VIII), cyclone airflow (IX), liquid pump (X), feed emulsion (XI), polymer solution (XII), and aqueous phase with leuprolide and gelatin (XII). Parameters and values tested (B). .....	39
Figure 2-2. Continuous monitoring of initial burst release of Lupron Depot® and spray dried microspheres. Formulations include: Lupron Depot® (A); $T_{inlet}$ 80, 70, 60 and 50 °C (B); $C_{feed}$ 20% and 30% (C); $AF_{nozzle}$ 10, 13, and 16 L/min (D); $Ratio_{A/L}$ 2.0, 3.0, 4.0, 6.0, and 8.0 (E); $S_{nozzle}$ 0.6, 0.8, 1.0, and 1.2 mm (F); $T_{feed}$ 4, 13, 25, and 37 °C (G). Analysis of each formulation was performed in duplicate with 1 <sup>st</sup> and 2 <sup>nd</sup> runs indicated. * refers to the standard condition, which is repeated in each panel to show the trend.....	41
Figure 2-3. Comparison of 24-h release of leuprolide from two determination systems under altered $T_{inlet}$ (A), $C_{feed}$ (B), $AF_{nozzle}$ (C), $Ratio_{A/L}$ (D), $S_{nozzle}$ (E) and $T_{feed}$ (F). General comparison (G) was summarized. * represents the basic formulation condition. Error bars show $\pm SE$ .....	48
Figure 2-4. External morphology (A, C) and internal structure (B, D) of Lupron Depot® (A,B) and standard condition spray-dried microspheres (C,D) from storage and after 0, 0.2, 1, 2, 5, 8, 12, 24, and 36 hours of incubation in the continuous monitoring system. Left image shows full microsphere. Right shows high magnification (field view = 7.2 $\mu m$ ) .....	50
Figure 2-5. Confocal images of dye penetration of bodipy-dextran in Lupron Depot® (A) and spray-dried microspheres made under standard conditions—loaded (B) and unloaded (C)—after 30 min incubation at 37°C with 0 (A), 0.2 (B), 1 (C), 2 (D), 8 (E), 12 (F), 24 (G) or 36 hr (H) of pre-incubation in the continuous monitoring.....	54
Figure 2-6. Effective diffusion of bodipy-dextran probe after preincubation in continuous monitoring (A-C); diffusion of spray-dried formulations after 0.2 hr (A) and 24 hr (B) preincubation (* $p < 0.05$ ; ** $p < 0.01$ ; *** $p < 0.001$ compared to LD; † and ‡ used when comparing to loaded and unloaded standard formulation, respectively). Changes in diffusion coefficient of LD compared to loaded and unloaded spray-dried standards over release period (C) and expanded over first 4 hr (C-inset). Error bars represent SEM (n=8-10). * and ** in labels represent loaded and unloaded standards.....	56

Figure 2-7. Results from aqueous diffusion study compared to features extracted from continuous monitoring in vitro release. 1° release was compared to the diffusion coefficient at 0.2 hr of preincubation (A) the characteristic diffusion time (B) (C); terminal release rate—the rate after the 1° release period—was compared to the diffusion coefficient at 24 hr (D). R<sup>2</sup> values are based on power law fits of all spray-dried data points except for (A), which uses a linear fit.

..... 59

Figure 2-8. Pharmacokinetic in rats after subcutaneous administration of microspheres with a dose equivalent to 3.5 mg/kg leuprolide. Plasma concentration-time profiles of the first 24 hours (A) and first 4 hours (A-inset). Cumulative fraction absorbed from numerical deconvolution of plasma profiles using a 2-compartment based on literature values, normalized to the exact amount administered (B). Error bars show ±SE (n=4).

..... 63

Figure 2-9. In-Vitro-In-Vivo Correlations of release by Continuous Monitoring. Individual Level-A IVIVC with no time scaling or shifting with fraction released obtained from continuous monitoring for Lupron Depot® (A) and spray-dried formulations: C<sub>feed</sub> 30% (B), Basic (C), AF<sub>nozzle</sub> L/min (D), and T<sub>feed</sub> 25 C (E); with linear fitting forced through the origin. Error bars show ±SE. Compiled IVIVC plots (F); linear fit includes data points from spray-dried formulations made with constant polymer concentration (C<sub>feed</sub> 20%)..... 64

Figure 2-10. Level C In-Vitro-In-Vivo Correlations with parameters from diffusion studies (A, B), continuous monitoring release (C, D), or conventional release (E, F) versus the fraction absorbed after 24 hours (A, C, E) or C<sub>max</sub> (B, D, F). Correlations were tested for spray-dried formulations with (blue) and without Lupron Depot® (green). Error bars show SE. .... 66

Figure S2-1. Schematic diagram of instrumental set-up for continuous monitoring system of the initial burst from PLGA microspheres. The continuous monitoring system includes sub-micron nylon mesh (B), sampling probe (C), magnetic stirrer (D), and water-jacketed beaker (G) at 37°C. Microspheres (E) are placed in phosphate-buffered saline with Tween 80 (F) with a seal (A) on the container. .... 77

Figure S2-2. Demonstration of feature extraction from cumulative release vs. time profiles and their numerical derivatives. (A) Estimation of t<sub>25%</sub>, t<sub>50%</sub>, and t<sub>75%</sub>; and (B) derivative-based extraction of maximum rate (upper left), terminal rate and end time of the burst release (upper right), the concentration at that time (lower left), and the calculation of the decay rate constant between the maximum rate and end of the burst (lower right). .... 77

Figure S2-3. External morphology (A, C) and internal structure (B, D) of unloaded standard condition spray-dried microspheres (A, B) and T<sub>inlet</sub> 50°C microspheres (C, D) from storage and after 0, 0.2, 1, 2, 5, 8, 12, 24, and 36 hours of incubation in the continuous monitoring system. Left image shows full microsphere. Right shows high magnification (field view = 7.2 μm) ..... 78

Figure S2-4. External morphology (A, C) and internal structure (B, D) of AF<sub>nozzle</sub> 13 (A, B) and 16 L/min microspheres (C, D) from storage and after 0, 0.2, 1, 2, 5, 8, 12, 24, and 36 hours of incubation in the continuous monitoring system. Left image shows full microsphere. Right shows high magnification (field view = 7.2 μm)..... 79

Figure S2-5. External morphology (A, C) and internal structure (B, D) of Ratio<sub>A/L</sub> 2 (A, B) and 8 microspheres (C, D) from storage and after 0, 0.2, 1, 2, 5, 8, 12, 24, and 36 hours of incubation in the continuous monitoring system. Left image shows full microsphere. Right shows high magnification (field view = 7.2 μm). ..... 80

Figure S2-6. External morphology (A, C) and internal structure (B, D) of S<sub>nozzle</sub> 0.6 (A, B) and 1.2 mm microspheres (C, D) from storage and after 0, 0.2, 1, 2, 5, 8, 12, 24, and 36 hours of incubation in the continuous monitoring system. Left image shows full microsphere. Right shows high magnification (field view = 7.2 μm). ..... 81

Figure S2-7. External morphology (A, C) and internal structure (B, D) of C<sub>feed</sub> 30% (A, B) and T<sub>feed</sub> 13°C microspheres (C, D) from storage and after 0, 0.2, 1, 2, 5, 8, 12, 24, and 36 hours of incubation in the continuous monitoring system. Left image shows full microsphere. Right shows high magnification (field view = 7.2 μm). ..... 82

Figure S2-8. External morphology (A, C) and internal structure (B, D) of T<sub>feed</sub> 25°C (A, B) and 37°C microspheres (C, D) from storage and after 0, 0.2, 1, 2, 5, 8, 12, 24, and 36 hours of incubation in the continuous monitoring system. Left image shows full microsphere. Right shows high magnification (field view = 7.2 μm). ..... 83

Figure S2-9. Confocal images of dye penetration of bodipy-dextran in *Tinlet* 50°C (A), C<sub>feed</sub> 30% (B), A<sub>fnozzle</sub> 13.0 (C) and 16.0 (D) L/min, Ratio<sub>A/L</sub> 2.0 (E) and 8.0 (F), S<sub>nozzle</sub> 0.6 (G) and 1.2 mm (H), and T<sub>feed</sub> 25°C (I) and 37°C (J) after 30 min incubation at 37°C with 0.2 hr (left) and 24 hr (right) of pre-incubation in the continuous monitoring ..... 84

Figure S2-10. C<sub>max</sub> heavily influences AUC<sub>0-24hr</sub> (A). Pharmacokinetic parameters are highly correlated in first 24 hr (A, B). C<sub>max</sub> (D, F) and the fraction absorbed at 24 hr (C, E) are compared to other calculated parameters from in vitro testing: effective diffusion coefficients at 0.2 hr (C, D) and cumulative fraction released at the end of the initial burst in the continuous monitoring system (E, F). Correlations are determined for all spray-dried formulations without (blue) or with (green) including Lupron Depot®. Error bars show ±SE. .... 85

Figure S2-11. Effective Diffusion coefficients of unconjugated bodipy from 30 minutes incubation at 37°C after different periods of pre-incubation in the continuous monitoring system. Error bars show ±SE (n=5-10) (A). Maximum rate compared to dimensionless times (B). ..... 86

Figure 3-1. Diagram of coaxial electrospray system. Syringe pumps (I) control the flow rate of outer, shell solution (II) and inner core solution (III) through a coaxial needle (IV). The coaxial needle is connected to voltage source (V). Core-shell micro-droplets (VIII) can be focused through a copper ring electrode (VII) connected to voltage source (VI) and collected into aluminum vessel (IX) containing the spray bath solution, which is connected to the common ground. .... 91

Figure 3-2. Cumulative release (A) and release kinetics (B) of cs-MPs made with and without system modifications. Relative crystallinity over the course of the first month for particles made without system modifications (C). (n = 3, mean ± SEM) ..... 93

Figure 3-3. Cumulative release (A) and release kinetics (B) of cs-MPs made with varying blends of Resomer <sup>®</sup> R203S and R205S. (n = 3, mean ± SEM) .....	95
Figure 3-4. Cumulative release (A, B) and release kinetics (C, D) of cs-MPs with shells containing PEG 45kDa (A, C) or PCL 45kDa (B, D).....	96
Figure S3-1. Accumulation of microparticles on black paper after 20 minutes of spraying without (A) and with (B) the ring electrode.....	101
Figure S3-2. DSC thermographs of pure etonogestrel, physical mixes with Resomer <sup>®</sup> R205S PLA, and electrosprayed microparticles made with and without the ring electrode. ....	102
Figure 4-1. Residual chloroform (A), ethanol and ethyl acetate (B) of lyophilized microparticles after spraying into ethanol or after post-spray treatments with ethanol (drying, vapor, or rinsing) and their effect on etonogestrel crystallinity (C).(n=3, mean ± SEM) ND = not detected. ....	110
Figure 4-2. Cumulative release (A) and release rates (B) of csMPs after treatment with ethanol during spraying (lower left), during drying (upper left), and after lyophilizing through rinsing (upper right) or exposure to ethanol vapor (lower right). Marker shape denote the concentration of ethanol in solution for all conditions except treatment with vapor, which is the incubation temperature (see legend).....	113
Figure 4-3. Morphology of core-shell particles without surface tension modifiers (A), 25% Ethanol (B) and 40% Ethanol (C).....	114
Figure 4-4. Morphology of core-shell particles with 250 μM Triton X-100 (A), 40 μM Tween 80 (B), 80 μM Span 80 (C), and 10 μM Pluronic L121 (D).....	117
Figure 4-5. Cumulative release (A) and release kinetics (B) of cs-MPs after inclusion of Pluronic L121 (upper left), Tween 80 (upper right), Span 80 (lower left), or Triton X-100 (lower right) in the spraying bath with (solid) and without (dotted) drying in 25% ethanol. ....	119
Figure S4-1. Higher magnification of 25% ethanol collector solution particles without surfactants. ....	126
Figure 5-1. Pharmacokinetic profiles in rats of ethanol-treated (A) microparticles and microparticles with varying shell compositions (B) after 15 mg/kg ENG dose (n=3). Inset displays log-linear plot of same data. Error bars show ± SEM. ....	133
Figure 5-2. Mean absorption kinetics of individually deconvoluted pharmacokinetics profiles.	134
Figure 5-3. Unscaled time-by-time in vivo-in vitro correlation. Data points show mean values for absorption and release at a given time. ....	135
Figure 5-4. Power law fit of in vivo/in vitro times to a given fraction absorbed/released (A). Power-scaled in vitro-in vivo correlation (B). ....	136

Figure 5-5. Mixed effects power law model of in vivo/in vitro times to a given fraction absorbed/released reduced by the random effect of the exponential term for the 25% ethanol rinse treatment (A) and all other formulation (B). Power-scaled in vitro-in vivo correlation (C) ..... 138

Figure S5-1. Noncompartmental parameters of studied formulations:  $C_{max}$  (A),  $T_{max}$  (B),  $AUC_{0-1 \text{ day}}$  (C), and  $AUC_{0-56 \text{ days}}$  (D). Error bars show  $\pm$  SEM. .... 146

Figure S5-3. Power law fit of in vivo/in vitro times to a given fraction absorbed/released excluding 25% Ethanol-Rinsed (A). Power-scaled in vitro-in vivo correlation (B)..... 147

Figure S5-2. Two-compartment model fit of intravenous injection for 25  $\mu\text{g}/\text{kg}$  (n=3) and 75  $\mu\text{g}/\text{kg}$  (n=1). Pre-exponential coefficients show ng/mL per mg dose. Higher dose is normalized to 25  $\mu\text{g}/\text{kg}$  for plot. .... 147

Figure S5-4. Full mixed effects power law model of in vivo/in vitro times to a given fraction absorbed/released for the 25% ethanol rinse treatment (A) and all other formulation (B). Power-scaled in vitro-in vivo correlation (C)..... 148

Figure S5-5. Pre-exponential term-reduced mixed effects power law model of in vivo/in vitro times to a given fraction absorbed/released for the 25% ethanol rinse treatment (A) and all other formulation (B). Power-scaled in vitro-in vivo correlation (C)..... 149

Figure S5-6. Predicted absorption from leave-one-out analysis of mixed effects power law scaled IVIVC compared to actual in vivo absorption. Error bars show  $\pm$ SEM.  $f_2$  refers to the  $f_2$  similarity of the actual absorption over time to the predicted absorption over time. .... 150

Figure S5-7. Predicted serum concentrations (black line) from leave-one-out analysis of IVIVC after convolution of predicted absorption. Actual data is shown by yellow stars with error bars representing  $\pm$ SEM. .... 151

## Abstract

Poly(lactic-*co*-glycolic acid) (PLGA) and poly(lactic acid) (PLA) injectable microparticles have been an excellent platform for the controlled-release of small and large molecules. While commercially used for more than 30 years, manufacturing of microparticles has been dominated by two encapsulation techniques, solvent evaporation and coacervation. Both techniques are difficult to scale and suffer from other issues such as limited or poor control of particle morphology and release kinetics during the early phases of drug release. The work herein focuses on characterizing particles made from two less used atomization techniques with potential advantages—spray drying and electrospraying—and mechanistic evaluation of their early and rapid release periods.

Leuprolide acetate, a model peptide drug, was encapsulated in low molecular weight acid-capped PLGA microparticles by spray-drying, a technique well-known for its excellent scalability. The 24-h release of 16 compositionally similar formulations were studied and compared to the commercial 1-month Lupron Depot<sup>®</sup> (LD) by using both the traditional sample-and-separate method and a previously validated continuous monitoring system. The morphology and internal structure as well as the effective diffusivity of a high molecular weight bodipy-dextran probe was examined at different points throughout the continuous monitoring release. Pore-healing behavior was observed as well as extensive swelling in some formulations. The continuous monitoring revealed a rapid primary (1<sup>°</sup>) phase followed by a constant-rate secondary (2<sup>°</sup>) release phase. The

primary phase duration was divided by the characteristic diffusion time of the probe to give a dimensionless diffusion time that was highly correlated to the extent of primary phase release. Spray-dried microspheres showed a strong *in vitro-in vivo* correlation (IVIVC) between the 24-h pharmacokinetic parameters, continuous monitoring *in vitro* release, and *in vitro* dimensionless times, whereas the sample-and-separate release was poorly correlated with *in vivo* absorption of leuprolide. The correlations found demonstrate that diffusion through the polymer matrix as a major release mechanism both *in vitro* and *in vivo* for highly porous spray-dried microspheres. However, the structurally dense LD did not follow these relationships. The poor correlation of LD and a fixed lower limit on the burst release implies that there exists one or more competing release mechanisms.

Coaxial electrospaying was investigated for producing morphologically novel core-shell microparticles (csMPs) for the purpose of achieving both elevated drug loading (~50% w/w) and slow and continuous release of the contraceptive hormone—etonogestrel (ENG)—for 3-6 months. While initial formulations achieved high drug loading, they suffered from elevated release rates over the first month as well as low yields, disk-shaped morphology, and elevated residual solvents. Incomplete drying in the air produced deformable embryonic microparticles that collapsed when they impacted the water surface and easily aggregated in solution. Loss was further increased by accumulation of polymer on the grounded collection container walls. System modifications, which aimed at focusing the electrospay, increased particles yield from 10-15% to 25-40%. High initial release rates were also associated with high fractions of amorphous drug and steady decreases in both parameters over the first month of drug release were observed. Additionally, some tunability in the rapid release fraction and long-term rates was demonstrated by using blends of PLA or alternative polymers such as high-molecular weight polyethylene glycol (PEG) in shell.

Various methods of exposure with ethanol for the newly formed csMPs were found to increase crystallinity and reduce residual solvents, which led to a slight decrease in the rapid release. Interestingly, 40% ethanol in the collector solution produced particles with a 5% rapid phase release compared to 20-40% in other treatments. SEM imaging showed that increasing ethanol concentrations created particles with increasing sphericity. These results were replicated using the strong surfactant, Triton X-100, in place of ethanol, which implicated the importance of collector solution surface tension in defining final csMP morphology.

Eight different disc-shaped csMP formulations were tested *in vivo* over 3 months. An IVIVC was developed using power law-scaling of *in vitro* and *in vivo* times ( $t_{in\ vivo} = At_{in\ vitro}^k$ ). Mixed effects modeling of the linearized power law time scaling was utilized to analyze individual formulations and compare pre-exponential,  $A$ , and exponential terms,  $k$ . Only treating particles with a 25% ethanol rinse were not well explained by this IVIVC model, since this group displayed a high near-constant *in vitro* release rate and no clear rapid phase. Adjustment of this group's pre-exponential term significantly improved the overall results and the IVIVC model based on *in vitro* release explained 81% of absorption variability. The predictive power was determined through a leave-one-out analysis. The predicted absorption curves with the exception of the 25% ethanol rinse displayed high  $f_2$  similarity, and log ratio accuracies of plasma concentrations were greater than 75% for a majority of formulations.

In summary, the present work demonstrates the utility of mechanistic evaluation of release and the potential of these analysis for the guided development of coaxial electrosprayed and spray-dried PLGA and PLA microparticles.

## **Chapter 1 Introduction**

### **1.1 Introduction to Controlled Release**

Many pharmaceuticals are hydrophobic small molecules and Biopharmaceutical Classification System (BCS) class II-IV, meaning they are poorly soluble and/or poorly permeable to the gastrointestinal wall. Additionally, there are many emerging or already established peptide and proteins, which are highly sensitive to denaturation and degradation. All these classes of drugs tend to show negligible oral bioavailability. For BSC II-IV drugs and biologics, the design of modified release dosage forms represents a method for overcoming the limitations of drug dosing. Controlled release dosage forms have shown significant success in limiting toxicity while improving efficacy and patient compliance by reducing the frequency of dosing. Biodegradable polymers such as PLGA and PLA are commonly used as matrices for drug encapsulation that allows constant release from the polymer as it erodes, and the drug diffuses out.

Poly(lactic-co-glycolic acid) (PLGA) is a biocompatible, biodegradable polymer that has been widely studied and utilized as a controlled-release carrier for therapeutics. PLGA has been in many formulations approved by the Food and Drug Administration for a variety of indications from cancer to diabetes. PLGA consists of lactide and glycolide monomers that are linked through ester bonds. In the presence of water, the hydrolysis of these ester bonds occurs, and, after significant degradation of the polymer chains, the microspheres will begin to erode or lose mass.

Often, it is this erosion that leads to drug release from the matrix. The characteristics of this polyester can be manipulated to control the degradation and release kinetics and ultimately maintain drug plasma kinetics within the therapeutic window of many pharmaceuticals. Increases in the glycolide to lactide ratio increases the hydrophilicity of the polymer and leads to increases in water uptake. Increased water uptake enhances hydrolysis and increases drug release rates. In addition, higher molecular weight polymers reduce degradation and slows erosion kinetics. Lowering crystallinity by using racemic mixtures of lactide and glycolide stereoisomers, the degradation and erosion is increased. The promise and versatility of PLGA and PLA as a biocompatible carrier for controlled drug delivery has led to its use in implants, in situ forming implants, and injectable microsphere formulations.

Implants like any other controlled release dosage form removes the need for frequent dosing. Additionally, implants have the benefit that they may be removed in the case of an adverse reaction. PLGA implants are often made through extrusion. Solvent extrusion is common for laboratory settings and requires dissolving the polymer and the drug in the same solvent. The mixture is then extruded through a small opening prior to complete evaporation and solidification of the polymer. Hot-melt extrusion is typically used in industry and is performed by heating a polymer drug mixture well above its glass transition temperature and extruding through a small die. For example, Zoladex<sup>®</sup> is a commercial product that utilizes hot-melt extrusion.

Microspheres is a commonly used method for controlled release because the ease of administration compared to implants and the lower burst release compared to in-situ forming depots [1]. PLGA microspheres are commonly manufactured through solvent evaporation or phase separation, but many different methods of microencapsulation have been explored. Currently, there are several FDA-approved PLGA microsphere formulations on the market such as Lupron

Depot<sup>®</sup> and Sandostatin<sup>®</sup>, which are made by solvent evaporation and phase separation, respectively [2]. Microspheres have shown great versatility in the encapsulation of both hydrophobic small molecules and macromolecules such as peptides and protein.

## **1.2 Microencapsulation of Peptides and Steroids**

Microencapsulation of drug molecules in PLGA is traditionally done through solvent evaporation. The simplicity of solvent evaporation methods makes them ideal for small scales, but control of evaporation and low encapsulation efficiency may present difficulties in scaling up. In addition, the inherent instability of peptide drugs makes them sensitive to emulsion and sterilization techniques. In addition, the problems of high initial burst release are prevalent in microsphere formulations especially when loaded with relatively water-soluble drugs. For these reasons, other methods of microencapsulation and the development of multi-layered particles are important areas of research.

### ***1.2.1 Solvent Evaporation***

Currently available FDA-approved PLGA microspheres such as Lupron Depot<sup>®</sup> and Vivitrol<sup>®</sup> utilize solvent evaporation in the manufacturing of these formulations [2]. Minimally, solvent evaporation requires the use of two solvents that will be used as primary components in an inner and outer phase of an emulsion. Solvent evaporation methods can be split into two categories: single and double emulsions.

#### ***1.2.1.1 Oil-in-water (o/w) Emulsion***

A common method for the microencapsulation of hydrophobic drugs such as steroids is the use of an oil-in-water (o/w) single emulsion followed by solvent evaporation. For this, both the drug and carrier polymer are dissolved in a water immiscible organic solvent. For PLGA, this

solvent is typically dichloromethane (DCM) and acetonitrile (ACN). This oil solution is added to relatively large volume of water containing an emulsifier such as polyvinyl alcohol (PVA). The solvent from the oil phase may be removed by continuous stirring, leaving the hardening microspheres in solution. These particles are often collected by centrifugation or filtration and then lyophilized [3].

#### ***1.2.1.2 Water-in-oil-in-water (w/o/w) Double Emulsion***

The use of a double emulsion technique is often utilized for water-soluble drugs and large macromolecules like peptides. In this method, the drug solution, which composes the inner water phase, is added to a larger oil polymer solution—often using DCM as a solvent. The mixture is emulsified and comprises the primary emulsion. The primary emulsion is added to a larger volume of water often containing an emulsifier such as PVA and homogenized to form the secondary emulsion. Then all methods for evaporation and collection are similar to a single emulsion [3].

#### ***1.2.2 Coacervation***

Coacervation or phase separation is another method that is widely used in the manufacturing of FDA-approved therapeutics such as Bydureon<sup>®</sup> or Sandostatin<sup>®</sup> LAR [2]. Coacervation is performed by using two immiscible oil phases. The inner oil phase is comprised of the polymer and drug dissolved in an organic solvent such as acetonitrile. Additionally, for the encapsulation of water-soluble drug, a w/o emulsion may be used for the inner phase as is the case for Bydureon<sup>®</sup> [4]. This solution or emulsion is then added to a non-solvent organic phase such as silicone oil that extracts the polymer solvent, which causes the precipitation of the polymer in droplets. To further harden the coacervation droplets, the mixture is mixed into a large volume of another solution (e.g., heptane/ethanol) [3,5].

### *1.2.3 Spray-drying*

Spray drying is a scalable technique, which may easily be incorporated in continuous processing, that has been widely used in food production as well electronics and cosmetics. In addition, it has been utilized in the pharmaceutical field for the formation of amorphous drugs and solid dispersions as well as for the homogenization of powders [6]. More recently, spray drying has been investigated as an alternative method to solvent evaporation for the microencapsulation of therapeutics in PLGA including water-soluble peptide drugs such as vancomycin [7]. One way to think about spray drying is that it is accelerated solvent evaporation. The desired compound to be spray dried and encapsulation is dissolved into oil solution with the polymer. If it is a water-soluble drug such as a peptide to be encapsulated in polymer, a w/o emulsion may be made instead for the feed solution [7]. Despite the versatility and benefits of spray drying, the complicated spatial and temporal nature of the heat and mass transfer and fluid dynamics are difficult to resolve [8] and may have a profound impact on formulation properties when used for microencapsulation.

The process of spray drying can be separated into three steps: atomization, drying, and separation of particles from the gas phase. In the first stage, the solution is divided into a fine mist of small droplets. There are several different atomizers that have been used in development of spray drying techniques. The two most common are two-fluid and pressure nozzles. In the pressure nozzle, the fluid is atomized by forcing high flow liquid through a small opening. While it is a relatively simple method, it results in a wide size distribution of particles. Two-fluid nozzles have smaller droplet sizes and narrower size distributions. The two-fluid nozzle atomizes the solution by subjecting it to a high-velocity gas. In addition, the initial droplet size has been correlated with the mass flow rate ratio of the gas and liquid and the Weber and Reynolds number of the liquid [9,10].

After atomization, the droplets enter a drying chamber with a co-current heated gas flow. The heated gas has a two-fold effect; by increasing vapor pressure of the solvent through an increase in temperature and by providing a sink through the low pressure of the solvent in the gas phase the gas drives the solvent out of the particles. As the droplet moves through the chamber, the droplet loses mass and shrinks after an initial temperature increase. During this process, the evaporation and shrinkage follows well-understood coupled heat and mass transport equations [11–13]. Eventually, a crust forms that slows diffusion and continues thickening until it reaches the center of the particle.

After the particle is formed in the drying chamber, it is necessary to separate the powder from the gas phase. Cyclone separation is a relatively simple and commonly used method for the collection of products. The cyclone separator forms vortex that uses centrifugal forces to remove particulates from the gas flow. Utilizing the proper atomization technique such as using two-fluid nozzles and sufficient evaporation time [9] can result in the generation of particles with a narrow size distribution. The size of the particles may be controlled through process variables such as the size and type of atomizer [6], the characteristics of the feed solution (e.g. temperature, viscosity, solute concentration) [6,11] and the ratio of the air flow rate to the fluid flow rate [6,8]. In addition, the drying gas temperature and flow rate could be expected to affect the solvent evaporation rate, density and uniformity of the particles by impacting the minimum residence time to dry and residence time, respectively.

#### ***1.2.4 Electrospray***

Electrohydrodynamics refers to the principles that govern the charged fluids and their behavior in an applied electric field. In an electrospray or electrospinning system, fluid flows through a needle that is connected to a cathode of a voltage supply. The fluid will be pulled toward

the anode or ground of the system and form a Taylor cone if the conductivity of the fluid and the voltage are high enough. This phenomenon is created by the hydrostatic pressure that is exerted on the fluid by the electrostatic field. Therefore, the viscosity and conductivity of the feed liquid have a profound impact on Taylor cone stability. From the tip of the Taylor cone, the solution may further break into micro-droplets if the cone is sufficiently stable. As the droplet falls, the solution evaporates similar to spray drying if the solvent is sufficiently volatile. After complete evaporation, particle will form and may be collected. A common method for particle collection is through spraying directly onto an aluminum foil ground [14,15]. Although other methods such as using cooling jacket [16] and an air-cross flow [17] have been used to ensure particle hardening and reduce deformations.

A coaxial electrospray system can be used to manufacture particles with core-shell morphology. The coaxial system involves using a dual-capillary needle that pushes separate inner and outer solutions. The ability for the outer fluid to engulf the inner fluid is highly dependent on the surface and interfacial tension between these two phases as well as the air. In addition, both liquids are influenced by the electric field, but one drives the formation of the Taylor Cone, which is necessary for droplet formation. The driving fluid is typically the one with high electric conductivity and will transfer electric stress to the other fluid [15]. If the conductivity and tension is within the proper ranges, complete engulfment of the inner fluid and the formation of multi-layered droplets can occur, which can become particles after solvent evaporation. This has been explored in different polymeric systems including PLGA and PLA micro- and nano-particles. Xu et al. [18] and Xie et. al [19] have both been able to successfully encapsulate aqueous solutions containing proteins inside PLA and PLGA microcapsules, respectively. Xie et. al also demonstrated protection from denaturation based on high bioactivity after release (90%) [19]. In

addition, there has been work on the encapsulation of solid small molecules [20] and PLGA-drug cores [21].

### ***1.2.5 Remote Loading***

#### ***1.2.5.1 Polymer Healing***

Methods that require solvent evaporation can leave the structure of the microspheres porous. The inner water phase creates spaces in the microspheres that the polymer will not be present. In addition, the leaching of salts and sugars that may improve the stability of the encapsulated therapeutic have a similar effect. These pores are interconnected and are evident on the surface of the particle. But the polymer is mendable and the pores on surface have been shown to heal over time through scanning electron microscopy and fluorescent imaging after dye incubation [22–24]. The self-healing of the polymer can be taken advantage for encapsulation of therapeutics through passive diffusion or active trapping. This reduces the need for sterile microsphere production as the drug may be encapsulated after sterilization is performed, which may otherwise damage the drug. In addition, the drug is not subjected to degradative and denaturing stresses of emulsification.

#### ***1.2.5.2 Pore Forming Agents***

The formation of pores for the remote loading can be induced by several agents called porosigens such as salts like  $\text{Mg}(\text{CO}_3)$  [24–26] or  $\text{Ca}(\text{CO}_3)$  or sugars. These components are included in the formulation of microspheres made through single or double-emulsion solvent evaporation techniques. Encapsulating these salts in the polymer phase of the microspheres or sugars in the inner water phase leads to increased osmotic pressure. The water that is driven into the polymer as well as the leaching of salts and sugars leaves pores in the microsphere. Similarly,

this may be achieved with the use of an immiscible water-soluble polymer that is included in the oil phase such as Pluronic<sup>®</sup> [23]. When the polymer is hardened, the water-soluble polymer is leached out leaving pores.

### ***1.2.5.3 Active Encapsulation***

To improve the encapsulation of compounds through remote loading, an agent may be encapsulated in the microspheres during the solvent evaporation procedures that interacts with the desired compound. Passive encapsulation has low encapsulation efficiency and requires high concentration of solute to drive the therapeutic into the microspheres through diffusion [27]. Through the use of an agent that coordinates with the therapeutic and entraps or precipitates it in the microspheres, the concentration gradient may be maintained, and the encapsulation efficiency improved. Active encapsulation of therapeutics has been used in other systems such as Doxil<sup>®</sup>, which uses ammonium sulfate to precipitate the drug [28]. For PLGA microspheres, Al(OH)<sub>3</sub> has proven to improve encapsulation efficiency to nearly 100% for proteins such as ovalbumin and tetanus toxoid [27,29] as well as peptides such as leuprolide acetate [27]. In addition, zinc salts have been used for other peptides like insulin [30].

### ***1.2.6 Other Methods***

#### ***1.2.6.1 Super Critical Fluid***

Supercritical fluids (SCF) have been researched as a method for the manufacturing of the PLGA and PLA particles and encapsulation of therapeutics. There are several variations of this technology based on the different levels of polymer solubility and solvent/co-solvent immiscibility, but they typically use CO<sub>2</sub> as the SCF. Rapid expansion of supercritical solutions (RESS) involves dissolving the polymer in the SCF. Since the solubility is often pressure and

temperature dependent, the solution is sprayed into a low-pressure system, which allows the polymer to phase separate and solidify in the SCF. Other systems such as gas antisolvent (GAS), supercritical antisolvent (SAS), and solution enhanced dispersion by supercritical fluids (SEDS) all use SCF as an anti-solvent that shifts the stability of a homogeneous solution and leads to the precipitation of the polymer but differ in how the SCF contacts the solution [31]. The benefits of RESS are that it eliminates the use of toxic organic solvents such as DCM which may be present in residual amounts in microspheres made by solvent evaporation.

#### ***1.2.6.2 Microfluidics***

Microfluidic particle formation has similarities to electrohydrodynamic particle formation, but fluid focusing occurs by changes in channel diameters in a microfluidic system rather than through the application of an electric field. Droplet formation occurs as an inner oil phase is driven into a moving continuous aqueous phase through a needle-like orifice. These droplets flow through the microfluidic channel to a larger collection solution, in which they undergo solvent evaporation. Microfluidic allows for the preparation of monodisperse particles [32]. In addition, by using crossflows [32] or coaxial flows [32,33], it is possible to form multi-layered particles similar to coaxial electrohydrodynamic atomizing.

### **1.3 Release from PLGA and PLA microparticles and Governing Mechanisms**

#### ***1.3.1 Initial Burst Release Phase***

Drug release from PLGA microspheres goes through several phases in which the mechanism and rate of release varies. The initial phase is an under-researched and poorly modeled area but represents considerable concern to the success of a long-acting release formulation. This initial phase, also known as the initial burst release, is characterized by a large release of the

encapsulated therapeutic, around 20-80% of total drug, in a short period—usually within the first 24 hours. Several mechanisms of release have been hypothesized during this initial burst period. For a hydrophilic water-soluble drug, diffusion through an aqueous phase is most probable considering the speed of release. Self-healing of the microsphere surface tends to occur at similar time points as the end of initial burst and the beginning of a lag period [25,34]. Therefore, the drug may diffuse through and out of a pore network created by the inner water phase during microsphere formation. In addition, water uptake and polymer swelling may induce convective flows further increasing diffusion out of the polymer.

### ***1.3.2 Water Uptake***

Water uptake occurs very rapidly and increases in water uptake tend to correlate with increases in the initial burst release [35]. Many factors can impact the water uptake, but generally it can be related to the hydrophilicity of the components of the microspheres [36]. When the glycolic acid content increases or the polymer is acid-capped [37], the hydrophilicity of the polymer increases, which facilitates the penetration of water into the polymer phase. The presence of salts that may be used as buffering species [38,39] and monomeric acids from the polymer will create an osmotic pressure gradient, which will drive water into the microspheres, and leave pores which allows water to occupy a separate aqueous phase. In addition, drug loading of water-soluble drugs is also positively correlated with water uptake [35] for similar reasons.

### ***1.3.3 Polymer Response to Water Uptake***

Water uptake can have several effects on the polymer, but the most obvious and well-studied for PLGA is degradation. The presence of water is necessary for the degradation of the polymer, but significant degradation is not expected in the initial burst period [40]. Polymer

swelling upon hydration occurs much more rapidly and deconvolution of in vivo drug concentrations has suggested it as an influencing factor in the initial burst release [41]. This mechanistic analysis was performed by using a semi-empirical method known as the Korsmeyers-Peppas Model or the Power Law [42,43]. In this model, release is considered to be proportional to the power of time ( $\frac{M_t}{M_\infty} = kt^n$ ). Originally for a porous PVA disc [42], it was revised for other geometries. At  $n=0.43$ , the release suggests standard Fickian diffusion release and the equation resembles the well-known Higuchi equation. At  $n=0.85$ , the release is swelling-controlled. It is possible that depending on the relaxation behavior of the polymer and the swelling velocity that crazing or cracking of the polymer can occur [44,45]. Crazing of the polymer may lead to the formation of microporous structures and enhance drug release. Because the penetration of water in both the polymer phase as well as the microporous structures, it is likely that the release is anomalous or somewhere in between pure diffusion and swelling-controlled [46] for PLGA microspheres.

Water also impacts the healing kinetics of pores in the microspheres. Water changes the mechanical properties of PLGA as it plasticizes the polymer and increases the mobility of polymer as evident by the depression of the glass transition temperature ( $T_g$ ) [47–50]. In addition, the healing kinetics of polymer films were greatly accelerated in PBST [47].

### ***1.3.3.1 Polymer-Drug Interactions***

Polymer-drug interactions may slow or prevent altogether the release of the drug. These interactions may limit complete release of the drug prior to self-healing of surfaces pores that would stifle faster aqueous diffusion. Alternatively, it is possible that, during the initial burst release, drug bound to the polymer through these interactions acts as a reservoir when drug concentrations are saturated within the microspheres, maintaining a high concentration gradient to

drive faster release. These interactions may be considered reversible or irreversible. For peptide drugs or drugs containing amine groups, acylation is an irreversible covalent bonding between the polymer and drug that has been heavily researched because it prevents the complete release of drug. The precursor to this reaction is hydrogen bonding or ionic interaction depending on pH between these two compounds [51], which has been shown to be disrupted through the use of divalent salts [52–54] or PEGylation [51,55]. Previously, the adsorption of leuprolide acetate specifically has been examined using confocal Raman spectroscopy [56] as well as used for increasing the encapsulation efficiency [57]. Altogether, it demonstrates that an ionic exchange is necessary to disrupt this interaction and desorb the peptide for release from the polymer.

#### ***1.3.4 Bioerosion***

Bio-erosion of the PLGA microspheres happens in the later phases of release and usually is responsible for most of the drug release. The rate of bio-erosion or mass loss from the microspheres is related to the degradation of the polymer chains [58]. As a result, the polymer chains become shorter and more solubility in water leading to dissolution of the polymer. Therefore, factors that inhibit hydrolysis as well as the characteristics of the polymer are linked to the erosion kinetics. Additionally, starting with a higher molecular weight will take longer for the polymer to erode [37,59], although it will degrade faster [60].

#### ***1.3.5 Hydrolysis***

As mentioned in 1.1, degradation of the polymer is the result of hydrolysis of the ester-linkage between different glycolides and lactides. This hydrolysis results in an acid terminus on one of the resulting polymer chains. The production of acids further increases the rate of reaction through acid-catalyzed hydrolysis. For this reason, polymer that are ester-capped show slower

rates of hydrolysis and erosion [37,59]. Additionally, hydrolysis is dependent on the presence of water. As previously discussed in 1.3.2, the hydrophobicity of the polymer decreases with increasing amounts of glycolide monomers and water uptake increases. Therefore, with decreasing lactide to glycolide ratios, hydrolytic activity and erosion is increased [60].

### ***1.3.6 Drug and Excipient Effects***

Both excipients and the drugs encapsulated have the capacity to alter the microclimate pH within the polymer and there by altering the degradation rates. The addition of basic additives such as  $Mg(OH)_2$  have been used as buffers to maintain the pH and reduce acid-catalyzed hydrolysis [38,39]. This has the additional benefit of stabilizing many protein drugs that are encapsulated. In the same manner, basic drugs can have similar effect. For example, increasing drug loading of caffeine lead to decreased mass loss [61].

### ***1.3.7 Media and Release Conditions***

Release media and conditions have been extensively investigated for their effects on PLGA and PLA degradation and erosion. Since hydrolysis can be catalyzed of acid species, the pH of the media has a significant effect on the erosion kinetics [59,60]. The buffer species may also have an impact on the erosion kinetics. In a study comparing PBST to HBST, HBST showed increased water uptake, but did not show significant differences in erosion or degradation [59]. Temperature is also an important characteristic. Increasing temperature leads to faster degradation rates and higher erosion kinetics [62,63]. The use of surfactants, such as PVA [63] and Tween 20 [64], and ethanol [64], a miscible organic solvent, have both shown to accelerate release although it's impact on degradation is not shown. The use of plasticizers like triethyl citrate have impacted erosion and

release kinetics [59], so the increases in release due to surfactants and ethanol may be related to plasticization of the polymer.

### ***1.3.8 Diffusion***

While bioerosion is commonly the rate-controlling mechanism for moderate molecular weight PLGAs, the release of drug from high molecular weight PLGAs and moderate to high molecular weight PLAs is likely to be diffusion-controlled because the high molecular weight and/or slow degradation leads to long lag times before erosion begins. Examples of this diffusion front release behaviors have been shown in PLA microspheres containing gentamicin [65] as well as estradiol valerate [66].

### ***1.3.9 Plasticizers and Residual Solvents***

Plasticizers, which would decrease the polymer  $T_g$  and polymer mobility, would lead to increased degradation and diffusion in polymers. Inclusion of triethyl citrate or acetyl triethyl citrate have been shown to increase the levels of hydrolysis in PLA films. Additionally, inclusion of PEG in polymer matrices have increased release, but the content was large enough for the PEG to be present as a separate phase and induce porosity [67]. Residual solvents left over from the manufacturing can also induce plasticization of the polymer [68]. These residual solvents can induce faster degradation and release from the polymer matrix [69]. In addition, limitations of residual solvents related to acceptable daily exposure are an important consideration in development of microparticle formulations. In particular, common polymer solvents such as methylene chloride and chloroform are considered Class 2 solvents and have stricter guidelines for residual levels [70].

## 1.4 References

- [1] R.A. Jain, C.T. Rhodes, A.M. Railkar, A.W. Malick, N.H. Shah, Comparison of various injectable protein-loaded biodegradable poly(lactide-co-glycolide) (PLGA) devices: in-situ-formed implant versus in-situ-formed microspheres versus isolated microspheres, *Pharm Dev Technol.* 5 (2000) 201–207. <https://doi.org/10.1081/PDT-100100535>.
- [2] R. Kumar, M.J. Palmieri, Points to Consider when Establishing Drug Product Specifications for Parenteral Microspheres, *Aaps Journal.* 12 (2010) 27–32. <https://doi.org/10.1208/s12248-009-9156-6>.
- [3] C. Wischke, S.P. Schwendeman, Principles of encapsulating hydrophobic drugs in PLA/PLGA microparticles, *Int J Pharm.* 364 (2008) 298–327. <https://doi.org/10.1016/j.ijpharm.2008.04.042>.
- [4] Y. Cai, L. Wei, L. Ma, X. Huang, A. Tao, Z. Liu, W. Yuan, Long-acting preparations of exenatide, *Drug Des Devel Ther.* 7 (2013) 963–970. <https://doi.org/10.2147/DDDT.S46970>.
- [5] R.A. Jain, The manufacturing techniques of various drug loaded biodegradable poly(lactide-co-glycolide) (PLGA) devices, *Biomaterials.* 21 (2000) 2475–2490. [https://doi.org/10.1016/S0142-9612\(00\)00115-0](https://doi.org/10.1016/S0142-9612(00)00115-0).
- [6] A. Ziaee, A.B. Albadarin, L. Padrela, T. Femmer, E. O'Reilly, G. Walker, Spray drying of pharmaceuticals and biopharmaceuticals: Critical parameters and experimental process optimization approaches, *Eur J Pharm Sci.* 127 (2019) 300–318. <https://doi.org/10.1016/j.ejps.2018.10.026>.
- [7] E. Gavini, P. Chetoni, M. Cossu, M.G. Alvarez, M.F. Saettone, P. Giunchedi, PLGA microspheres for the ocular delivery of a peptide drug, vancomycin using

- emulsification/spray-drying as the preparation method: in vitro/in vivo studies, *European Journal of Pharmaceutics and Biopharmaceutics*. 57 (2004) 207–212.  
<https://doi.org/10.1016/j.ejpb.2003.10.018>.
- [8] S. Lo, Application of computational fluid dynamics to spray drying, *Lait*. 85 (2005) 353–359. <https://doi.org/10.1051/lait:2005024>.
- [9] I.C. Kemp, T. Hartwig, R. Herdman, P. Hamilton, A. Bisten, S. Bermingham, Spray drying with a two-fluid nozzle to produce fine particles: Atomization, scale-up, and modeling, *Drying Technology*. 34 (2016) 1243–1252.  
<https://doi.org/10.1080/07373937.2015.1103748>.
- [10] A. Mansour, N. Chigier, Air-blast atomization of non-Newtonian liquids, *J Nonnewton Fluid Mech*. 58 (1995) 161–194. [https://doi.org/https://doi.org/10.1016/0377-0257\(95\)01356-Z](https://doi.org/https://doi.org/10.1016/0377-0257(95)01356-Z).
- [11] F. Wan, M. Yang, Design of PLGA-based depot delivery systems for biopharmaceuticals prepared by spray drying, *Int J Pharm*. 498 (2016) 82–95.  
<https://doi.org/10.1016/j.ijpharm.2015.12.025>.
- [12] R. Vehring, W.R. Foss, D. Lechuga-Ballesteros, Particle formation in spray drying, *J Aerosol Sci*. 38 (2007) 728–746. <https://doi.org/10.1016/j.jaerosci.2007.04.005>.
- [13] W.E. Ranz, W.R. Marshall, Evaporation from Drops .1., *Chem Eng Prog*. 48 (1952) 141–146.
- [14] F. Wang, Z.Q. Li, K. Tamama, C.K. Sen, J.J. Guan, Fabrication and Characterization of Prosurvival Growth Factor Releasing, Anisotropic Scaffolds for Enhanced Mesenchymal Stem Cell Survival/Growth and Orientation, *Biomacromolecules*. 10 (2009) 2609–2618.  
<https://doi.org/10.1021/bm900541u>.

- [15] L. Zhang, J. Huang, T. Si, R.X. Xu, Coaxial electrospray of microparticles and nanoparticles for biomedical applications, *Expert Rev Med Devices*. 9 (2012) 595–612. <https://doi.org/10.1586/erd.12.58>.
- [16] R. Bocanegra, A.G. Gaonkar, A. Barrero, I.G. Loscertales, D. Pechack, M. Marquez, Production of cocoa butter microcapsules using an electrospray process, *J Food Sci*. 70 (2005) E492–E497. [https://doi.org/DOI 10.1111/j.1365-2621.2005.tb11520.x](https://doi.org/DOI%2010.1111/j.1365-2621.2005.tb11520.x).
- [17] L. Ding, T. Lee, C.H. Wang, Fabrication of monodispersed Taxol-loaded particles using electrohydrodynamic atomization, *J Control Release*. 102 (2005) 395–413. <https://doi.org/10.1016/j.jconrel.2004.10.011>.
- [18] Y. Xu, M.A. Hanna, Morphological and structural properties of two-phase coaxial jet electrosprayed BSA-PLA capsules, *J Microencapsul*. 25 (2008) 469–477. <https://doi.org/10.1080/02652040802049513>.
- [19] J. Xie, W.J. Ng, L.Y. Lee, C.H. Wang, Encapsulation of protein drugs in biodegradable microparticles by co-axial electrospray, *J Colloid Interface Sci*. 317 (2008) 469–476. <https://doi.org/10.1016/j.jcis.2007.09.082>.
- [20] Y.H. Lee, F. Mei, M.Y. Bai, S. Zhao, D.R. Chen, Release profile characteristics of biodegradable-polymer-coated drug particles fabricated by dual-capillary electrospray, *J Control Release*. 145 (2010) 58–65. <https://doi.org/10.1016/j.jconrel.2010.03.014>.
- [21] H.W. Yeh, D.R. Chen, In vitro release profiles of PLGA core-shell composite particles loaded with theophylline and budesonide, *Int J Pharm*. 528 (2017) 637–645. <https://doi.org/10.1016/j.ijpharm.2017.06.032>.

- [22] S. Fredenberg, M. Wahlgren, M. Reslow, A. Axelsson, Pore formation and pore closure in poly(D,L-lactide-co-glycolide) films, *J Control Release*. 150 (2011) 142–149.  
<https://doi.org/10.1016/j.jconrel.2010.11.020>.
- [23] H.K. Kim, H.J. Chung, T.G. Park, Biodegradable polymeric microspheres with “open/closed” pores for sustained release of human growth hormone, *J Control Release*. 112 (2006) 167–174. <https://doi.org/10.1016/j.jconrel.2006.02.004>.
- [24] R.B. Shah, S.P. Schwendeman, A biomimetic approach to active self-microencapsulation of proteins in PLGA, *J Control Release*. 196 (2014) 60–70.  
<https://doi.org/10.1016/j.jconrel.2014.08.029>.
- [25] J. Kang, S.P. Schwendeman, Pore closing and opening in biodegradable polymers and their effect on the controlled release of proteins, *Mol Pharm*. 4 (2007) 104–118.  
<https://doi.org/10.1021/mp060041n>.
- [26] S.E. Reinhold, S.P. Schwendeman, Effect of polymer porosity on aqueous self-healing encapsulation of proteins in PLGA microspheres, *Macromol Biosci*. 13 (2013) 1700–1710. <https://doi.org/10.1002/mabi.201300323>.
- [27] S.E. Reinhold, K.G. Desai, L. Zhang, K.F. Olsen, S.P. Schwendeman, Self-healing microencapsulation of biomacromolecules without organic solvents, *Angew Chem Int Ed Engl*. 51 (2012) 10800–10803. <https://doi.org/10.1002/anie.201206387>.
- [28] G. Haran, R. Cohen, L.K. Bar, Y. Barenholz, Transmembrane ammonium sulfate gradients in liposomes produce efficient and stable entrapment of amphipathic weak bases, *Biochim Biophys Acta*. 1151 (1993) 201–215. [https://doi.org/10.1016/0005-2736\(93\)90105-9](https://doi.org/10.1016/0005-2736(93)90105-9).

- [29] K.G. Desai, S.P. Schwendeman, Active self-healing encapsulation of vaccine antigens in PLGA microspheres, *J Control Release*. 165 (2013) 62–74.  
<https://doi.org/10.1016/j.jconrel.2012.10.012>.
- [30] C. Manoharan, J. Singh, Insulin loaded PLGA microspheres: effect of zinc salts on encapsulation, release, and stability, *J Pharm Sci*. 98 (2009) 529–542.  
<https://doi.org/10.1002/jps.21445>.
- [31] S.D. Yeo, E. Kiran, Formation of polymer particles with supercritical fluids: A review, *Journal of Supercritical Fluids*. 34 (2005) 287–308.  
<https://doi.org/10.1016/j.supflu.2004.10.006>.
- [32] S. Rezvantalab, M.K. Moraveji, Microfluidic assisted synthesis of PLGA drug delivery systems, *RSC Adv*. 9 (2019) 2055–2072. <https://doi.org/10.1039/c8ra08972h>.
- [33] T.T. Kong, J. Wu, K.W.K. Yeung, M.K.T. To, H.C. Shum, L.Q. Wang, Microfluidic fabrication of polymeric core-shell microspheres for controlled release applications, *Biomicrofluidics*. 7 (2013). <https://doi.org/Artn 044128 10.1063/1.4819274>.
- [34] J. Wang, B.M. Wang, S.P. Schwendeman, Characterization of the initial burst release of a model peptide from poly(D,L-lactide-co-glycolide) microspheres, *J Control Release*. 82 (2002) 289–307. <https://www.ncbi.nlm.nih.gov/pubmed/12175744>.
- [35] K.G. Desai, S.R. Mallery, S.P. Schwendeman, Formulation and characterization of injectable poly(DL-lactide-co-glycolide) implants loaded with N-acetylcysteine, a MMP inhibitor, *Pharm Res*. 25 (2008) 586–597. <https://doi.org/10.1007/s11095-007-9430-1>.
- [36] A.G. Ding, S.P. Schwendeman, Acidic microclimate pH distribution in PLGA microspheres monitored by confocal laser scanning microscopy, *Pharm Res*. 25 (2008) 2041–2052. <https://doi.org/10.1007/s11095-008-9594-3>.

- [37] A.C. Doty, D.G. Weinstein, K. Hirota, K.F. Olsen, R. Ackermann, Y. Wang, S. Choi, S.P. Schwendeman, Mechanisms of in vivo release of triamcinolone acetonide from PLGA microspheres, *Journal of Controlled Release*. 256 (2017) 19–25.  
<https://doi.org/10.1016/j.jconrel.2017.03.031>.
- [38] G. Zhu, S.R. Mallery, S.P. Schwendeman, Stabilization of proteins encapsulated in injectable poly (lactide- co-glycolide), *Nat Biotechnol*. 18 (2000) 52–57.  
<https://doi.org/10.1038/71916>.
- [39] G.Z. Zhu, S.P. Schwendeman, Stabilization of proteins encapsulated in cylindrical poly(lactide-co-glycolide) implants: Mechanism of stabilization by basic additives, *Pharm Res*. 17 (2000) 351–357. <https://doi.org/Doi 10.1023/A:1007513425337>.
- [40] #x, S. Souza, R. Dorati, P.P. DeLuca, Effect of Hydration on Physicochemical Properties of End-Capped PLGA, *Advances in Biomaterials*. 2014 (2014) 9.  
<https://doi.org/10.1155/2014/834942>.
- [41] I. Tomic, M. Mueller-Zsigmondy, A. Vidis-Millward, J.M. Cardot, In vivo release of peptide-loaded PLGA microspheres assessed through deconvolution coupled with mechanistic approach, *Eur J Pharm Biopharm*. 125 (2018) 21–27.  
<https://doi.org/10.1016/j.ejpb.2017.12.007>.
- [42] R.W. Korsmeyer, R. Gurny, E. Doelker, P. Buri, N.A. Peppas, Mechanisms of Solute Release from Porous Hydrophilic Polymers, *Int J Pharm*. 15 (1983) 25–35.  
[https://doi.org/Doi 10.1016/0378-5173\(83\)90064-9](https://doi.org/Doi 10.1016/0378-5173(83)90064-9).
- [43] P.L. Ritger, N.A. Peppas, A simple equation for description of solute release II. Fickian and anomalous release from swellable devices, *Journal of Controlled Release*. 5 (1987) 37–42. [https://doi.org/https://doi.org/10.1016/0168-3659\(87\)90035-6](https://doi.org/https://doi.org/10.1016/0168-3659(87)90035-6).

- [44] J. Klier, N.A. Peppas, Anomalous Penetrant Transport in Glassy-Polymers .4. Stresses in Partially Swollen Polymers, *Polymer (Guildf)*. 28 (1987) 1851–1859. [https://doi.org/Doi 10.1016/0032-3861\(87\)90290-4](https://doi.org/Doi 10.1016/0032-3861(87)90290-4).
- [45] N.A. Peppas, K.G. Urdahl, Anomalous Penetrant Transport in Glassy-Polymers .8. Solvent-Induced Cracking in Polystyrene, *Eur Polym J*. 24 (1988) 13–20. [https://doi.org/Doi 10.1016/0014-3057\(88\)90119-X](https://doi.org/Doi 10.1016/0014-3057(88)90119-X).
- [46] T. Alfrey, E.F. Gurnee, W.G. Lloyd, Diffusion in Glassy Polymers, *Journal of Polymer Science Part C-Polymer Symposium*. (1966) 249-.
- [47] J.M. Mazzara, M.A. Balagna, M.D. Thouless, S.P. Schwendeman, Healing kinetics of microneedle-formed pores in PLGA films, *J Control Release*. 171 (2013) 172–177. <https://doi.org/10.1016/j.jconrel.2013.06.035>.
- [48] S.S. Shah, Y. Cha, C.G. Pitt, Poly (glycolic acid-co-dl-lactic acid): diffusion or degradation controlled drug delivery?, *Journal of Controlled Release*. 18 (1992) 261–270. [https://doi.org/https://doi.org/10.1016/0168-3659\(92\)90171-M](https://doi.org/https://doi.org/10.1016/0168-3659(92)90171-M).
- [49] N. Passerini, D.Q.M. Craig, An investigation into the effects of residual water on the glass transition temperature of polylactide microspheres using modulated temperature DSC, *Journal of Controlled Release*. 73 (2001) 111–115. [https://doi.org/Doi 10.1016/S0168-3659\(01\)00245-0](https://doi.org/Doi 10.1016/S0168-3659(01)00245-0).
- [50] J.M. Mazzara, L.J. Ochyl, J.K.Y. Hong, J.J. Moon, M.R. Prausnitz, S.P. Schwendeman, Self-healing encapsulation and controlled release of vaccine antigens from PLGA microparticles delivered by microneedle patches, *Bioeng Transl Med*. 4 (2019) 116–128. <https://doi.org/10.1002/btm2.10103>.

- [51] D.H. Na, P.P. DeLuca, PEGylation of octreotide: I. Separation of positional isomers and stability against acylation by poly(D,L-lactide-co-glycolide), *Pharm Res.* 22 (2005) 736–742. <https://doi.org/10.1007/s11095-005-2589-4>.
- [52] Y. Zhang, A.M. Sophocleous, S.P. Schwendeman, Inhibition of peptide acylation in PLGA microspheres with water-soluble divalent cationic salts, *Pharm Res.* 26 (2009) 1986–1994. <https://doi.org/10.1007/s11095-009-9914-2>.
- [53] Y. Zhang, S.P. Schwendeman, Minimizing acylation of peptides in PLGA microspheres, *J Control Release.* 162 (2012) 119–126. <https://doi.org/10.1016/j.jconrel.2012.04.022>.
- [54] A.M. Sophocleous, Y. Zhang, S.P. Schwendeman, A new class of inhibitors of peptide sorption and acylation in PLGA, *J Control Release.* 137 (2009) 179–184. <https://doi.org/10.1016/j.jconrel.2009.03.006>.
- [55] W.L. Jiang, S.P. Schwendeman, Stabilization and controlled release of bovine serum albumin encapsulated in poly(D, L-lactide) and poly(ethylene glycol) microsphere blends, *Pharm Res.* 18 (2001) 878–885. <https://doi.org/10.1023/A:1011009117586>.
- [56] A.M. Sophocleous, K.G. Desai, J.M. Mazzara, L. Tong, J.X. Cheng, K.F. Olsen, S.P. Schwendeman, The nature of peptide interactions with acid end-group PLGAs and facile aqueous-based microencapsulation of therapeutic peptides, *J Control Release.* 172 (2013) 662–670. <https://doi.org/10.1016/j.jconrel.2013.08.295>.
- [57] H. Okada, One- and three-month release injectable microspheres of the LH-RH superagonist leuprorelin acetate, *Adv Drug Deliv Rev.* 28 (1997) 43–70. <https://www.ncbi.nlm.nih.gov/pubmed/10837564>.

- [58] F.G. Hutchinson, B.J.A. Furr, Biodegradable Polymer Systems for the Sustained-Release of Polypeptides, *Journal of Controlled Release*. 13 (1990) 279–294. [https://doi.org/Doi10.1016/0168-3659\(90\)90018-O](https://doi.org/Doi10.1016/0168-3659(90)90018-O).
- [59] A.C. Doty, Y. Zhang, D.G. Weinstein, Y. Wang, S. Choi, W. Qu, S. Mittal, S.P. Schwendeman, Mechanistic analysis of triamcinolone acetonide release from PLGA microspheres as a function of varying in vitro release conditions, *European Journal of Pharmaceutics and Biopharmaceutics*. 113 (2017) 24–33. <https://doi.org/10.1016/j.ejpb.2016.11.008>.
- [60] X.S. Wu, N. Wang, Synthesis, characterization, biodegradation, and drug delivery application of biodegradable lactic/glycolic acid polymers. Part II: Biodegradation, *Journal of Biomaterials Science-Polymer Edition*. 12 (2001) 21–34. <https://doi.org/Doi10.1163/156856201744425>.
- [61] S.M. Li, Hydrolytic degradation characteristics of aliphatic polyesters derived from lactic and glycolic acids, *J Biomed Mater Res*. 48 (1999) 342–353. [https://doi.org/Doi10.1002/\(Sici\)1097-4636\(1999\)48:3<342::Aid-Jbm20>3.0.Co;2-7](https://doi.org/Doi10.1002/(Sici)1097-4636(1999)48:3<342::Aid-Jbm20>3.0.Co;2-7).
- [62] Y. Aso, S. Yoshioka, A.L.W. Po, T. Terao, Effect of Temperature on Mechanisms of Drug-Release and Matrix Degradation of Poly(D,L-Lactide) Microspheres, *Journal of Controlled Release*. 31 (1994) 33–39. [https://doi.org/Doi10.1016/0168-3659\(94\)90248-8](https://doi.org/Doi10.1016/0168-3659(94)90248-8).
- [63] M. Shameem, H. Lee, P.P. DeLuca, A short term (accelerated release) approach to evaluate peptide release from PLGA depot-formulations, *AAPS PharmSci*. 1 (1999) E7. <https://doi.org/10.1208/ps010307>.

- [64] D.R. Janagam, L. Wang, S. Ananthula, J.R. Johnson, T.L. Lowe, An Accelerated Release Study to Evaluate Long-Acting Contraceptive Levonorgestrel-Containing in Situ Forming Depot Systems, *Pharmaceutics*. 8 (2016). <https://doi.org/10.3390/pharmaceutics8030028>.
- [65] T.T.T. Trang, M. Mariatti, H.Y. Badrul, K. Masakazu, X.T.T. Nguyen, A.A.H. Zuratul, Drug release profile study of gentamicin encapsulated poly(lactic Acid) microspheres for drug delivery, in: *Mater Today Proc*, 2019. <https://doi.org/10.1016/j.matpr.2019.06.370>.
- [66] S.R.P. MacHado, L.O. Lunardi, A.P. Tristo, J.M. Marchetti, Preparation and characterization of D, L-PLA loaded 17 - Estradiol valerate by emulsion/evaporation methods, *J Microencapsul*. 26 (2009). <https://doi.org/10.1080/02652040802233786>.
- [67] W. Bao, X. Zhang, H. Wu, R. Chen, S. Guo, Synergistic effect of ultrasound and polyethylene glycol on the mechanism of the controlled drug release from polylactide matrices, *Polymers (Basel)*. 11 (2019). <https://doi.org/10.3390/polym11050880>.
- [68] S.G. Wright, T. Christensen, T. Yeoh, M.E. Rickey, J.M. Hotz, R. Kumar, H.R. Costantino, Polymer-based sustained release device, US8431685B2, 2005.
- [69] M.E. Rickey, J.M. Ramstack, D.H. Lewis, J. Mesens, Preparation of extended shelf-life biodegradable, biocompatible microparticles containing a biologically active agent, US5792477A, 1997.
- [70] USP, USP-467 RESIDUAL SOLVENTS, USP. (2007).

## **Chapter 2 Mechanistic Evaluation of the Initial Burst Release of Leuprolide from Poly(Lactic-co-Glycolic Acid) Spray-dried Microspheres**

### **2.1 Abstract**

Spray-dried poly(lactic-co-glycolic acid) (PLGA) peptide-loaded microspheres have demonstrated similar long-term in vitro release kinetics compared to those produced by the solvent evaporation method and commercial products. However, the difficult-to-control initial burst release over the first 24 hours after administration presents an obstacle to product development and establishing bioequivalence. Currently, detailed information about underlying mechanisms of the initial burst release from microspheres is limited. We investigated the mechanism and extent of initial burst release using 16 previously developed spray-dried microsphere formulations of the hormone drug, leuprolide acetate, with similar composition to the commercial 1-month Lupron Depot<sup>®</sup> (LD). The burst release kinetics was measured with a previously validated continuous monitoring system as well as traditional sample-and-separate methods. The changes in pore structure and polymer permeability were investigated by SEM imaging and the uptake of a bodipy-dextran probe. In vitro results were compared to pharmacokinetics in rats over the same interval. High-burst, spray-dried microspheres were differentiated in the well-mixed continuous monitoring system but reached an upper limit when measured by the sample-and-separate method. Pore-like occlusions observed by confocal microscopy in some formulations indicated that particle swelling

may have contributed to probe diffusion through the polymer phase and showed the extensive internal pore structure of spray-dried particles. Continuous monitoring revealed a rapid primary ( $1^\circ$ ) phase followed by a constant-rate secondary ( $2^\circ$ ) release phase, which comprised  $\sim 80\%$  and  $20\%$  of the 24-hr release, respectively. The ratio of  $1^\circ$  phase duration ( $t_{1^\circ}$ ) and the characteristic probe diffusion time ( $\tau$ ) was highly correlated to  $1^\circ$  phase release for spray dried particles. Of the four spray-dried formulations administered in vivo, three spray-dried microspheres with similar polymer density showed nearly ideal linear correlation between in vivo absorption and well-mixed in vitro release kinetics over the first 24 hours. By contrast, the more structurally dense LD and a more-dense in-house formulation showed a slight lag phase in vivo relative to in vitro. Furthermore, in vitro dimensionless times ( $t_{burst}/\tau$ ) were highly correlated with pharmacokinetic parameters for spray-dried microspheres but not for LD. While the correlation of increases in effective probe diffusion and  $1^\circ$  phase release strongly suggests diffusion through the polymer matrix as a major release mechanism both in vitro and in vivo, a fixed lower limit for this release fraction implies an alternative release mechanism.

## 2.2 Introduction

Long-acting release (LAR) products are a common method for enhancing the safety and efficacy of drug therapy. In terms of biodegradable controlled-release products, injectable poly(lactic-co-glycolic acid) and poly(lactide-co-glycolide) (PLGA) microspheres are one of the most prevalent, and there are a large number of products that have received FDA approval [1,2]. The effects of in vitro conditions on drug release rates and mechanisms from PLGA has been studied extensively for several biomolecules [3–11] including small peptide hormones.

Leuprolide acetate—a short synthetic peptide—is a luteinizing hormone-releasing hormone (LHRH) receptor agonist used for the palliative treatment of several indications including

cancer and endometriosis [12]. While transient and pulsatile administration of leuprolide can lead to increase in gonadotropin levels, continuous release of LHRH agonists (LHRHa) causes desensitization and reduces steroidogenesis. The mechanism of action of leuprolide along with its low bioavailability and short plasma half-life (~3 hr) made it a prime candidate for controlled release. The Lupron Depot® includes a family of PLGA and poly(lactic acid) (PLA) microsphere products with injection intervals of one, three, four, or even six months and is produced by double-emulsion/solvent evaporation with the drug dissolved in the inner water phase with or without gelatin [13]. Despite Lupron Depot® being marketed for over 30 years, there are currently no approved generic formulations in the US, which may be related to the difficulty in manufacturing and establishing equivalent in vitro and in vivo performance. To better understand critical characteristics for release, our group has previously reverse-engineered the composition (gelatin type, polymer type, polymer molecular weight, etc.) of the 1-month US Lupron Depot® product [14].

The effect of manufacturing conditions on encapsulation and long-term release also has been investigated by our lab for double-emulsion (w/o/w) solvent evaporation [15] and spray drying [16], the latter of which can serve as an alternative method for microencapsulation of leuprolide. Spray drying is a controllable, continuous production approach used in the pharmaceutical industry, which has a unique particle formation process. Process parameters of spray drying displayed a significant influence on long-acting release profiles [16]. Like most PLGA LAR microspheres, Lupron Depot® possesses a substantial initial burst release (20-40% drug loading in vitro) [14,15,17] in the first 24 hr, and while being able to create compositionally equivalent formulations with similar long-term release profiles as the commercial product, we saw significant variation in initial burst by the sample-and-separate method, especially for spray-dried

formulations. Spray dried microspheres might have unique particle microstructure features that are influenced by process parameters, resulting in distinctive release behaviors. The initial burst of leuprolide from these microparticles has important implications for regulation and development of generic formulations because the high initial plasma concentrations produce temporary flares in gonadotropin levels, which have been associated with a transient increase in the severity of symptoms [12,18], while this surge may also be important for desensitization. Accordingly, it is important to characterize the process of initial burst release of microspheres made by spray drying quantitatively and work to control or minimize burst.

Initial burst release has been hypothesized to be controlled primarily by at least one of three mechanisms: (1) polymer phase diffusion; (2) aqueous diffusion through network of pores; (3) osmotic-mediated release/osmotic-pumping [19]. Immediate release of surface-bound drug from the polymer also contributes to the burst, but this release may be minimized through washing steps after particle formation. For compositionally similar microspheres, the subtle changes in encapsulation efficiency and residual solvents are not expected to cause significant changes in osmotic gradients, which would result in the differences in initial burst previously seen, but the structure and density of these microspheres are expected to be heavily influenced by the manufacturing conditions. Previously, the changes in release rates and the end of the initial release have coincided with closing of pores on the surface of particles—pore healing—for high molecular weight, hydrophilic molecules such as peptides [3,20–22]. More specifically for Lupron Depot®, while the pore network could play a key role for controlling the initial burst, leuprolide has demonstrated a potential to partition into the polymer phase for low molecular weight PLGAs [5]. Both these could be impacted by the manufacturing conditions. Therefore, determining whether the rate controlling mechanism during the initial burst is polymer phase diffusion or through a pore

network is important for helping guide future formulation development, but more importantly, for establishing appropriate *in vitro* release conditions for comparison with *in vivo* absorption.

Release from PLGA microspheres is often multi-phasic, and each of these phases may be hindered or accelerated by the *in vivo* environment. Often, a significant fraction of release from PLGA microspheres occurs during an erosion-controlled phase that happens after a slow-releasing lag phase, which itself is preceded by a fast-releasing initial burst. For low molecular weight uncapped PLGAs, the lag phase is often minimal or even absent, giving rise to continuous near zero order release [23]. In recent studies with leuprolide acetate, release from PLGA microspheres and the commercial product, Lupron Depot® has occurred at a faster time scale *in vivo* when compared to *in vitro* [24]. The degradation and erosion of PLGA microspheres is commonly understood to be accelerated *in vivo* and hypothesized to be related to inflammatory responses and endogenous components [10,11,25]. While these previous studies with leuprolide have demonstrated some predictability in the long-term release from PLGA microspheres, it required separating formulations into high and low burst groups and did not investigate the differences in initial burst release *in vitro* compared to *in vivo* [24].

The purpose of this study was to investigate the associations between *in vitro* initial burst release by both traditional sample-and-separate [16] and continuous monitoring methods [3] as well as *in vitro* parameters and *in vivo* absorbance and pharmacokinetic parameters during the initial burst period. Specifically, we examined these relationships in the context of changes in process variables of previously characterized in-house spray-dried microsphere formulations [16] in comparison to Lupron Depot® and utilized *in vitro* release characterization during the initial burst to elucidate plausible contributions to the initial release mechanisms.

## 2.3 Materials and Methods

### 2.3.1 Materials

The 7.5 mg leuprolide dose for 1-month administration Lupron Depot<sup>®</sup> (LD, AbbVie Inc., North Chicago, IL, USA) was purchased from the pharmacy department at the University of Michigan Health System. Type B gelatin derived from bovine bone with bloom number 250 was supplied from Nitta Gelatin Inc. (Osaka, Japan). Poly(lactic-co-glycolic acid) 7515 (PLGA 75/25) polymer (catalog no. 823-11966) was purchased from Wako Pure Chemical Industries, Ltd. Leuprolide acetate with purity >98% by HPLC assay was provided by Bachem Inc. (Bubendorf, Switzerland). Methylene chloride, acetonitrile and tetrahydrofuran (THF) were provided by Aldrich Chemical (Milwaukee, WI, USA). Filter paper (Nylon, 0.45um) was supplied by Micron Separations Inc. (Westboro, MA). Bodipy<sup>™</sup> FL Hydrazide was purchased from Invitrogen<sup>™</sup> (Eugene, OR). Dextran (9-11kDa) was purchased from Sigma-Aldrich (St. Louis, MO). All solvents used were HPLC grade and were purchased from Fisher Scientific. All chemicals were used as received.

### 2.3.2 Preparation of poly(lactic-co-glycolic acid) microspheres encapsulating leuprolide by spray-drying

As described previously [16], the spray drying method was performed to formulate Lupron Depot<sup>®</sup>-like microspheres according to a formulation table (Table S2-1). The water phase consisted of a suitable amount of leuprolide and gelatin in 1 mL of water and was maintained at 60°C. PLGA 75/25 was dissolved in methylene chloride (DCM) to make the final concentration at 50–300 mg/mL. The water phase and the oil phase were mixed by vortexing for 20 s and then emulsified for 2 min using a homogenizer at a speed of 15000 rpm (Virtis Tempest I.Q.2

Homogenizer, Sentry Microprocessor, Kent City, Michigan) to form a W/O emulsion. The obtained W/O emulsion was cooled in an ice-bath for 1 minute to decrease the evaporation of methylene chloride in the emulsion. The W/O emulsion was subjected to spray drying by a ProCepT 4M8-TriX spray dryer (ProCepT, Zelzate, Belgium) with a 0.6-1.2 mm bi-fluid nozzle and a 7-16 L/min airflow in the nozzle. Cyclone air was open at a value of 0.12 m<sup>3</sup>/min and cooling air was shut down. The emulsion solutions were fed at a rate of 50–100 mL/min and atomized at an inlet airflow of 0.4–0.7 m<sup>3</sup>/min at 50–80°C. The parameters of the spray dryer and leuprolide/PLGA formulations made by spray drying are shown in Table S2-1. The spray-dried powders were collected by the product receiver. The crude powders by spray drying were rinsed with 50 mL of cold water at 4°C and centrifuged at a speed of 4000 rpm, and the procedure was performed three times to wash off the unencapsulated drug. The microspheres were freeze-dried under reduced pressure for at least 48 hr using a lyophilizer (Labconco, Kansas, USA).

### **2.3.3 Drug loading**

As described previously [16], the spray drying method was performed to formulate Lupron Depot®-like microspheres according to a formulation table (Table S2-1). The water phase consisted of a suitable amount of leuprolide and gelatin in 1 mL of water and was maintained at 60°C. PLGA 75/25 was dissolved in methylene chloride (DCM) to make the final concentration at 50–300 mg/mL. The water phase and the oil phase were mixed by vortexing for 20 s and then emulsified for 2 min using a homogenizer at a speed of 15000 rpm (Virtis Tempest I.Q.2 Homogenizer, Sentry Microprocessor, Kent City, Michigan) to form a W/O emulsion. The obtained W/O emulsion was cooled in an ice-bath for 1 minute to decrease the evaporation of methylene chloride in the emulsion. The W/O emulsion was subjected to spray drying by a ProCepT 4M8-TriX spray dryer (ProCepT, Zelzate, Belgium) with a 0.6-1.2 mm bi-fluid nozzle

and a 7-16 L/min airflow in the nozzle. Cyclone air was open at a value of 0.12 m<sup>3</sup>/min and cooling air was shut down. The emulsion solutions were fed at a rate of 50–100 mL/min and atomized at an inlet airflow of 0.4–0.7 m<sup>3</sup>/min at 50–80°C. The parameters of the spray dryer and leuprolide/PLGA formulations made by spray drying are shown in Table S1. The spray-dried powders were collected by the product receiver. The crude powders by spray drying were rinsed with 50 mL of cold water at 4°C and centrifuged at a speed of 4000 rpm, and the procedure was performed three times to wash off the unencapsulated drug. The microspheres were freeze-dried under reduced pressure for at least 48 hr using a lyophilizer (Labconco, Kansas, USA).

#### ***2.3.4 In vitro initial burst evaluated by continuous monitoring system***

The custom designed continuous monitoring system was used to measure the continuous initial burst release profiles of leuprolide-loaded microspheres, as similarly described [3]. Pre-weighed microspheres (~2mg leuprolide equivalence) were added into release medium (Figure S2-1). Release medium was 40 mL of 10 mM phosphate-buffered saline with 0.02% tween 80 (PBST) (containing 0.02% sodium azide) at pH 7.4. The continuous monitoring instrumental set-up, which circulates the release media through an HPLC dual UV detector from a probe that was covered with a submicron nylon mesh and placed inside the release vessel, is described in Figure S2-1 and the data processing was performed as described [3]. Initial burst release monitoring was conducted over 36 hr at 37 °C.

#### ***2.3.5 Single-point monitoring of 24-hr in vitro initial burst***

Ten mg of leuprolide-loaded spray-dried microspheres or 11.8 mg of Lupron Depot® microspheres (~1mg leuprolide equivalence) were dispersed in 1 mL of 10 mM phosphate-buffered saline with 0.02% tween 80 (PBST) (containing 0.02% sodium azide) at pH 7.4 and 37°C

using 2.0-mL round-bottom tube. Then, the microspheres were incubated at 37 °C with agitation at 240 rpm (KS 130 basic, IKA Works Inc., Wilmington, NC, USA) and after centrifugation at 8000 rpm for 5 min, the media (~0.8 mL) were collected. The amount of leuprolide in aqueous phase was determined using UPLC (Acquity, Waters, Milford, MA, USA) composed of a BEH C18 column (Waters, Milford, MA, USA) and a UV detector with an absorption wavelength of 280 nm and an injection volume of 2 µL. A gradient of acetonitrile with 0.1% (v/v) TFA (solvent A) and ddH<sub>2</sub>O with 0.1% TFA (solvent B) at a flow rate of 0.5 mL/min was performed as follows: 0 min (25:75, A:B), 2 min (35:65, A:B) and 2.5 min (25:75, A:B) for a 1 min recovery to initial conditions.

### ***2.3.6 Dynamic changes of external and internal morphology during initial burst in vitro***

External and internal morphology of microspheres during the initial burst release period was observed by scanning electron microscopy (SEM). Microspheres were incubated in the release medium (PBST, pH7.4) at 37°C using the continuous monitoring system established before. After 0, 0.2, 1, 2, 5, 8, 12, 24, and 36 hr of incubation, microspheres were recovered from the release media and were immediately subjected to freeze-drying for 2 days to remove water. The dry samples were mounted onto aluminum specimen stubs using double-sided adhesive tape and fractured with a razor blade. The samples were then sputter coated with gold/palladium for analysis by a Hitachi S3200N scanning electron microscope (SEM) (Hitachi, Tokyo, Japan).

### ***2.3.7 Preparing a bodipy-dextran fluorescent probe***

Dextran was labeled with Bodipy™ FL in a similar method as previously described [22]. Bodipy™ FL hydrazide (1 mg/mL) was dissolved with Dextran (9-11 kDa) in 1 mL of dimethyl sulfoxide (DMSO) at a 1:1 molar ratio (dye : dextran). The mixture was incubated at 70°C for 22

hr. After cooling to room temperature and diluting with 19 mL water, the unreacted dye and DMSO were removed through 3 cycles of ultra-filtration and water dilution using an Amicon® Ultra centrifugal filter with 3kDa MWCO (Merck Millipore, Tullagreen, Ireland). The bodipy-dextran dye obtained after ultrafiltration and transferring with 4 mL water was lyophilized and stored at -20°C for future use. Conjugation was confirmed using UPLC size-exclusion chromatography (BEH SEC 125Å, Waters, Milford, MA, USA) with a gradient of methanol (solvent A) and ddH<sub>2</sub>O with 0.1% TFA (solvent B) at 50°C and a flow rate of 0.4 mL/min as follows: 0 min (5:95), 6 min (10:90), 8 min (15:85), 15 min (5:95). The concentration was determined by a fluorescence detector at excitation of 490 nm and emission of 525 nm.

### ***2.3.8 Dynamic changes of effective diffusion coefficients and characteristic times during in vitro initial burst***

Microspheres collected from continuous monitoring systems at various time points were incubated with bodipy-dextran conjugate in 0.25 mL of PBST for 30 min. Bodipy-dextran conjugate at 2.5 mg/mL was pre-warmed at 37 °C and followed by incubation at 37 °C for 30 min. Probe distribution in PLGA microspheres was imaged by confocal laser scanning microscopy (Nikon A1, Tokyo, Japan). An excitation of 488 nm was used, and emission was captured using a FITC filter set. Laser power was set at 4% with a gain of 80 for all images. Images were captured at the approximate center of the microspheres. Effective diffusion was calculated as in previous studies [4,26]. Pixel intensities ( $I$ ) at position ( $r$ ) of a particle of radius,  $a$ , were average and fit by the following equation of Fick's second law of diffusion:

$$\frac{I}{I_0} = \frac{C}{C_0} = \frac{1}{r/a} \sum_{n=0}^{\infty} \operatorname{erfc} \frac{(2n+1) - r/a}{\sqrt{D_{eff}t/a^2}} - \operatorname{erfc} \frac{(2n+1) + r/a}{\sqrt{D_{eff}t/a^2}}$$

where  $t$  is time exposed with dye,  $D_{eff}$  is the effective diffusion coefficient of the dye in the microspheres, and  $C$  and  $C_0$  are the dye concentration in the microspheres and at the surface, respectively ( $C/C_0$  is equivalent to  $I/I_0$ ). The data fitting was performed using a nonlinear least squares regression with MATLAB built-in function, “fitlm”, and using  $n=100$ . This analysis was performed at 0, 0.2, 1, 2, 8, 12, 24, and 36 hr of preincubation in the continuous monitoring system for Lupron Depot® (LD) and spray-dried microspheres—loaded and unloaded—made under the standard conditions. The analysis was also performed for other selected formulations at 0.2 and 24 hr. Additionally, a characteristic diffusion time was defined as:

$$\tau = \frac{R_{4,3}^2}{6D_{eff}}$$

where  $R_{4,3}$  is the volume-mean radius determined by laser diffraction previously [16]. This characteristic time was calculated only for 0.2 hr. The length of the primary release phase ( $t_{1^\circ}$ ) was normalized by the characteristic diffusion time to define a dimensionless burst time ( $\Theta_{1^\circ}$ ):

$$\Theta_{1^\circ} = \frac{t_{1^\circ}}{\tau}$$

### 2.3.9 *In vivo* release study

Leuprolide-microspheres suspended in 0.8 mL of diluent solution from Lupron Depot® were injected subcutaneously into male Sprague Dawley rats (9 weeks of age) at a dose of 3.5 mg/kg based on microsphere drug loading. Approximately 250  $\mu$ L of blood were withdrawn from the jugular vein under isoflurane anesthesia for 7 weeks and kept on ice. Blood collection time points included 0.25, 0.5, 1, 2, 4, 6, 8, 12, and 24 hr. At least 100  $\mu$ L of serum was separated after centrifuging at a speed of 8000 rpm at below 4 °C and was stored at below -80 °C until assay of the leuprolide concentration.

### ***2.3.10 Residual drug quantification after administration***

The drug remaining in the syringe after administration was determined by rinsing the components of the syringe with DCM to dissolve any residual microspheres. The residual leuprolide was determined by two-phase extraction of the DCM followed by UPLC analysis as done for drug loading determination.

### ***2.3.11 Serum sample analysis of leuprolide***

Serum leuprolide concentrations were analyzed using ultra-high-performance liquid chromatography coupled with single quadrupole mass spectrometry (UPLC-QDa-MS). Alarelin was used as an internal standard solution. 50  $\mu$ L of plasma was added into 0.5 mL tube. Then, 7.5  $\mu$ L of internal standard solution to samples. 10  $\mu$ L of acetic acid and 150  $\mu$ L methanol, 17.5  $\mu$ L water was added serially. The mixture solution was mixed and vortexed for 30 s and centrifuged at 4 °C at 10000rpm for 5 min. Supernatant was filtered by a 0.45  $\mu$ m filter and subjected to further analysis by UPLC-MS. A UPLC-MS (Acquity, Waters, Milford, MA, USA) composed of a BEH C18 column (Waters, Milford, MA, USA) and a UV detector with an absorption wavelength of 215. UPLC-MS conditions were set as follows: Flow rate is at 0.4 min/mL. Column temperature is 40 °C. Injection volume is 10  $\mu$ L. A gradient of H<sub>2</sub>O with 0.1% formic acid (solvent A) and acetonitrile with 0.1% formic acid (solvent B) was performed as follows: 0 min (95:5, A:B), 1 min (65:35, A:B) and 2.5 min (95:5, A:B) for a 1 min recovery to initial conditions. The mass detector was set in positive ion mode with a spray voltage of 0.8 kV and a cone voltage of 15 V. The m/z peak of the [+2] ion, corresponding to a m/z of 605.7, was used for quantification.

### ***2.3.12 Non-compartmental pharmacokinetic analysis and numerical deconvolution***

Non-compartmental pharmacokinetic parameters were obtained by analysis in MATLAB. AUC values were obtained by trapezoidal numerical integration of plasma concentrations. Numerical deconvolution was performed using a custom MATLAB code through a point-area technique [27]. The unit-dose input response that was used was based on a 2-compartment model using values published in literature for healthy Sprague Dawley rats [17]. The weights of the rats at the beginning of the study were used to estimate the volume of distribution throughout the study. To improve the resolution and the accuracy of the deconvolution, the data was interpolated to 1 data point per hour using a modified Akima interpolation (built-in MATLAB interpolation scheme). This resolution was selected because it had the lowest residuals when the experimental plasma curve was compared to the calculated plasma curve, which was obtained by re-convoluting the calculated absorption rate with the 2-compartment model. The absorption rate was used to estimate an absolute amount absorbed.

### ***2.3.13 Statistical analysis***

Statistical analysis was performed using Excel software. Data were expressed as the mean  $\pm$  standard deviation (SD) and statistical analysis was performed using an unpaired Student's t-test. Data were considered significantly distinct from controls at  $p < 0.05$ ,  $p < 0.01$  or  $p < 0.001$  was also given to reflect the degree of significance.

## 2.4 Results and discussion

The components of the spray dryer are illustrated in Figure 2-1A including: (1) the chamber for the atomization process during spray drying; (2) the cyclone for the separation of microparticles; (3) the product receiver; (4) the control panel for inlet airflow, inlet air temperature and cyclone air temperature; and (5) the pump to control fluid feed rates. As shown in Figure 2-1B, six processing factors were selected to identify the key influencing parameters during spray drying process based on previous process characterization and development [16]. For completeness, the leuprolide loading of all the formulations originally examined [16] is reproduced in the Supplementary Information (see Table S1). A “basic” formulation was established according to the criteria of drug loading (~10%) and gelatin loading (1.7%) and used as a standard condition. Process parameters were adjusted from this standard condition at various levels with no

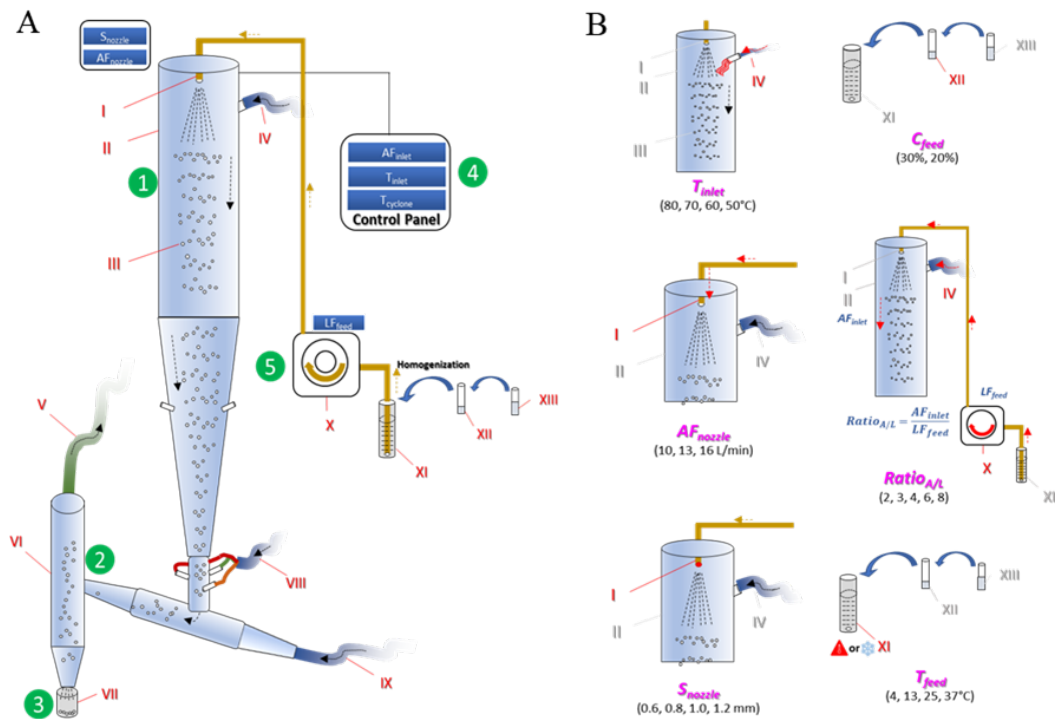


Figure 2-1. Diagram of the spray dryer components (A) including: the atomizing nozzle (I), drying/atomization chamber (II), microparticles (III), inlet air flow (IV), outlet air/exhaust (V), separation cyclone (VI), collection vessel (VII), cooling airflow (VIII), cyclone airflow (IX), liquid pump (X), feed emulsion (XI), polymer solution (XII), and aqueous phase with leuprolide and gelatin (XII). Parameters and values tested (B).

interactions between different parameters ( $T_{inlet} = 50\sim 80\text{ }^{\circ}\text{C}$ ,  $C_{feed} = 5\%\sim 30\%$ ,  $AF_{nozzle} = 7\sim 16\%$ ,  $Ratio_{A/L} = 2.0\sim 10.0$  and  $S_{nozzle} = 0.6\sim 1.2\text{ mm}$  and  $T_{feed} = 4\sim 37\text{ }^{\circ}\text{C}$ ). Microspheres prepared by the standard condition spray drying method were spherical,  $18.9\pm 6.5\text{ }\mu\text{m}$  in diameter (volume-average  $\pm$  S.D.) and had a drug loading of  $9.6\pm 0.4\%$  and a gelatin loading of  $1.68\pm 0.09\%$ . These characteristics are similar with commercial product Lupron Depot<sup>®</sup>, which had a  $15.5\pm 0.3\text{ }\mu\text{m}$  diameter,  $8.8\pm 0.2\%$  drug loading and  $1.69\pm 0.08\%$  gelatin loading based on amino acid analysis. Note that the drug loading in the microspheres of Lupron Depot<sup>®</sup> is reduced from  $\sim 10\%$  w/w because of the addition of mannitol to the surface of the microspheres before drying [14]. Therefore, only spray-dried mannitol-free microspheres with drug loading around 9~11% and gelatin loading around 1.4~1.8%, which would be highly similar in composition with commercial product, were selected for initial burst release characterization. Some formulations such as  $C_{feed}$  10% [drug loading ( $7.47\pm 0.04\%$ )],  $C_{feed}$  5% [drug loading ( $5.39\pm 0.01\%$ )],  $Ratio_{A/L}$  10.0 [drug loading ( $8.8\pm 0.2\%$ )] were not considered because their drug loading was out of the range of 9~11% to be compositionally equivalent with LD. In addition, an empty microsphere produced under standard conditions was used to examine the effect of the drug.

#### ***2.4.1 Evaluation of the initial burst by continuous monitoring system***

As shown in Figure S2-1, the custom-designed continuous monitoring system [3], which our group had previously used to study the initial burst release of octreotide acetate, was used to monitor the continuous release profiles of leuprolide-loaded microspheres during the first 24 hr in PBST at pH 7.4 and  $37\text{ }^{\circ}\text{C}$ . In Figure 2-2, the cumulative leuprolide release over the first 24 hr from Lupron Depot<sup>®</sup> and spray-dried biodegradable microspheres is shown. Experiments were performed twice for each formulation. Continuous release curves generated from both runs were virtually superimposable. As shown in Figure 2-2, generally, initial burst trends in all microspheres

were similar and followed two stages: (I) a primary (1°) release phase, which is characterized by immediate, rapid release stage (< ~0.5 hr) followed by diminishing release rates (~0.5-4 hr); and

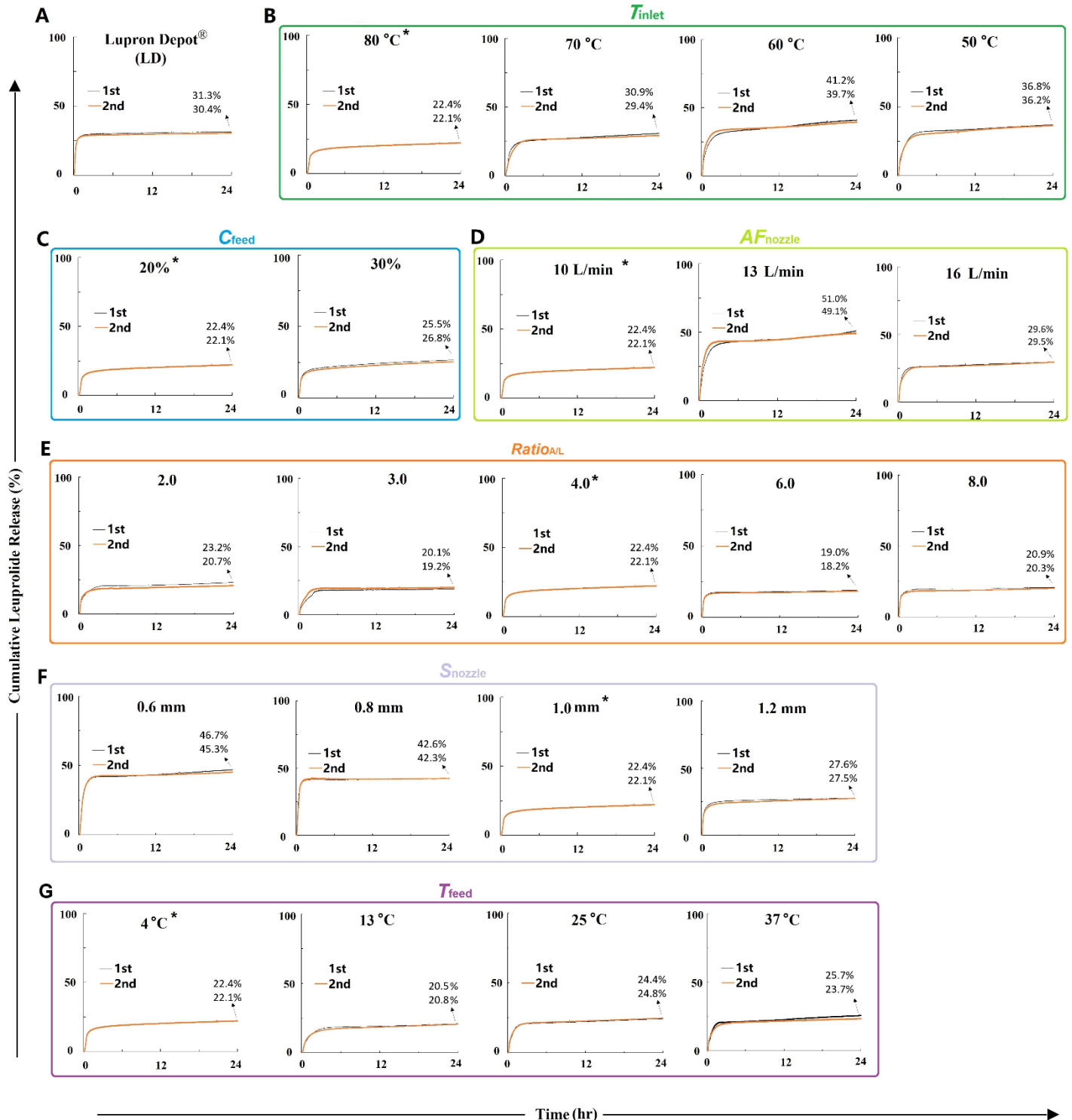


Figure 2-2. Continuous monitoring of initial burst release of Lupron Depot® and spray dried microspheres. Formulations include: Lupron Depot® (A);  $T_{inlet}$  80, 70, 60 and 50 °C (B);  $C_{feed}$  20% and 30% (C);  $A_{Fnozzle}$  10, 13, and 16 L/min (D);  $Ratio_{AL}$  2.0, 3.0, 4.0, 6.0, and 8.0 (E);  $S_{nozzle}$  0.6, 0.8, 1.0, and 1.2 mm (F);  $T_{feed}$  4, 13, 25, and 37 °C (G). Analysis of each formulation was performed in duplicate with 1<sup>st</sup> and 2<sup>nd</sup> runs indicated. \* refers to the standard condition, which is repeated in each panel to show the trend.

(II) a slow, secondary ( $2^\circ$ ) phase with near-constant release rates ( $> \sim 4$  hr). The drug release in the  $1^\circ$  phase represented a significant fraction ( $> 80\%$ ) of the release for the entire 24 hours. Not only did the extent of release differ between formulations, ranging from 20~50% of drug loading, but the duration of the burst release also changed depending on the process parameters of spray drying. While there were similarities between the initial phases of release for leuprolide in this system compared previous work with octreotide in a mildly acidic acetate buffer (pH 4) [3], octreotide showed a faster release ( $> 6$  hr) after an initial slow phase. Both octreotide and leuprolide have demonstrated interactions with low molecular weight, acid-capped PLGAs and absorption into the polymer phase [5], but the inclusion of gelatin in the formulations that are being investigated may provide additional binding for leuprolide and alter polymer behavior that will lead to slower release after the stage I.

Compared to in-house formulations, LD had a faster  $1^\circ$  phase ( $\sim 2$  hr) (Figure 2-2A). The 24-hr cumulative fraction released from LD was around 30~31%. Many spray-dried microspheres had lower 24-hr release compared to LD, but some parameters had significant effects on the release, leading to release exceeding 40% for some formulations. Both decreases of  $T_{inlet}$  (Figure 2-2B) and increasing  $AF_{nozzle}$  to 13 L/min (Figure 2-2D) lead to increases in the 24-hr release, which may be related to the rate and extent of droplet drying. 24-hr release of  $T_{inlet}$  80 °C formulation was around 22% and increased to around 36% when the temperature was decreased to 50°C, while  $AF_{nozzle}$  13 L/min caused a 24-hr release is close to 50%. Shown in Figure 2-2G, smaller nozzle sizes (0.6 mm and 0.8 mm) also resulted in higher initial burst with release reaching to 42% and 45%, respectively.  $C_{feed}$  (Figure 2-2C),  $Ratio_{AL}$  (Figure 2-2E) and  $T_{feed}$  (Figure 2-2G) had minor impacts on the 24-hr release. Both  $C_{feed}$  (20% and 30%) and the different levels of  $T_{feed}$  had a similar  $1^\circ$  phase and 24-h release is around 22~27%.  $Ratio_{AL}$ , which was thought to be an

important parameter for the initial burst release had similar 1° phase behaviors for all levels, and their 24-hr release was around 19~23%.

#### **2.4.2 Extraction of features from dynamic monitoring**

To characterize the extent and speed of the different phases of the initial burst, we adopted two methods. Further, features extracted from these methods could be used to help determine possible release mechanisms. For first method, as shown in Figure S2-2A, we defined 24-hr release as 100% burst release and determined the corresponding release times ( $t_{25\%,IBR}$ ,  $t_{50\%,IBR}$  and  $t_{75\%,IBR}$ ) for 25%, 50% and 75% burst release, respectively, which could allow us to compare the relative lengths of the different stages of the initial burst release. The results can be seen in Table 2-1 (Nearest-Point Estimation). Overall, the Lupron Depot and spray-dried particles had  $t_{25\%,IBR}$  values around 0.2~0.5 hr,  $t_{50\%,IBR}$  from 0.2 to 0.9 hr, and  $t_{75\%,IBR}$  of about 0.5~2 hr. Lupron Depot® had the fastest initial burst with a  $t_{25\%,IBR}$ ,  $t_{50\%,IBR}$  and  $t_{75\%,IBR}$  of 0.2 hr, 0.28 hr, and 0.46 hr, respectively. Most spray-dried microspheres had more prolonged initial bursts. About half of the spray-dried formulations displayed higher  $t_{25\%,IBR}$  values that within 0.1 hr of Lupron Depot. Higher  $T_{inlet}$  (especially for 70 °C) and lower  $T_{feed}$  or  $AF_{nozzle}$  caused higher  $t_{25\%,IBR}$  levels. All microspheres made by spray drying displayed an obvious prolongation of the initial burst show primarily through  $t_{50\%,IBR}$  and  $t_{75\%,IBR}$  values.  $T_{inlet}$  below 80°C caused higher  $t_{50\%,IBR}$ —close to 0.8 hr. Higher  $C_{feed}$  (PLGA 30%) led to the lower  $t_{50\%,IBR}$  (0.4 hr). Lower residence time in the drying chamber by higher  $AF_{nozzle}$  (16.0 L/min) and  $Ratio_{A/L}$  (6 and 8) accelerated the initial burst somewhat and yielded lower  $t_{50\%,IBR}$  and  $t_{75\%,IBR}$ . . All  $T_{inlet}$  formulations had similar  $t_{75\%,IBR}$  values. While midway through was faster, higher  $C_{feed}$  (PLGA 30%) resulted in the longer  $t_{75\%,IBR}$ . While  $S_{Nozzle}$  affected these times, no obvious relationship appeared. Higher  $T_{feed}$  with the exception of the standard condition of 4°C shorten the burst length measured by  $t_{50\%,IBR}$  and  $t_{75\%,IBR}$ .

For the second method, we analyzed the relative release rates of the different formulations and the commercial product. Concentration-time profiles from the custom continuous monitoring system were used to calculate the release rate. In a custom MATLAB code, the average rate was determined for every 120 time points (2 min) through a linear regression of the points and used to represent the rate at the midpoint of the interval. Several features were extracted from the normalized release rate versus time profiles, as shown in Figure S2-2B. The first feature, the maximum release rate, appeared to be somewhat variable, leading to only significantly higher maximum release rates for  $Ratio_{A/L}$  2.0,  $Ratio_{A/L}$  8.0 and  $S_{nozzle}$  0.6 mm when compared to the basic formulation. No clear trend was observed for this feature when comparing different levels of spray drying parameters except for the airflow in nozzle which may show increasing maximum rate with increasing flow rate (Table 2-1, Numerical-Based Derivative Analysis) Additionally, Lupron Depot<sup>®</sup> appeared to have a higher maximum rate but was not a significant difference when compared to basic formulation. Since the maximum rate occurred at similar times (~12-15 min) into release, it could be expected that these values would show similar rank order to  $t_{25\%}$ ,  $IBR$ , but no obvious similarities were found between these values or any other estimated times. The next feature, the length of the 1<sup>o</sup> release phase ( $t_{1^o}$ ), was determined by examining the release rate in the last 5 hr of testing when the release was in the 2<sup>o</sup> phase and the rate of release was nearly constant. The standard deviation of this 2<sup>o</sup> phase rate was used to construct a boundary between the rates of the 1<sup>o</sup> and 2<sup>o</sup> release phases. After smoothing the release rate data using gaussian-weighted averaging, the time at which the rate dropped below this boundary line was determined and used as  $t_{1^o}$  (method shown in Figure S2-2B, upper right). Additionally, the cumulative release at this time was used for the 1<sup>o</sup> phase release fraction. No significant differences were observed in the time until the end of the 1<sup>o</sup> phase except for when decreasing the nozzle size from 1.0 mm

to 0.8 mm. However, Lupron Depot® appeared to last shorter than most of the spray dried formulations. Unsurprisingly, the time calculated for the beginning of the 2° phase from release rates was similar in rank order to the  $t_{75\%}$ ,  $IBR$  estimate, although the exact magnitude differed greatly. The 2° phase release rate of Lupron Depot® was significantly lower than a majority of the spray dried formulations while the rate amongst spray dried formulations were relatively similar. For the 1° phase cumulative release fraction, the calculation was relatively consistent when testing each formulation, leading to comparisons with higher significance. Lupron Depot® had a significantly difference 1° phase release compared to most of the spray dried formulations, excluding  $T_{inlet}$  50°C and 60°C,  $AF_{nozzle}$  16.0 L/min and  $T_{feed}$  13°C. With increasing  $T_{inlet}$ , the 1° phase release tended to increase until it reached a maximum. Other parameters did not have any clear trends although  $AF_{nozzle}$  13.0 L/min and decreasing  $S_{nozzle}$  lead to significantly higher 1° phase release. Another parameter, the rate decay constant, was extracted based on the observation that the rates appeared to decay exponentially in the period between the maximum rate and  $t_{1^\circ}$ . The exponential decay behavior could suggest a first-order rate-controlling mechanism such as desorption from the polymer after initial peak in the release rates. This constant, which was determined by a log-linear fit of this interval (Figure S2-2B, lower right), seemed to mirror changes in the maximum rate for most cases. This can be expected since the terminal rate and time to the end of the burst period are relatively the same between most spray dried formulations and therefore the maximum rate would provide leverage in changing the decay. In addition, the similarity in the timescales for the 1° release phase suggests a mechanism like surface healing, which could be similar between particles with similar diameters and pore sizes as critical, for dictating how the rapid release is terminated.

#### ***2.4.3 Measurements by single-point sample-and-separate method***

While the continuous monitoring provides higher resolution and better precision for determining relative release rates, the use of this system has not been investigated for leuprolide, so the sample-and-separate method was used as a standard method with which to compare. Sample-and-separate is a conventional method for the determining both long-term and initial burst release of leuprolide [4,5,14,24,28] and other peptide/proteins [29–32] from PLGA microspheres. The 24-hr cumulative release from Lupron Depot<sup>®</sup> (LD) and all spray-dried formulations, which had been assessed in the continuous monitoring, were evaluated using this method. The results of this study are shown in Table 2-1 (Endpoint). All spray-dried formulations showed lower release at 24 hr than LD (29.52.24%) with several showing significant decreases. LD also appeared to show higher variability in this measurement than in-house-prepared formulations. Of the spray-dried formulations,  $AF_{nozzle}$  13.0 L/min had the highest burst release ( $27.5\pm 0.55\%$ ), which is consistent in its rank order in the continuous monitoring method, and significantly higher than the standard conditions (basic formulation), but this formulation showed much higher release at the end of the continuous monitoring study than this study.  $T_{feed}$  25°C had the lowest 24-hr fraction released ( $14.7\pm 0.29\%$ ), which was significantly lower than the standard condition, but this value was also significantly lower than the continuous monitoring release (less than 2/3). In general, decreasing  $T_{inlet}$ ,  $T_{feed}$ , and  $S_{nozzle}$  tended to lead to increases in the fraction released at 24 hr, while decreasing  $Ratio_{A/L}$  and  $C_{feed}$  lead to decreases.  $AF_{nozzle}$  appeared to have positive correlation with the release, but the relationship is not as clear.

Table 2-1. Characteristics of Release Profiles.

Formulation	Nearest-Point Estimation			Numerical Derivative-Based Analysis					Endpoint	
	t <sub>25%,IBR</sub> (hr)	t <sub>50%,IBR</sub> (hr)	t <sub>75%,IBR</sub> (hr)	1°Burst Release (%)	t <sub>1°</sub> (hr)	Max Rate (% hr <sup>-1</sup> )	2° phase Rate Rate (% hr <sup>-1</sup> ) x10 <sup>2</sup>	Rate Decay Constant (hr <sup>-1</sup> )	24-hr Continuous (%)	24-hr Sample-and-Separate (%)
<i>Lupron Depot</i> <sup>®</sup>	0.20 (0.02)	0.28 (0.02)	0.46 (0.02)	29.23 (0.43)	2.17 (0.42)	106.6 (6.6)	4.8 (0.4)	2.69 (0.55)	30.87 (0.47)	29.53 (2.25)
<i>Basic/Standard Formulation</i>	0.35 (0.01)	0.52 (0.02)	1.74 (0)	18.19 (0.06)	3.33 (0.22)	36.6 (0.9)	15.1 (0.9)	1.09 (0.13)	22.25 (0.16)	17.41 (0.19)
<i>T<sub>inlet</sub> 70°C</i>	0.44 (0.01)	0.78 (0.13)	1.78 (0.08)	25.75 (0.45)	3.45 (0.35)	37.8 (6.2)	19.8 (2.9)	1.22 (0.16)	30.16 (0.74)	20.44 (0.02)
<i>T<sub>inlet</sub> 60°C</i>	0.29 (0.04)	0.67 (0.18)	2.08 (0.65)	32.48 (0.93)	2.97 (0.18)	68.0 (16.6)	33.9 (0.8)	1.28 (0.15)	40.43 (0.43)	20.80 (0.41)
<i>T<sub>inlet</sub> 50°C</i>	0.34 (0.03)	0.85 (0.03)	1.92 (0.08)	30.84 (1.05)	3.68 (0.03)	49.4 (2.2)	21.3 (0.0)	1.28 (0.01)	26.12 (0.29)	19.89 (0.36)
<i>C<sub>feed</sub> 30%</i>	0.26 (0.01)	0.44 (0.01)	2.05 (0.11)	20.86 (0.26)	3.93 (0.62)	53.6 (3.8)	19.2 (0.5)	1.00 (0.19)	50.06 (0.96)	22.00 (0.53)
<i>AF<sub>nozzle</sub> 13 L/min</i>	0.36 (0.01)	0.64 (0.23)	1.62 (0.43)	41.69 (0.82)	2.72 (0.23)	63.5 (9.6)	52.9 (19.0)	1.47 (0.27)	30.25 (0.65)	27.46 (0.55)
<i>AF<sub>nozzle</sub> 16 L/min</i>	0.26 (0.01)	0.45 (0.02)	1.14 (0.19)	25.58 (0.17)	2.48 (0.27)	71.8 (8.2)	16.5 (4.0)	1.90 (0.45)	21.95 (1.25)	21.49 (0.14)
<i>Ratio<sub>NL</sub> 2</i>	0.25 (0.01)	0.49 (0.12)	1.41 (0.32)	19.33 (1.42)	3.10 (0.42)	49.4 (1.1)	15.3 (4.1)	1.13 (0.22)	20.58 (0.29)	15.58 (0.16)
<i>Ratio<sub>NL</sub> 3</i>	0.34 (0.05)	0.86 (0.21)	1.76 (0.45)	18.51 (0.81)	3.10 (0.08)	30.6 (9.6)	7.3 (0.9)	1.09 (0.13)	19.65 (0.45)	18.25 (0.17)
<i>Ratio<sub>NL</sub> 6</i>	0.22 (0.01)	0.29 (0.01)	0.49 (0.01)	17.06 (0.27)	1.98 (0.03)	63.3 (10.7)	10.3 (0.1)	2.36 (0.04)	18.59 (0.39)	18.67 (0.62)
<i>Ratio<sub>NL</sub> 8</i>	0.20 (0.01)	0.30 (0.01)	0.59 (0.01)	18.82 (0.86)	2.27 (0.28)	61.4 (2.6)	11.1 (2.8)	2.05 (0.27)	20.58 (0.29)	20.31 (1.48)
<i>S<sub>nozzle</sub> 0.6 mm</i>	0.32 (0.01)	0.53 (0.01)	1.03 (0.06)	41.91 (0.38)	2.35 (0.20)	73.6 (3.2)	25.9 (3.1)	1.96 (0.13)	46.00 (0.70)	20.79 (0.46)
<i>S<sub>nozzle</sub> 1.2 mm</i>	0.22 (0)	0.34 (0.01)	0.87 (0.13)	24.38 (0.62)	2.88 (0.03)	78.0 (12.4)	13.0 (3.4)	0.82 (0.05)	29.72 (2.08)	15.43 (0.19)
<i>T<sub>feed</sub> 13°C</i>	0.38 (0.01)	0.92 (0.08)	2.37 (0.17)	20.04 (3.04)	3.35 (1.00)	46.8 (23.9)	20.2 (2.1)	1.16 (0.34)	20.68 (0.15)	16.05 (0.34)
<i>T<sub>feed</sub> 25°C</i>	0.28 (0.02)	0.66 (0.03)	1.43 (0.11)	21.13 (0.23)	2.92 (0.40)	46.8 (6.5)	17.3 (0.4)	1.45 (0.12)	24.64 (0.21)	14.67 (0.29)
<i>T<sub>feed</sub> 37°C</i>	0.27 (0.01)	0.68 (0.02)	1.45 (0.07)	20.36 (0.40)	2.47 (0.52)	49.9 (7.5)	16.4 (3.6)	1.74 (0.38)	24.70 (1.00)	16.50 (0.17)

Values are shown as mean (SEM) and are calculated from release curves (n=2)

### 2.4.4 Comparison of initial burst by continuous monitoring and sample-and-separate methods

During the initial burst release period, drug release at 24 hr was determined by two types of release systems as mentioned above. Generally, 24-hr release results determined by two systems deviate from each other for a majority of spray-dried microspheres while Lupron Depot® showed excellent agreement between the two methods (Figure 2-3). Because leuprolide acetate as a water-

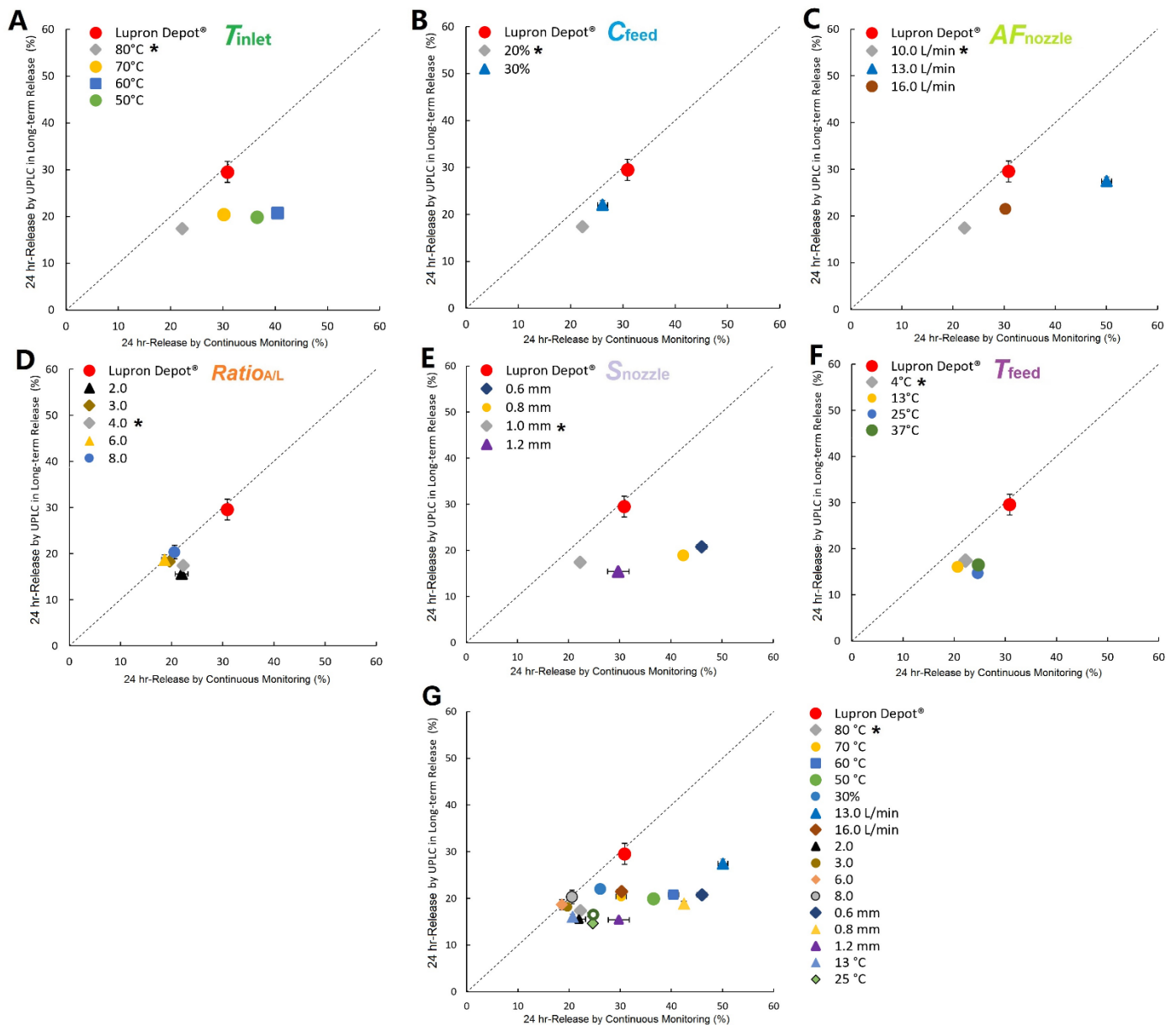


Figure 2-3. Comparison of 24-h release of leuprolide from two determination systems under altered  $T_{inlet}$  (A),  $C_{feed}$  (B),  $AF_{nozzle}$  (C),  $Ratio_{A/L}$  (D),  $S_{nozzle}$  (E) and  $T_{feed}$  (F). General comparison (G) was summarized. \* represents the basic formulation condition. Error bars show  $\pm SE$ .

soluble drug has high solubility ( $\gg 10$  mg/mL) in PBS, both determination systems easily meet sink conditions. It should be noted that the continuous monitoring system was 20 times more dilute than the tube incubation for sample-and-separate. The extent of the difference between the burst values for the two methods can be seen from the degree of deviation from a central line in Figure 2-3.  $T_{inlet}$  and  $S_{nozzle}$  were influential on the deviation from the central line (Figure 2-3A and E) and increases resulted lower deviations with the standard condition ( $T_{inlet}$  80°C,  $S_{nozzle}$  1.0 mm) showing the best agreement between the two methods.  $AF_{nozzle}$  had some impact on the deviation in Figure 2-3C. Noteworthy,  $AF_{nozzle}$  13.0 L/min formulation induced the significant deviation from the central line, but the effect of other values was more muted. Overall, the general influence on the deviation was obvious for three process parameters ( $T_{inlet}$ ,  $AF_{nozzle}$  and  $S_{nozzle}$ ) while, other variables had less impact on the deviation. The rank order of the effect on this deviation from the greatest to the weakest was as follows:  $AF_{nozzle} > S_{nozzle} > T_{inlet} > T_{feed} \approx Ratio_{A/L} > C_{feed}$ . Additionally, deviation between these methods appears to occur when release from the continuous monitoring system exceeds 20%, while the conventional method excluding Lupron Depot<sup>®</sup> plateaus at this value. External and internal morphology change possibly played an important role in the deviation during the initial burst. Exploration on dynamic morphological changes during initial burst is helpful to understand these initial burst phenomena.

#### **2.4.5 Dynamic changes of external and internal morphology during initial burst**

Because of the similarity of the compositions between microspheres, the interactions between the polymer and drug of the different formulations may be expected to be similar amongst spray-dried particles. Variation in release behavior and extent could be related to structural differences resulting during microsphere formation (changes in residence times, evaporation rates, etc.) and healing during release, since the high water-solubility of leuprolide can facilitate release

through an internal aqueous pore network. Scanning electron microscopy was used to examine structural changes throughout release. After microspheres were incubated for different time

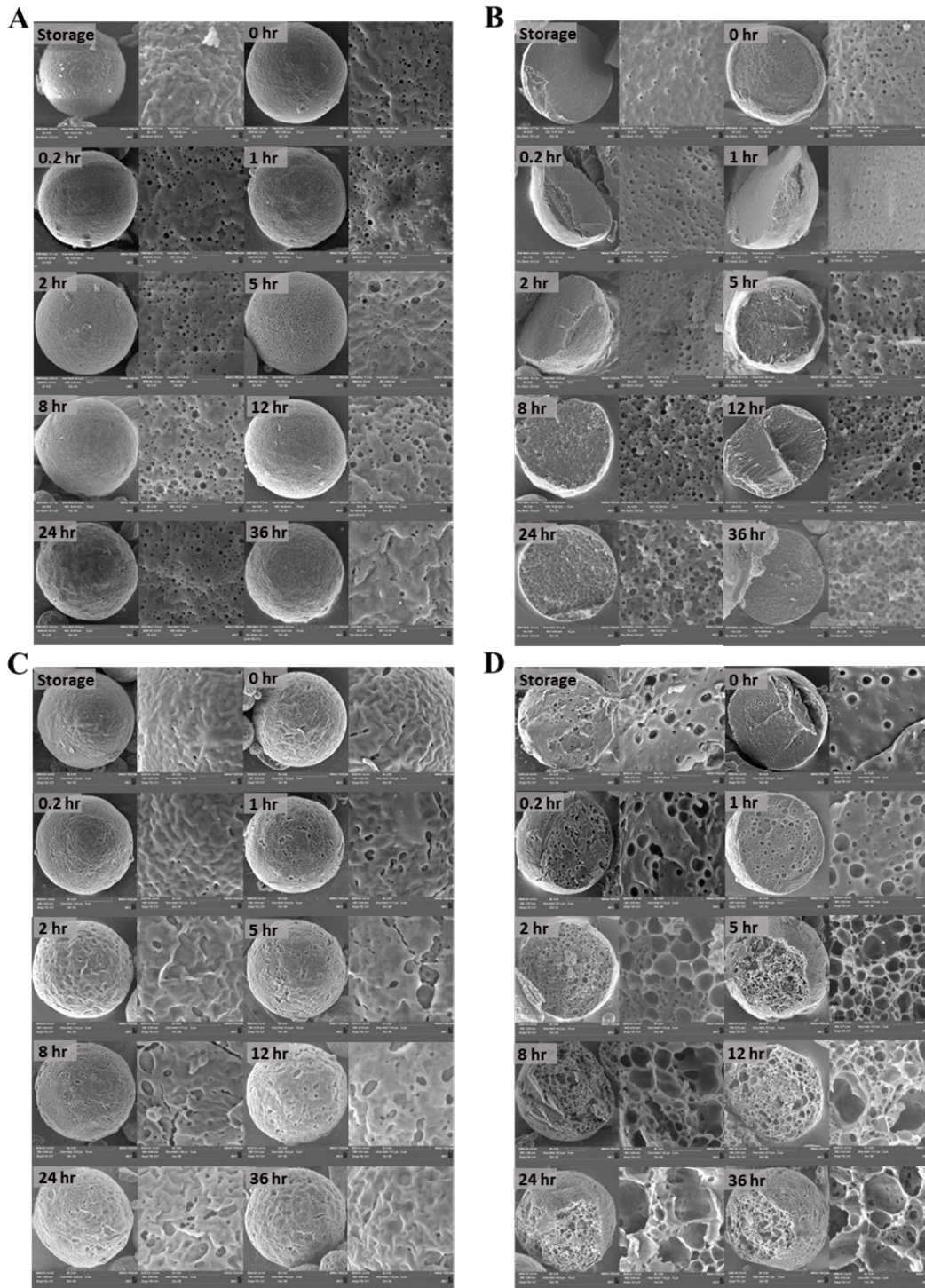


Figure 2-4. External morphology (A, C) and internal structure (B, D) of Lupron Depot® (A,B) and standard condition spray-dried microspheres (C,D) from storage and after 0, 0.2, 1, 2, 5, 8, 12, 24, and 36 hours of incubation in the continuous monitoring system. Left image shows full microsphere. Right shows high magnification (field view = 7.2  $\mu\text{m}$ )

periods (0, 0.2, 1, 2, 5, 8, 12, 24 and 36 hr) in the continuous monitoring system, their external and internal morphology was observed using SEM. In addition, these microspheres were examined prior to incubation or under “storage” conditions. In contrast to these storage condition observations, 0 hr were microspheres that were immediately collected after adding to the continuous monitoring system. SEM results of LD and typical spray-dried microspheres were shown in Figure 2-4. Under storage conditions for LD (Figure 2-4A), the pore number on the surface was low and pore sizes were small (20~100 nm). After exposure to release media, the pore number increased, and pore size became larger until 12 hr (300~500 nm). After 12 hr, pore numbers decreased dramatically and began to close over time and demonstrated the self-healing process that had been found shown in previous studies [3,22,33–35]. Observations of the internal structure during this period have not been observed before though. Under the storage condition (Figure 2-4B), the internal pore number and pore sizes were similar with those on the surface and gradually increased over time but did not show an obvious reduction in porosity later like the surface did. At 36 hr, the pore size increased to about 300~600 nm—similar to the size on the surface before healing began. The observation further deepened our understanding of the self-healing process. Self-healing of pores mainly occurred on the surface but not in the internal region. Driven likely by surface tension [35], internal pores appear to heal by becoming more circular, but swelling of the polymer may prevent size reduction. The density of microspheres made by the solvent evaporation method like LD [13] might be more uniform than spray-dried microspheres. Spray-dried microspheres had structure profiles that were distinct compared to LD. For the standard formulation, the structure on the surface was relatively smooth under storage (Figure 2-4C). The initial pore size present internally was larger than that in LD, close to 500-700 nm (Figure 2-4D). At the start of incubation, there were minor changes on the surface of microspheres

over time. The surface pores were superficial and irregular/non-circular pores compared to LD as well as fewer in number. Spray-dried microspheres also showed a denser “skin” layer in the initial 4 hours with fewer and smaller pores closer to the particle surface (Figure 2-4D). However, internal pore size and number increased gradually over time. From 1 hr to 2 hr, there was a sudden increase in internal pore number likely due to swelling. At the end of initial burst (24 hr and 36 hr), pore sizes were around approximately 3  $\mu\text{m}$ . All other spray-dried formulations evaluated during the initial burst period showed similar structural changes as the standard condition (Figure S2-3 through Figure S2-8) except when the  $C_{feed}$  was increased to 30% (Figure S2-7A, B).  $C_{feed}$  30% appeared to be denser and had smaller internal pore size growth than other formulations. The structural changes of this formulation may be most similar to the commercial product, LD. Empty/unloaded spray-dried microspheres were fabricated based on the composition and condition of basic formulation. The external morphology was relatively intact over time (Figure S2-3A) while large internal cavities and pores appeared after 0.2 to 1 hour (Figure S2-3B). While pore size did increase gradually, pore numbers did not increase obviously, which may be attributed to swelling in the absence of mass loss from drug release. The onset time of structural changes in microsphere formulations during the initial burst release period is different for some spray dried microspheres and related to process parameters. The decrease of  $T_{inlet}$ ,  $C_{feed}$ ,  $S_{nozzle}$  and increase of  $AF_{nozzle}$  resulted in earlier increases in internal porosity, possibly due to less dense matrices.

#### ***2.4.6 Dynamic changes in effective diffusion of bodipy-dextran probe through aqueous pore networks***

To further examine structural changes throughout the release period, the penetration of a dextran fluorescent dye was used to obtain a measure of microsphere permeability when exposed to the release media. The dextran-bodipy conjugate was originally expected to be capable of only

penetrating the pores of the polymer based on previous studies with aliphatic ester end-capped PLGA microspheres whose water uptake are initially less than a few percent water [22]. The diffusivity of a probe was measured through confocal imaging of individual microspheres and the extent of probe penetration determined through pixel intensity. Images were captured at several time points for Lupron Depot® (LD) and loaded and unloaded spray-dried particles made under standard conditions (labeled as basic and empty). LD showed an apparent increase in dye penetration after 1 hr of preincubation that dropped later in the study (Figure 2-5A). This initial spike in the diffusion of the pore probe at 1 hr was calculated as an effective diffusion coefficient of  $2.1 \times 10^{-11} \text{ cm}^2/\text{s}$  and then significantly decreased 54.6% to  $9.55 \times 10^{-12} \text{ cm}^2/\text{s}$  without any significant changes for the remainder of the study (Figure 2-6A). The initial spike in diffusivity suggests an initial phase of pore opening although the change was not statistically significant while the decrease is consistent with previous healing hypothesis and SEM images appear to also show healing, but noticeable changes are not observed until later in the study (Figure 2-4A, B). While the diffusivity of the probe through LD at 24 hours was higher than the effective diffusion coefficient measured for Bodipy FL at the same time point in a comparable leuprolide formulation [4], polymer-phase diffusion or less extensive healing from increased swelling in the highly agitated continuous monitoring might have led to a higher extent of diffusion measured at the plateau since it was within an order of magnitude. The distribution and shape of the dye penetration may also reveal whether the diffusion of high-molecular weight dye through pores is rate-controlling, or the extensive swelling caused penetration of the dextran dye into the polymer phase. Some evidence of microporous diffusion for LD can be seen at 8 hr (Figure 2-5A-8) by a circular

region of dye penetration, which is typical of pore structures [3,22,35]. More homogenous diffusion in earlier time points suggest polymer phase or nanoporous diffusion (Figure 2-5A-0 to A-1). Diffusion through nanoporous structures would be consistent with the internal and external

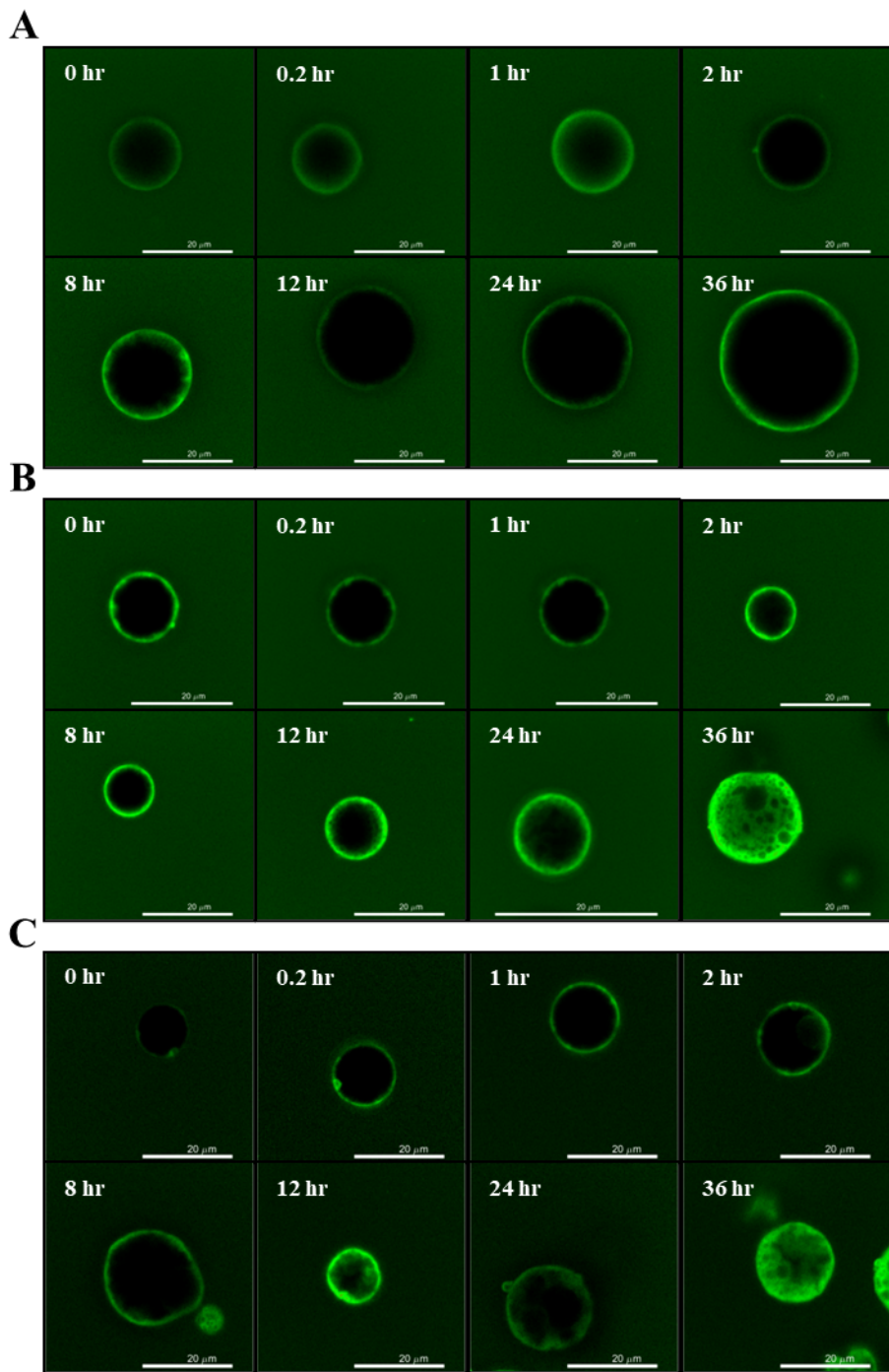


Figure 2-5. Confocal images of dye penetration of bodipy-dextran in Lupron Depot<sup>®</sup> (A) and spray-dried microspheres made under standard conditions—loaded (B) and unloaded (C)—after 30 min incubation at 37°C with 0 (A), 0.2 (B), 1 (C), 2 (D), 8 (E), 12 (F), 24 (G) or 36 hr (H) of pre-incubation in the continuous monitoring

morphology of LD (Figure 2-4A, B). Additionally, unconjugated dye showed a similar, but more pronounced, behavior over time for LD, and the diffusion coefficients measured were on average higher than the dextran-dye as expected (Figure S2-11A). The higher diffusion coefficient of the free bodipy in LD was likely still a measure of the access to the pore network as the drop in early diffusivity is unlikely to coincide in a change in polymer phase diffusion.

Both loaded and unloaded spray dried microspheres made under the basic conditions showed significantly lower probe diffusion initially compared to LD based on both probe penetration (Figure 2-5B, C) and calculated diffusion coefficients. Loaded microspheres also showed an increase in the measured diffusion coefficient similar to LD, but the decline from 1 to 2 hr was smaller in magnitude (26.2%) and not statistically significantly, before continuing to increase to similar levels as LD. In addition, loaded spray dried microspheres showed significantly higher initial probe diffusion compared to unloaded, which may suggest the role of osmotic pressure and/or changes in polymer stability caused by polymer-peptide interactions (i.e., changes in pore opening/closing kinetics). The increases in probe diffusion seem to coincide with increases in internal pore sizes, which are observed through SEM (Figure 2-4D and Figure S2-3B). Increases in internal pore sizes may be the result of residual solvent leaching, which may leave voids, or swelling as the polymer expands faster than it can relax. Larger particles were observed in confocal imaging as the study progressed, although the exact extent has not been evaluated. Despite increases in effective diffusion and increasing internal pore sizes of spray dried formulations, release remained relatively steady during the 2<sup>o</sup> release period, which strongly suggests that aqueous diffusion through a pore network is not the primary controlling mechanism after the 1<sup>o</sup> phase. In addition, at 36 hours, the regions of dye penetration are more irregular with circular occlusions. This distribution of dye demonstrates that the effective diffusion measured might be

the result of increased void volume of the swollen polymer, which may allow polymer phase diffusion of the high molecular-weight, water-soluble dye. Conversely, the circular surface regions at earlier time points (Figure 2-5B, C) are consistent with diffusion through the microporous structure of the spray-dried particles. Further, unlike LD, the spray-dried formulation showed an

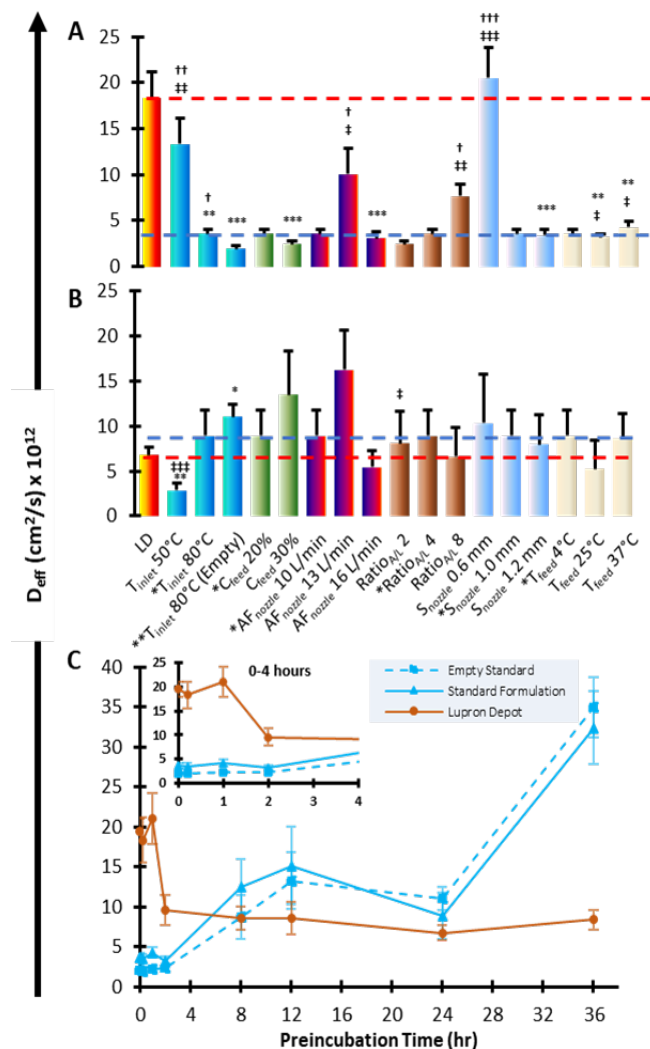


Figure 2-6. Effective diffusion of bodipy-dextran probe after preincubation in continuous monitoring (A-C); diffusion of spray-dried formulations after 0.2 hr (A) and 24 hr (B) preincubation (\*  $p < 0.05$ ; \*\*  $p < 0.01$ ; \*\*\*  $p < 0.001$  compared to LD; † and ‡ used when comparing to loaded and unloaded standard formulation, respectively). Changes in diffusion coefficient of LD compared to loaded and unloaded spray-dried standards over release period (C) and expanded over first 4 hr (C-inset). Error bars represent SEM ( $n=8-10$ ). \* and \*\* in labels represent loaded and unloaded standards.

early three-fold increase in diffusivity of the unconjugated dye around 2 hr (Figure S2-11A) that coincided with swelling in SEM images without the analogous increase in dextran-dye diffusion. Previous studies have shown that diffusion through hygroscopic, polymer membranes increased with smaller hydrodynamic radii and increasing swelling until it reaches unity with aqueous diffusion [36]. Therefore, spray-dried particles appeared to swell to the extent in early time points that made polymer phase diffusion additive to aqueous diffusion for the low molecular-weight free dye, while significant polymer phase diffusion of the high molecular-weight dextran pore probe did not occur until the polymer swells extensively around 36 hours. Although changes in diffusion

occur through the study period, interactions between leuprolide and the polymer or depletion of drug in surface-connected pores may limit release from aqueous pore diffusion after the first 2-4 hours.

The effective diffusion of the probe was measured at 0.2 hr for other spray dried formulations ( $T_{\text{inlet}}$  50 °C,  $C_{\text{feed}}$  30%,  $AF_{\text{nozzle}}$  13.0 and 16.0 L/min,  $Ratio_{A/L}$  2.0 and 8.0,  $S_{\text{nozzle}}$  0.6 and 1.2 mm, and  $T_{\text{feed}}$  25°C and 37 °C) through the probe penetration as well (Figure S2-9). While the peak in diffusivity appeared to occur at 1 hour for both LD and the basic formulation, 0.2 hr was selected for observation because the difference between these two time points was not significant and the maximum release rate determined through continuous monitoring release occurred closer to 0.2 hour for almost all formulations. More than half the tested spray dried formulations ( $C_{\text{feed}}$  30%,  $AF_{\text{nozzle}}$  16.0 L/min,  $Ratio_{A/L}$  2.0,  $S_{\text{nozzle}}$  1.2 mm, and all changes in  $T_{\text{feed}}$ ) showed significantly lower effective diffusion of the probe compared to LD (Figure 2-6A). In general, those that did not show significant decreases and those with higher diffusivity also showed higher 1° phase release. The diffusivity of the probe was also measured for these formulations at 24 hr (Figure 2-6B). 24 hr was selected since this was the typical release period for characterizing the initial burst in *in vitro* tests even though more significant differences between the commercial product and the spray dried formulations existed at 36 hr (Figure 2-6C). The only formulations that showed significant differences from LD were  $T_{\text{inlet}}$  50 °C and unloaded basic microspheres, which showed a lower and higher effective diffusion, respectively. There were no significant differences between loaded microspheres. The measurements of effective diffusion coefficients at this time point had high variability, which made evaluating changes difficult.

#### ***2.4.7 Correlations between in vitro release and probe diffusion***

To confirm the possibility of diffusion as a rate-controlling mechanism during the 1° phase, the diffusion study was related to features extracted from release. In general, measurements of diffusion were in decent agreement with the extent of the 1° phase release that was calculated from the continuous monitoring system (Figure 2-7A). Circular pore-like occlusions at 0.2 hr for  $T_{inlet} 50^{\circ}C$ ,  $AF_{nozzle} 13 L/min$ , and  $S_{nozzle} 0.6 mm$  strongly suggest the probe is distributed into the polymer phase (Figure S2-9A, C, G). In addition, the depth of the penetration was clearly related to the apparent porosity shown in SEM images of the internal structure. For example, using a nozzle size of 0.6 mm created microspheres that were highly porous at 0.2 hr (Figure S2-6B) with deep dye penetration (Figure S2-9G) and the highest effective diffusion (Figure 2-6A) while the dye was localized to the surface of microspheres in formulations like  $T_{feed} 25^{\circ}C$  (Figure S2-9I), which were denser at the same time point (Figure S2-8B), leading to a low effective diffusion. All three formulations with apparent polymer phase diffusion showed high porosity in SEM that began at this time point and fast effective diffusion and appeared to demonstrate that rapid swelling could lead to void formation in the matrix and increased matrix diffusion.

To take into the differences in the diffusion path length, the volume mean radius of the particles was incorporated into a characteristic diffusion time,  $\tau$ . Use of characteristic time improved the correlation to the 1° phase release (Figure 2-7B) (excludes  $C_{feed} 30\%$ ) and the spread of the data. In addition, the characteristic diffusion time displayed a power law relationship to the 1° phase release and showed increasing fraction released when the characteristic time was similar in magnitude to the length of the 1° phase. The value calculated  $C_{feed} 30\%$  suggests that a plateau in 1° phase release may occur with increasing diffusion time. In other words, when the typical time to diffuse out of microspheres is longer, it is less likely to contribute to this phase. Based on this phenomenon,  $t_{1^{\circ}}$  was normalized to the characteristic diffusion time to give rise to a new

dimensionless 1° phase duration ( $\Theta_{1^\circ}$ ). The high correlation of  $\Theta_{1^\circ}$  to the 1° phase extent reinforces that the relationship between probe effective diffusivity and the 1° phase release is dependent on how long the burst occurs (Figure 2-7C). Above unity, leuprolide has sufficient time to diffuse out of the matrix and could be limited by the amount of leuprolide that is unbound to long PLGA chains. The hypothesized leuprolide fraction, unbound or bound to very low MW PLGA chains,

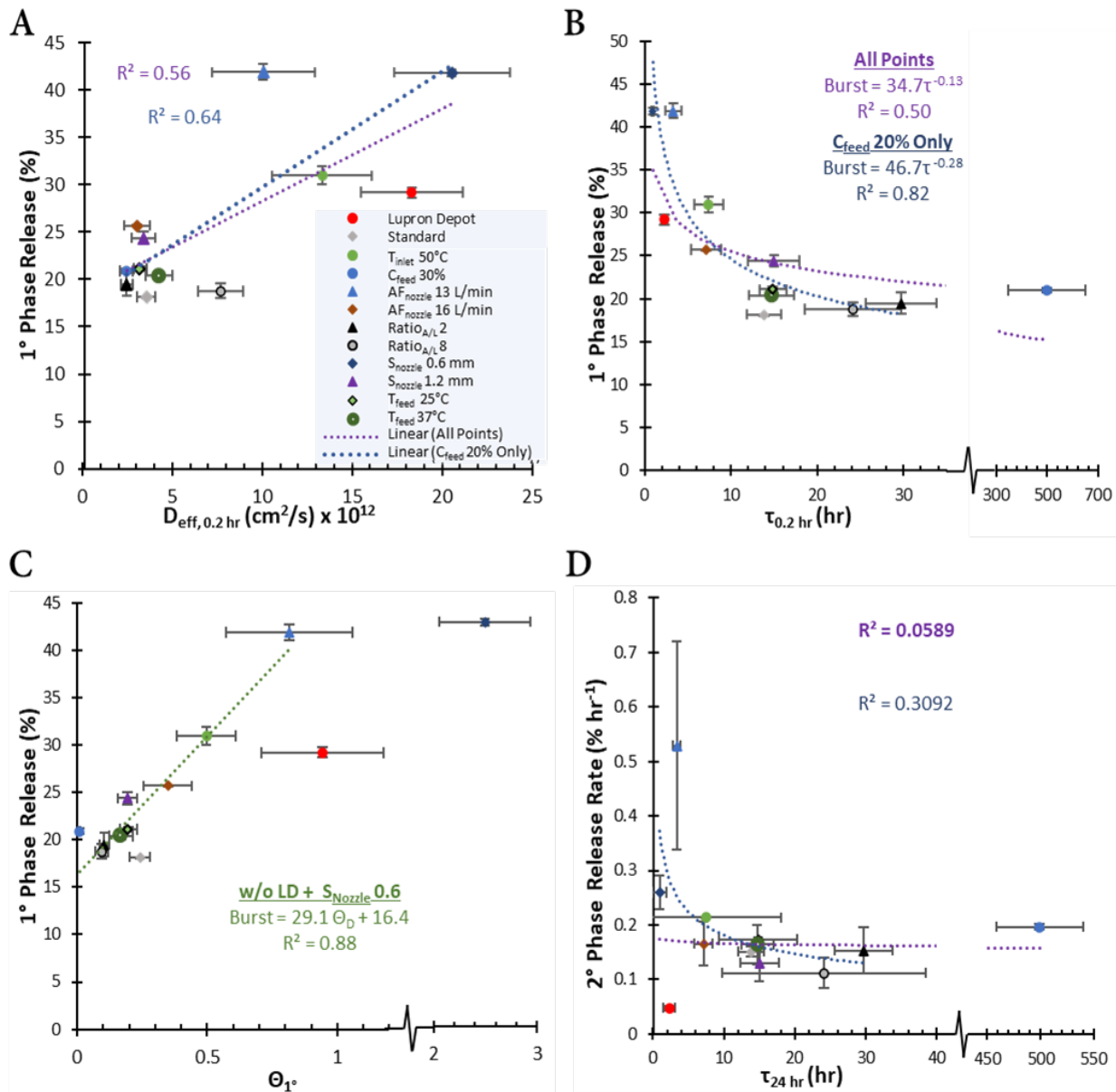


Figure 2-7. Results from aqueous diffusion study compared to features extracted from continuous monitoring in vitro release. 1° release was compared to the diffusion coefficient at 0.2 hr of preincubation (A) the characteristic diffusion time (B) (C); terminal release rate—the rate after the 1° release period—was compared to the diffusion coefficient at 24 hr (D).  $R^2$  values are based on power law fits of all spray-dried data points except for (A), which uses a linear fit.

appears to be at least 40% and the high dimensionless time of  $S_{nozzle}$  0.6 mm suggests that this could be the maximum. Between 0.2 and unity, a significant portion of the release is dictated by PLGA matrix diffusion, but at the lowest, the drug does not have sufficient time to release by this mechanism. The minimal 1° phase release that could be achieved was ~16% (~20% at 24 hr) from continuous monitoring based on the intercept of the dimensionless time and may be related to desorption of leuprolide from ion pairs of peptide with very low molecular weight polymer chains, which is independent of pore diffusion. Interestingly, if compared to the sample-and-separate methods (Table 2-1, Endpoint), the minimal release that was shown to occur for 24 hours in the continuous monitoring system was around 20% of their total drug loading while nearly all microspheres released around or below 20% for the sample-and-separate method. The strong relationship between the continuous monitoring and pore probe diffusion combined with this information could suggest that any contribution of diffusion through an inter-connected aqueous pore network in the microspheres is hindered when using the sample-and-separate method to evaluate the initial burst release.

Other continuous monitoring release parameters did not share as strong relationships to diffusion values. Although the maximum release rate tends to occur around 0.2 hours and could be expected to trend with  $\Theta_{1^{\circ}}$ , the dimensionless times did not correlate well ( $R^2 < 0.5$ ) with the maximum release rate (Figure S2-11B). The rapid decay of these rates may make it difficult to capture the relationship between the effective probe diffusion since over the course of the incubation with the pore probe the rate could have decreased significantly. Shown in Figure 2-7D, the characteristic diffusion time of the pore probe at 24 hr of preincubation showed relatively poor correlation to the terminal release rates that were measured in the continuous monitoring system (Table 2-1, Numerical-Based Derivative Analysis), which could further demonstrate a change in

release mechanisms after the 1<sup>o</sup> phase. Spray-dried particles appeared to transition from low to high effective diffusivity between 1 to 36 hr (Figure 2-6A). During this transitional phase, there is a distribution of low and high diffusion in microspheres that is evident by penetration of the probe in confocal images and the high variability in the effective diffusion coefficient measurements. Based on SEM observations at 24 hr, the particles appeared to undergo visible swelling and polymer void formation. The exact extent of swelling was not accounted for in the characteristic time at 24 hr, since particle size was not measured at this time with high statistical power through a method like laser diffraction. Instead, the original dry particle size was used in the calculation. Accounting for swelling may help to improve the correlation.

While the continuous monitoring system may facilitate the initial burst release, an *in vitro* release method where microspheres are less dispersed such as the sample-and-separate method may be more similar to the *in vivo* environment in which the microspheres will be confined to the injection site. Therefore, it is important to compare these methods to the *in vivo* release.

#### ***2.4.8 Pharmacokinetic evaluation of selected spray dried formulations in rats***

Four in-house microsphere formulations (Basic Formulation,  $C_{\text{feed}}$  30%,  $AF_{\text{nozzle}}$  13.0 L/min, and  $T_{\text{feed}}$  25°C) were selected for a pharmacokinetic study of the initial burst period based on their differences in *in vitro* initial burst release, deviations in the two release methods, and internal morphology and were compared to the commercial product Lupron Depot<sup>®</sup> (LD). To estimate the exact dose delivered, residual drug remaining in the syringe after administration was determined by rinsing with DCM and analysis through UPLC. The residual drug ranged from ~4-12% of the total dose. The residual drug was 8.5±0.4%, 9.1±0.6%, 10.9±0.4%, 9.1±1.0%, and 6.0±1.1 for LD, Basic Formulation,  $C_{\text{feed}}$  30%,  $AF_{\text{nozzle}}$  13.0 L/min, and  $T_{\text{feed}}$  25 °C, respectively. Levels in the first 24 hr were similar amongst all microspheres with  $AF_{\text{nozzle}}$  13.0 L/min reaching

Table 2-2. Pharmacokinetics parameters for subcutaneous administration (3mg/kg) in rats (n=4)

Formulation	Non-Compartment Parameters			Numerical Deconvolution
	C <sub>max</sub> (ng/mL)	t <sub>max</sub> (hr)	AUC <sub>0-24hr</sub> (ng-hr/mL)	F <sub>abs,24hr</sub> (% Administered)
<i>Lupron Depot</i>	87.6 (21.0)	1.00 (0.00)	322.4 (64.7)	7.32 (1.40)
<i>Basic/Standard</i>	149.8 (42.1)	0.63 (0.22)	381.4 (100.1)	9.33 (2.99)
<i>C<sub>feed</sub> 30%</i>	143.7 (60.3)	1.00 (0.00)	369.1 (181.3)	7.93 (3.81)
<i>AF<sub>nozzle</sub> 13 L/min</i>	280.5 (70.4)	0.50 (0.18)	507.1 (110.9)	12.35 (2.80)
<i>feed 25°C</i>	160.9 (11.8)	0.88 (0.13)	409.0 (29.9)	9.46 (0.68)

the lowest levels after a high initial concentration (Figure 2-8A). All spray dried microspheres appeared to have had a higher C<sub>max</sub> than LD with AF<sub>nozzle</sub> being the highest, but only T<sub>feed</sub> 25 °C had a statistically significant increase because the high inter-animal variability for the other formulations. Additionally, no significant differences in AUC were observed in the first 24 hr (Table 2-2) or in the t<sub>max</sub> but spray dried formulations may have released faster initially based on slightly shorter time until maximum plasma concentrations (Table 2-2). The short half-life of leuprolide in rats (~26 min) [17] and limitation on the frequency of collecting blood samples may have added to the variability and inability to capture significant differences in non-compartmental parameters. Larger studies or studies in larger rodents (rabbits) with longer leuprolide plasma half-lives may be necessary to better extract differences in these earlier periods.

#### 2.4.9 Numerical deconvolution of pharmacokinetic data

Numerical deconvolution based on a point-area method was used to estimate the amount absorbed during the pharmacokinetic study (Figure 2-8B). Because the length of the study could not capture the bioavailability, the amount absorbed was normalized by the amount administered to obtain a cumulative fraction absorbed. The amount administered was calculated based on the

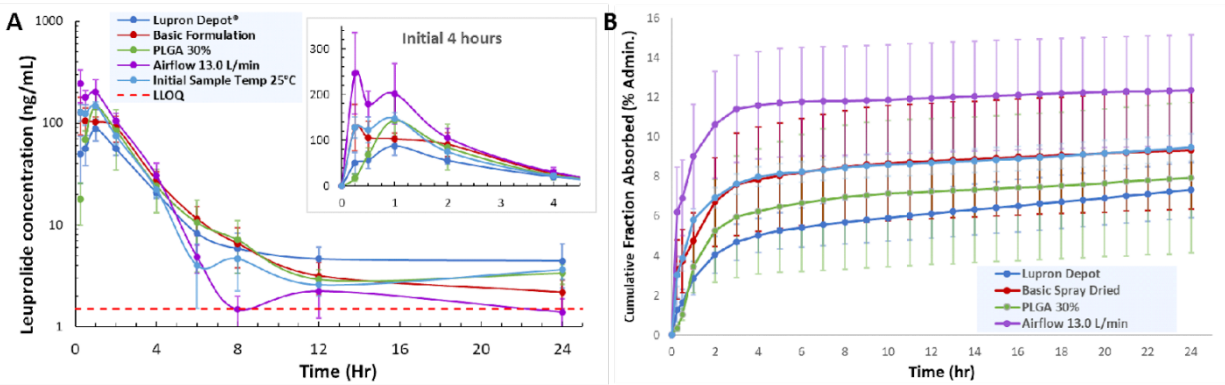


Figure 2-8. Pharmacokinetic in rats after subcutaneous administration of microspheres with a dose equivalent to 3.5 mg/kg leuprolide. Plasma concentration-time profiles of the first 24 hours (A) and first 4 hours (A-inset). Cumulative fraction absorbed from numerical deconvolution of plasma profiles using a 2-compartment based on literature values, normalized to the exact amount administered (B). Error bars show  $\pm SE$  ( $n=4$ ).

actual amount given of microspheres and drug loading of each formulation and was corrected for residual drug left in the syringes.

Similar to *in vitro* release testing,  $AF_{\text{nozzle}}$  13.0 L/min showed the highest apparent absorption rate and highest fraction absorbed in the first 24 hr. Unlike *in vitro* tests, Lupron Depot® showed the lowest fraction absorbed in the first 24 hr (Table 2-2). While the rates did not peak as high as spray dried formulations, LD showed a higher rate near the end of the first 24 hr. In terms of initial burst characteristics,  $C_{\text{feed}}$  30% appears to have cumulative fraction absorbed (Table 2-1) and absorption rates that is most similar to LD in the first 24 hr. The accuracy of these measurements may be limited by the proximity of plasma concentrations to the LLOQ and could have added to the variability of the calculated absorption rates.

#### 2.4.10 *In-vitro in-vivo correlations during initial burst*

While no guidance for bioequivalence exists for LAR products, the U.S. FDA guidance for extended-release oral products may be used as a basis for the development of IVIVCs. The guidance describes three different levels of IVIVC correlations [37]: (*level A*) a point-by-point relationship between the fraction released *in vitro* to the fraction absorbed *in vitro* (calculated after

deconvolution of pharmacokinetic data); (*level B*) a single-point relationship between the mean time to fraction released (e.g., 50%) and the mean time to the fraction absorbed; and (*level C*) a

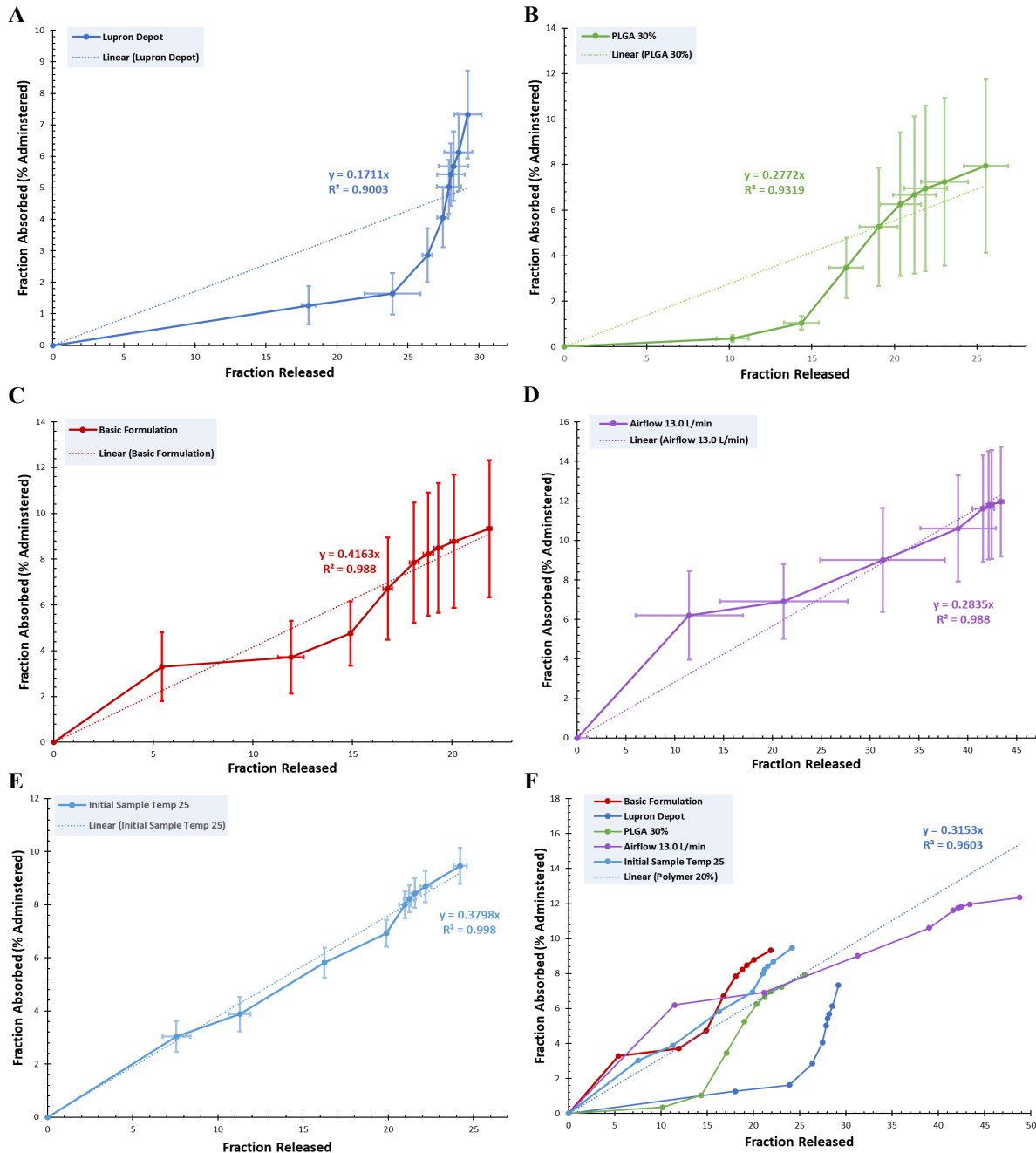


Figure 2-9. In-Vitro-In-Vivo Correlations of release by Continuous Monitoring. Individual Level-A IVIVC with no time scaling or shifting with fraction released obtained from continuous monitoring for Lupron Depot® (A) and spray-dried formulations:  $C_{feed}$  30% (B), Basic (C),  $AF_{nozzle}$  L/min (D), and  $T_{feed}$  25 C (E); with linear fitting forced through the origin. Error bars show  $\pm SE$ . Compiled IVIVC plots (F); linear fit includes data points from spray-dried formulations made with constant polymer concentration ( $C_{feed}$  20%).

relationship between an *in vitro* dissolution/release parameter to a pharmacokinetic parameter (e.g.,  $C_{max}$ , AUC).

Three *in vitro* methods were used to assess the initial burst release period: Sample-and-Separate 24-hr Release, Continuous Monitoring Release, and Probe Diffusion. To assess the potential of a Level A correlation [37], a time-by-time comparison of the fraction released in the continuous monitoring release and the calculated fraction absorbed from *in vivo* pharmacokinetic study was created for the first 24 hr (Figure 2-9). For this analysis only definite time points for *in vivo* absorption are used (no interpolated points used). Without any time-scaling/time-shifting, the basic formulation,  $AF_{nozzle}$  13.0 L/min, and  $T_{feed}$  25°C showed a high correlation between *in vitro* and *in vivo* release ( $R^2 > 0.9$ ) (Figure 2-9C, D, E). Both  $C_{feed}$  30% and LD showed an apparent lag in *in vivo* absorption compared to *in vitro* release (Figure 2-9A, B). In terms of physical characteristics,  $C_{feed}$  30% had reduced pore sizes and delayed increases in the internal pore structure as observed through SEM (Figure S2-7. External morphology (A, C) and internal structure (B, D) of  $C_{feed}$  30% (A, B) and  $T_{feed}$  13°C microspheres (C, D) from storage and after 0, 0.2, 1, 2, 5, 8, 12, 24, and 36 hours of incubation in the continuous monitoring system. Left image shows full microsphere. Right shows high magnification (field view = 7.2  $\mu$ m). A, B), which may be more comparable to LD than other spray dried formulations. Time-shifting may help improve the correlation of  $C_{feed}$  30% and LD, but a Levy plot could not be performed because the amount absorbed could not be properly normalized by amount absorbed at infinity (i.e., correcting for bioavailability/inter-animal variability). When grouped together, spray dried formulations with a constant  $C_{feed}$  had a good correlation with *in vitro* release from continuous monitoring ( $R^2 = 0.79$ ) (Figure 2-9F). The predictability of the IVIVC has not been assessed.

*In vitro* tests were also assessed for Level C IVIVCs (Figure 2-10). The fraction released at 24 hr from the continuous monitoring system was compared to the fraction absorbed at 24 hr,

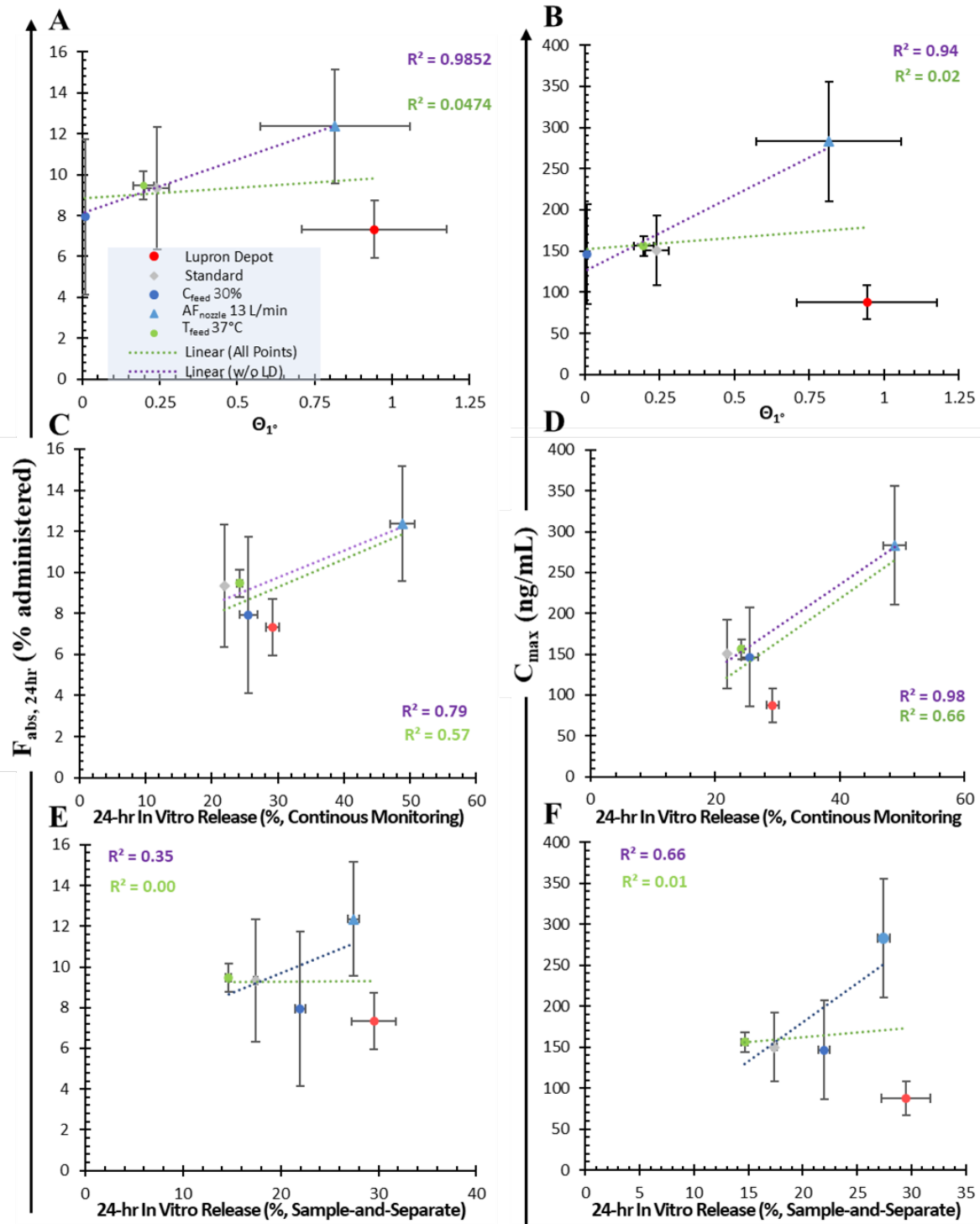


Figure 2-10. Level C In-Vitro-In-Vivo Correlations with parameters from diffusion studies (A, B), continuous monitoring release (C, D), or conventional release (E, F) versus the fraction absorbed after 24 hours (A, C, E) or  $C_{max}$  (B, D, F). Correlations were tested for spray-dried formulations with (blue) and without Lupron Depot® (green). Error bars show SE.

$F_{abs,24hr}$  (Figure 2-10C) and showed a high correlation amongst spray dried formulations ( $R^2 > 0.9$ ). During the first 24 hr, the  $C_{max}$  contributes heavily to the AUC (Figure S2-10A) and fraction absorbed is highly correlated with AUC (Figure S2-10B), therefore, the fraction released in continuous monitoring also showed a high correlation with  $C_{max}$  (Figure 2-10D). However, in both cases, the commercial product, LD, appeared as an outlier severely reducing the correlation when included ( $R^2 < 0.65$ ). In addition, the  $F_{abs,24hr}$  and  $C_{max}$  was compared to the in vitro burst release and diffusion studies through the dimensionless time— $\Theta_{1^\circ}$  (Figure 2-10A, B). Amongst spray dried formulations, the in vitro release by continuous monitoring appear to a good predictor of the  $F_{abs,24hr}$  and  $C_{max}$ , but no correlation was found when LD was included. Interestingly, the effective diffusion coefficients alone appeared to be a better predictor of *in vivo* performance (Figure S2-10C, D) as well. Since the characteristic time is based on dry particle sizes, differences in particle wettability and subsequent swelling that were more subtle in well-mixed *in vitro* conditions may be further distinguished *in vivo*. In general, the results of Level A and Level C IVIVCs shows there is an apparent disparity between the *in vitro* release and *in vivo* absorbance for LD when compared to spray dried formulations, which showed better correlations. In the context of diffusion studies and SEM imaging, this suggests the mechanism of release may be different between single-emulsion w/o spray dried particles and the commercial product for the initial burst period. The non-compartmental parameters were also compared to the fraction release after 24 hr from conventional sample-and-separate. The conventional method showed a poor Level C relationship to both  $F_{abs,24hr}$  (Figure 2-10E) and  $C_{max}$  (Figure 2-10F). Overall, the conventional method appears to have exaggerated the differences in the release of the spray dried formulations that showed little differences *in vivo*. Therefore, this method does not seem appropriate for evaluating the initial burst release of spray dried formulations, and measurements of pore probe

diffusion and continuous monitoring release may better reproduce *in vivo* release during this period.

## 2.5 Conclusions

Changes in spray-drying process parameters produce microsphere formulations with significant variability in the *in vitro* initial burst release that was observed in the continuous monitoring system. Parameters that affect evaporation rates such as inlet air temperature ( $T_{\text{inlet}}$ ) or droplet velocity/residence time in the drying chamber such as nozzle airflow ( $AF_{\text{nozzle}}$ ) and nozzle size ( $S_{\text{nozzle}}$ ) appear to have the most profound effect on the burst release.  $AF_{\text{nozzle}}$  has a positive relationship to the release while  $S_{\text{nozzle}}$  and  $T_{\text{inlet}}$  exhibit a negative correlation. A majority of spray-dried formulations also display lower initial burst values than the Lupron Depot<sup>®</sup>. Differences in release are more muted and with lower magnitude in the conventional, single-point “sample-and-separate” method for evaluating the initial burst period. Release from in-house spray-dried microspheres in the continuous monitoring system is typically higher than the conventional sample-and-separate method and show reasonable correlation to constants calculated from the diffusion studies.

Overall, the spray-dried formulations tend to show lower initial diffusional uptake of a fluorescent dextran probe than does the Lupron Depot<sup>®</sup>, but diffusion rates are similar by 24 hr. At early timepoints, increases in diffusivity in spray-dried particles appear to coincide with changes in apparent internal porosity from SEM images that can be attributed to increased access to the particle interior from surface-connected pores, which allow for deeper penetration. Images of dye-defined circular pore-like occlusions strongly suggest that swelling may have led to polymer phase diffusion. At 24 hours, probe effective diffusion coefficients are unrelated to terminal rates and release. This lack of relationship, along with the apparent sharp increase in

probe diffusion rates at 36 hr likely caused by swelling, suggests that diffusion through the polymer matrix is not the rate-controlling mechanism after the initial burst period. Overall, the peptide mass transfer during the initial burst appears to involve an interplay between aqueous pore network diffusion, polymer-phase diffusion and interactions between leuprolide and the carboxylic ends of the polymer.

The in-house-prepared spray-dried microsphere formulations exhibit little to no significant differences in non-compartment parameters and fractions absorbed when compared to Lupron Depot<sup>®</sup>.  $T_{\text{feed}} 25\text{ }^{\circ}\text{C}$ ,  $AF_{\text{nozzle}} 13.0\text{ L/min}$ , and the standard conditions for spray drying (basic formulation) show the potential for a Level A relationship between *in vivo* absorbance and fraction released in the continuous monitoring while the more dense,  $C_{\text{feed}} 30\%$  and LD, display similar delays in *in vivo* absorption relative to continuous monitoring *in vitro* release, and also show similar absorption rates and pharmacokinetic parameters during the first 24 hr. Overall, the continuous monitoring method and pore probe diffusion studies show the greatest potential for being a predictor of pharmacokinetic parameters amongst spray-dried formulations but cannot predict LD absorption using the same relationship.

## 2.6 References

- [1] H. Zhong, G. Chan, Y. Hu, H. Hu, D. Ouyang, A Comprehensive Map of FDA-Approved Pharmaceutical Products, *Pharmaceutics*. 10 (2018).  
<https://doi.org/10.3390/pharmaceutics10040263>.
- [2] Y. Wang, Q. Wen, S.H. Choi, FDA's Regulatory Science Program for Generic PLA/PLGA-Based Drug Products, *Am Pharm Rev*. 19 (2016) 5–9.
- [3] J. Wang, B.M. Wang, S.P. Schwendeman, Characterization of the initial burst release of a model peptide from poly(D,L-lactide-co-glycolide) microspheres, *J Control Release*. 82 (2002) 289–307. <https://www.ncbi.nlm.nih.gov/pubmed/12175744>.
- [4] K. Hirota, A.C. Doty, R. Ackermann, J. Zhou, K.F. Olsen, M.R. Feng, Y. Wang, S. Choi, W. Qu, A.S. Schwendeman, S.P. Schwendeman, Characterizing release mechanisms of leuprolide acetate-loaded PLGA microspheres for IVIVC development I: In vitro evaluation, *J Control Release*. 244 (2016) 302–313.  
<https://doi.org/10.1016/j.jconrel.2016.08.023>.
- [5] A.M. Sophocleous, K.G. Desai, J.M. Mazzara, L. Tong, J.X. Cheng, K.F. Olsen, S.P. Schwendeman, The nature of peptide interactions with acid end-group PLGAs and facile aqueous-based microencapsulation of therapeutic peptides, *J Control Release*. 172 (2013) 662–670. <https://doi.org/10.1016/j.jconrel.2013.08.295>.
- [6] Y. Aso, S. Yoshioka, A.L.W. Po, T. Terao, Effect of Temperature on Mechanisms of Drug-Release and Matrix Degradation of Poly(D,L-Lactide) Microspheres, *Journal of Controlled Release*. 31 (1994) 33–39. [https://doi.org/10.1016/0168-3659\(94\)90248-8](https://doi.org/10.1016/0168-3659(94)90248-8).

- [7] D.R. Janagam, L. Wang, S. Ananthula, J.R. Johnson, T.L. Lowe, An Accelerated Release Study to Evaluate Long-Acting Contraceptive Levonorgestrel-Containing in Situ Forming Depot Systems, *Pharmaceutics*. 8 (2016).  
<https://doi.org/10.3390/pharmaceutics8030028>.
- [8] M. Shameem, H. Lee, P.P. DeLuca, A short term (accelerated release) approach to evaluate peptide release from PLGA depot-formulations, *AAPS PharmSci*. 1 (1999) E7.  
<https://doi.org/10.1208/ps010307>.
- [9] K.G. Desai, S.R. Mallery, S.P. Schwendeman, Formulation and characterization of injectable poly(DL-lactide-co-glycolide) implants loaded with N-acetylcysteine, a MMP inhibitor, *Pharm Res*. 25 (2008) 586–597. <https://doi.org/10.1007/s11095-007-9430-1>.
- [10] A.C. Doty, D.G. Weinstein, K. Hirota, K.F. Olsen, R. Ackermann, Y. Wang, S. Choi, S.P. Schwendeman, Mechanisms of in vivo release of triamcinolone acetonide from PLGA microspheres, *Journal of Controlled Release*. 256 (2017) 19–25.  
<https://doi.org/10.1016/j.jconrel.2017.03.031>.
- [11] F. Alexis, Factors affecting the degradation and drug-release mechanism of poly(lactic acid) and poly[(lactic acid)-co-(glycolic acid)], *Polym Int*. 54 (2005) 36–46.  
<https://doi.org/DOI 10.1002/pi.1697>.
- [12] A.C. Wilson, S. V Meethal, R.L. Bowen, C.S. Atwood, Leuprolide acetate: a drug of diverse clinical applications, *Expert Opin Investig Drugs*. 16 (2007) 1851–1863.  
<https://doi.org/10.1517/13543784.16.11.1851>.
- [13] H. Okada, Y. Ogawa, T. Yashiki, *Method for Producing Microcapsule*, 1985.

- [14] J. Zhou, K. Hirota, R. Ackermann, J. Walker, Y. Wang, S. Choi, A. Schwendeman, S.P. Schwendeman, Reverse engineering the 1-month Lupron Depot®, *AAPS J.* 20 (2018) 105.
- [15] J. Zhou, J. Walker, R. Ackermann, K. Olsen, J.K.Y. Hong, Y. Wang, S.P. Schwendeman, Effect of Manufacturing Variables and Raw Materials on the Composition-Equivalent PLGA Microspheres for 1-Month Controlled Release of Leuprolide, *Mol Pharm.* 17 (2020) 1502–1515. <https://doi.org/10.1021/acs.molpharmaceut.9b01188>.
- [16] N.Q. Shi, J. Zhou, J. Walker, L. Li, K.Y. Hong, K.F. Olsen, J. Tang, R. Ackermann, Y. Wang, B. Qin, A. Schwendeman, S.P. Schwendeman, Microencapsulation of luteinizing hormone-releasing hormone agonist in poly (lactic-co-glycolic acid) microspheres by spray drying, *J Control Release.* (2020). <https://doi.org/10.1016/j.jconrel.2020.01.023>.
- [17] H. Okada, Y. Inoue, T. Heya, H. Ueno, Y. Ogawa, H. Toguchi, Pharmacokinetics of once-a-month injectable microspheres of leuprolide acetate, *Pharm Res.* 8 (1991) 787–791. <https://doi.org/10.1023/a:1015818504906>.
- [18] I.M. Thompson, Flare Associated with LHRH-Agonist Therapy, *Rev Urol.* 3 Suppl 3 (2001) S10-4.
- [19] S. Fredenberg, M. Wahlgren, M. Reslow, A. Axelsson, The mechanisms of drug release in poly(lactic-co-glycolic acid)-based drug delivery systems--a review, *Int J Pharm.* 415 (2011) 34–52. <https://doi.org/10.1016/j.ijpharm.2011.05.049>.
- [20] S. Fredenberg, M. Wahlgren, M. Reslow, A. Axelsson, Pore formation and pore closure in poly(D,L-lactide-co-glycolide) films, *J Control Release.* 150 (2011) 142–149. <https://doi.org/10.1016/j.jconrel.2010.11.020>.

- [21] H.K. Kim, H.J. Chung, T.G. Park, Biodegradable polymeric microspheres with “open/closed” pores for sustained release of human growth hormone, *J Control Release*. 112 (2006) 167–174. <https://doi.org/10.1016/j.jconrel.2006.02.004>.
- [22] J. Kang, S.P. Schwendeman, Pore closing and opening in biodegradable polymers and their effect on the controlled release of proteins, *Mol Pharm*. 4 (2007) 104–118. <https://doi.org/10.1021/mp060041n>.
- [23] S.P. Schwendeman, R.B. Shah, B.A. Bailey, A.S. Schwendeman, Injectable controlled release depots for large molecules, *J Control Release*. 190 (2014) 240–253. <https://doi.org/10.1016/j.jconrel.2014.05.057>.
- [24] J. V Andhariya, R. Jog, J. Shen, S. Choi, Y. Wang, Y. Zou, D.J. Burgess, In vitro-in vivo correlation of parenteral PLGA microspheres: Effect of variable burst release, *J Control Release*. 314 (2019) 25–37. <https://doi.org/10.1016/j.jconrel.2019.10.014>.
- [25] X.S. Wu, N. Wang, Synthesis, characterization, biodegradation, and drug delivery application of biodegradable lactic/glycolic acid polymers. Part II: Biodegradation, *Journal of Biomaterials Science-Polymer Edition*. 12 (2001) 21–34. <https://doi.org/10.1163/156856201744425>.
- [26] J.C. Kang, S.P. Schwendeman, Determination of diffusion coefficient of a small hydrophobic probe in poly(lactide-co-glycolide) microparticles by laser scanning confocal microscopy, *Macromolecules*. 36 (2003) 1324–1330. <https://doi.org/10.1021/ma021036+>.
- [27] Z. Yu, J.B. Schwartz, E.T. Sugita, H.C. Foehl, Five modified numerical deconvolution methods for biopharmaceutics and pharmacokinetics studies, *Biopharm Drug Dispos*. 17

- (1996) 521–540. [https://doi.org/10.1002/\(SICI\)1099-081X\(199608\)17:6<521::AID-BDD974>3.0.CO;2-A](https://doi.org/10.1002/(SICI)1099-081X(199608)17:6<521::AID-BDD974>3.0.CO;2-A).
- [28] J. V Andhariya, R. Jog, J. Shen, S. Choi, Y. Wang, Y. Zou, D.J. Burgess, Development of Level A in vitro-in vivo correlations for peptide loaded PLGA microspheres, *J Control Release*. 308 (2019) 1–13. <https://doi.org/10.1016/j.jconrel.2019.07.013>.
- [29] Y.Y. Yang, T.S. Chung, N.P. Ng, Morphology, drug distribution, and in vitro release profiles of biodegradable polymeric microspheres containing protein fabricated by double-emulsion solvent extraction/evaporation method, *Biomaterials*. 22 (2001) 231–241.
- [30] R.B. Shah, S.P. Schwendeman, A biomimetic approach to active self-microencapsulation of proteins in PLGA, *J Control Release*. 196 (2014) 60–70. <https://doi.org/10.1016/j.jconrel.2014.08.029>.
- [31] H. Yushu, S. Venkatraman, The effect of process variables on the morphology and release characteristics of protein-loaded PLGA particles, *J Appl Polym Sci*. 101 (2006) 3053–3061. <https://doi.org/10.1002/app.23933>.
- [32] C. Cui, V.C. Stevens, S.P. Schwendeman, Injectable polymer microspheres enhance immunogenicity of a contraceptive peptide vaccine, *Vaccine*. 25 (2007) 500–509. <https://doi.org/10.1016/j.vaccine.2006.07.055>.
- [33] K.G. Desai, S.P. Schwendeman, Active self-healing encapsulation of vaccine antigens in PLGA microspheres, *J Control Release*. 165 (2013) 62–74. <https://doi.org/10.1016/j.jconrel.2012.10.012>.

- [34] J. Huang, J.M. Mazzara, S.P. Schwendeman, M.D. Thouless, Self-healing of pores in PLGAs, *J Control Release*. 206 (2015) 20–29.  
<https://doi.org/10.1016/j.jconrel.2015.02.025>.
- [35] J.M. Mazzara, M.A. Balagna, M.D. Thouless, S.P. Schwendeman, Healing kinetics of microneedle-formed pores in PLGA films, *J Control Release*. 171 (2013) 172–177.  
<https://doi.org/10.1016/j.jconrel.2013.06.035>.
- [36] N.A. Peppas, C.T. Reinhart, Solute diffusion in swollen membranes. Part I. A new theory, *J Memb Sci*. 15 (1983). [https://doi.org/10.1016/S0376-7388\(00\)82304-2](https://doi.org/10.1016/S0376-7388(00)82304-2).
- [37] F.T. Análisis, P. Costa, J.M. Sousa Lobo, T. Data, P. Quetiapine, M.R. Tablets, B. Grintjes, A.M. Gmt, F.F.B.R.P. L, J. Pharm, L. Summary, The Mendeley Support Team, H.A. Andreetta, P. Blends, F. Dosage, U. Sampling, E. Costa, A. Arancibia, J. Aïache, S. Feature, Q.G.D. Lisci, Q.F.B. María, E. Girard, G.D.N. Materiales, R.E. N, D. Ph, P.D. Prasad, N.U. Lakshmi, D.A. Kumar, M. Jhansee, M. Kumar, P. Product, N. Seroquel, S. Xr, C. Qu, C.N. Recommendations, C.D. Release, M. Release, S. Oral, D. Forms, M.E. Addendum, S. De Seguridad, P.H. Service, H. Services, N.R. Tebes, M. Towers, Guidance for Industry: Extended Release Oral Dosage Forms: Development, Evaluation, and Application of In Vitro/In Vivo Correlations, Food and Drug Administration. 24 (2010).

## 2.7 Supplementary Data

Table S2-1. The compositions and formulations of spray-dried leuprolide-PLGA microspheres with altered spray drying parameters including inlet air temperature ( $T_{inlet}$ ), PLGA concentration ( $C_{feed}$ ), airflow in nozzle ( $AF_{nozzle}$ ), ratio between atomization gas flow rate and the liquid mass flow rate ( $Ratio_{A/L}=AF_{inlet}/LF_{nozzle}$ ), nozzle size ( $S_{nozzle}$ ) and initial sample temperature ( $T_{feed}$ ).

Formulations	$T_{inlet}$ (°C)	$C_{feed}$ (%)	$AF_{nozzle}$ (L/min)	$Ratio_{A/L}$ (mL/min/ mL/min)	$S_{nozzle}$ (mm)	$T_{feed}$ (°C)	Drug (mg)	PLG (mg)	Gelatin (mg)	DCM (mL)	H <sub>2</sub> O (mL)	Drug Loading (%)	Encapsulation Efficiency (%)	Gelatin Loading (%)	EE (%)
Standard/Basic	80	20	10	4.0 (400/100)	1	4	150	1000	19.9	5	1	9.81 (0.04)	76.3 (0.3)	1.72 (0.04)	100.9 (2.1)
$T_{inlet}$ 70°C	70	20	10	4.0 (400/100)	1	4	150	1000	19.9	5	1	9.80 (0.23)	76.4 (1.8)	1.59 (0.14)	93.8 (7.9)
$T_{inlet}$ 60°C	60	20	10	4.0 (400/100)	1	4	150	1000	19.9	5	1	9.24 (0.16)	72.0 (1.3)	1.68 (0.12)	98.8 (6.7)
$T_{inlet}$ 50°C	50	20	10	4.0 (400/100)	1	4	150	1000	19.9	5	1	9.58 (0.13)	74.7 (1.0)	1.59 (0.01)	93.2 (0.4)
$C_{feed}$ 30%	80	30	10	4.0 (400/100)	1	4	225	1500	29.85	5	1	10.41 (0.80)	81.2 (1.0)	1.70 (0.04)	100.3 (2.1)
$AF_{nozzle}$ 13 L/min	80	20	13	4.0 (400/100)	1	4	150	1000	19.9	5	1	9.35 (0.03)	72.73 (0.03)	1.77 (0.11)	103.8 (6.2)
$AF_{nozzle}$ 16 L/min	80	20	16	4.0 (400/100)	1	4	150	1000	19.9	5	1	9.25 (0.01)	88.6 (1.5)	1.73 (0.07)	101.8 (4.2)
$Ratio_{A/L}$ 2	80	20	10	2.0 (400/200)	1	4	150	1000	19.9	5	1	9.61 (0.02)	74.7 (0.1)	1.76 (0.28)	103.5 (0.2)
$Ratio_{A/L}$ 3	80	20	10	3.0 (300/100)	1	4	150	1000	19.9	5	1	9.54 (0.04)	74.3 (0.3)	1.75 (0.04)	102.94 (0.03)
$Ratio_{A/L}$ 6	80	20	10	6.0 (600/100)	1	4	150	1000	19.9	5	1	9.52 (0.03)	73.9 (0.2)	1.48 (0.02)	86.8 (12.0)
$Ratio_{A/L}$ 8	80	20	10	8.0 (640/80)	1	4	150	1000	19.9	5	1	9.57 (0.04)	74.5 (0.3)	1.76 (0.28)	102.9 (16.5)
$S_{nozzle}$ 1.2 mm	80	20	10	4.0 (400/100)	1.2	4	150	1000	19.9	5	1	9.50 (0.05)	73.9 (0.4)	1.47 (0.01)	85.7 (0.4)
$S_{nozzle}$ 0.8 mm	80	20	10	4.0 (400/100)	0.8	4	150	1000	19.9	5	1	9.01 (0.01)	70.0 (0.6)	1.57 (0.10)	91.8 (5.8)
$S_{nozzle}$ 0.6 mm	80	20	10	4.0 (400/100)	0.6	4	150	1000	19.9	5	1	9.10 (0.14)	70.7 (1.1)	1.53 (0.05)	89.8 (2.9)
$T_{feed}$ 13°C	80	20	10	4.0 (400/100)	1	13	150	1000	19.9	5	1	9.36 (0.14)	72.8 (1.1)	1.71 (0.08)	100.88 (0.05)
$T_{feed}$ 25°C	80	20	10	4.0 (400/100)	1	25	150	1000	19.9	5	1	9.02 (0.04)	70.1 (0.3)	1.74 (0.04)	102.63 (0.004)
$T_{feed}$ 37°C	80	20	10	4.0 (400/100)	1	37	150	1000	19.9	5	1	9.78 (0.21)	76.1 (1.6)	1.75 (0.01)	102.06 (0.02)

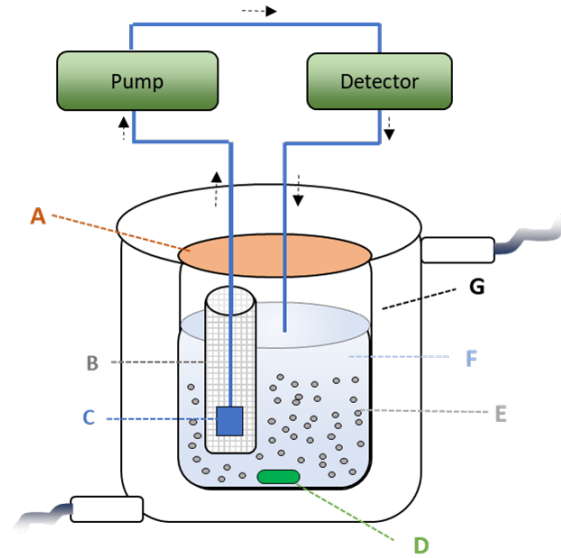


Figure S2-1. Schematic diagram of instrumental set-up for continuous monitoring system of the initial burst from PLGA microspheres. The continuous monitoring system includes sub-micron nylon mesh (B), sampling probe (C), magnetic stirrer (D), and water-jacketed beaker (G) at 37°C. Microspheres (E) are placed in phosphate-buffered saline with Tween 80 (F) with a seal (A) on the container.

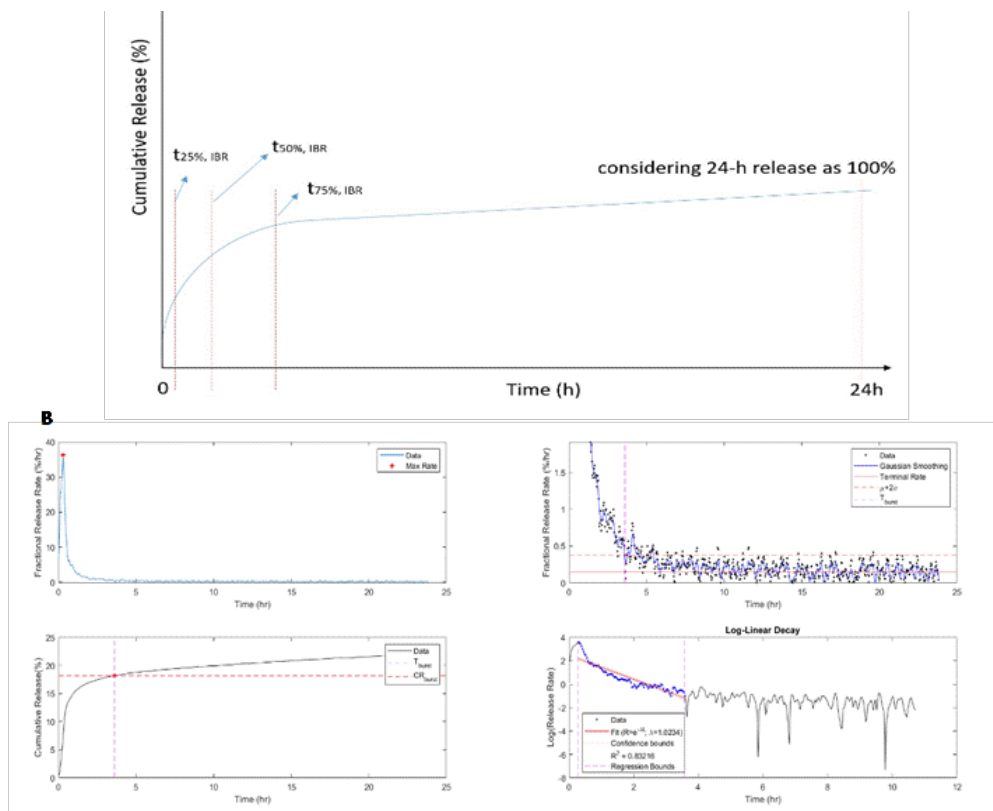


Figure S2-2. Demonstration of feature extraction from cumulative release vs. time profiles and their numerical derivatives. (A) Estimation of  $t_{25\%}$ ,  $t_{50\%}$ , and  $t_{75\%}$ ; and (B) derivative-based extraction of maximum rate (upper left), terminal rate and end time of the burst release (upper right), the concentration at that time (lower left), and the calculation of the decay rate constant between the maximum rate and end of the burst (lower right).

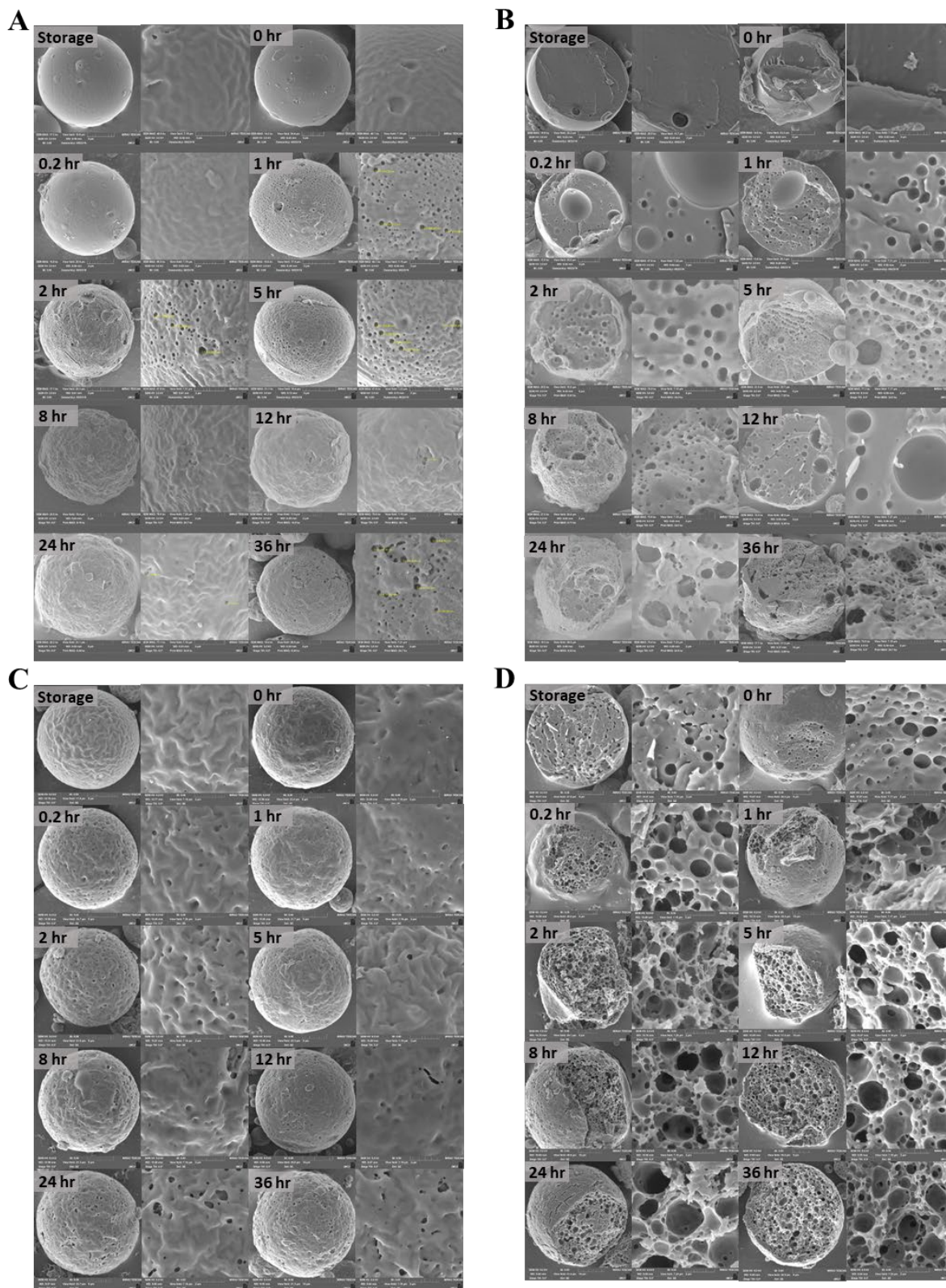


Figure S2-3. External morphology (A, C) and internal structure (B, D) of unloaded standard condition spray-dried microspheres (A, B) and  $T_{inlet} 50^{\circ}\text{C}$  microspheres (C, D) from storage and after 0, 0.2, 1, 2, 5, 8, 12, 24, and 36 hours of incubation in the continuous monitoring system. Left image shows full microsphere. Right shows high magnification (field

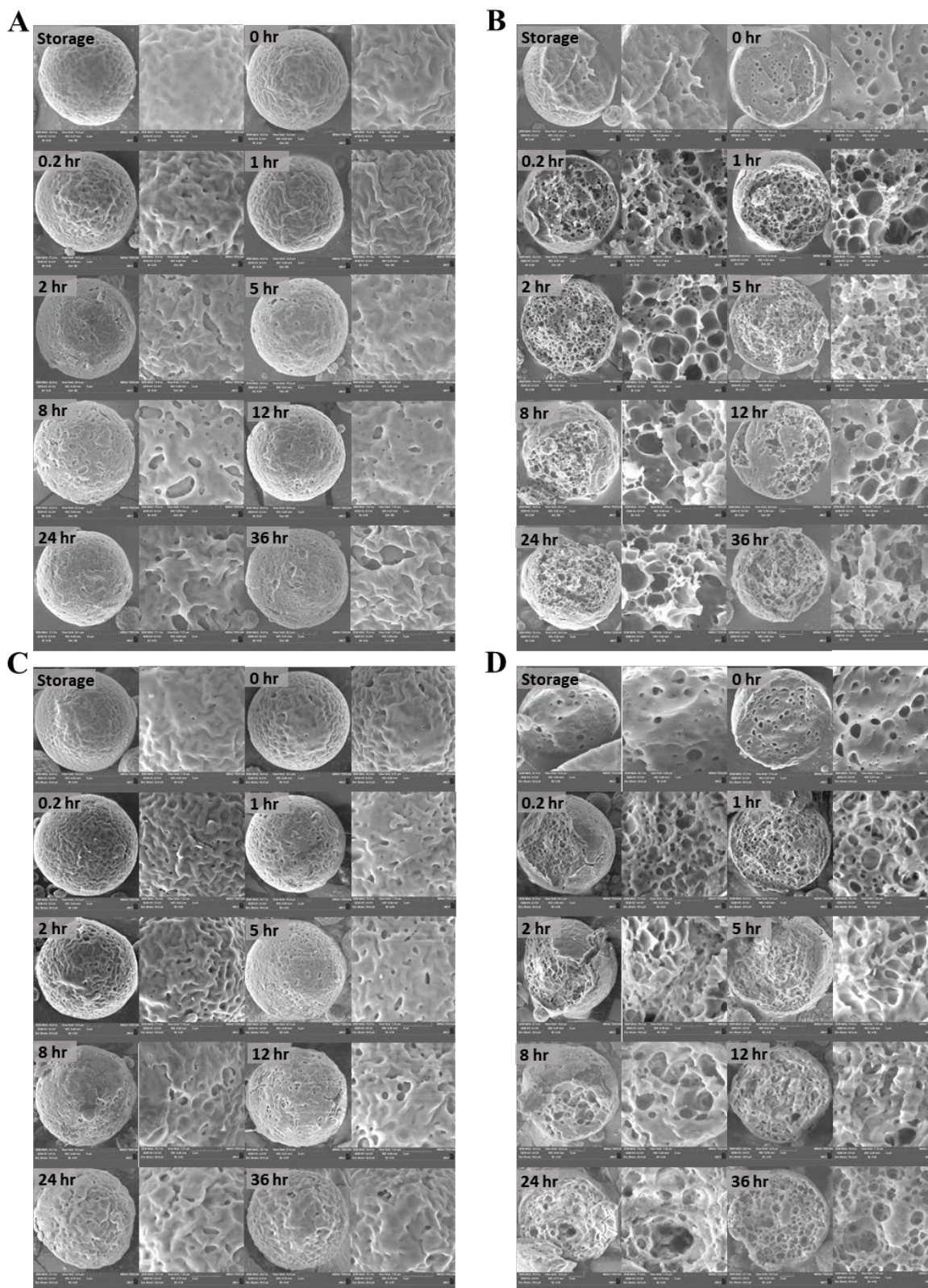


Figure S2-4. External morphology (A, C) and internal structure (B, D) of  $AF_{nozzle}$  13 (A, B) and 16 L/min microspheres (C, D) from storage and after 0, 0.2, 1, 2, 5, 8, 12, 24, and 36 hours of incubation in the continuous monitoring system. Left image shows full microsphere. Right shows high magnification (field view =  $7.2 \mu m$ )

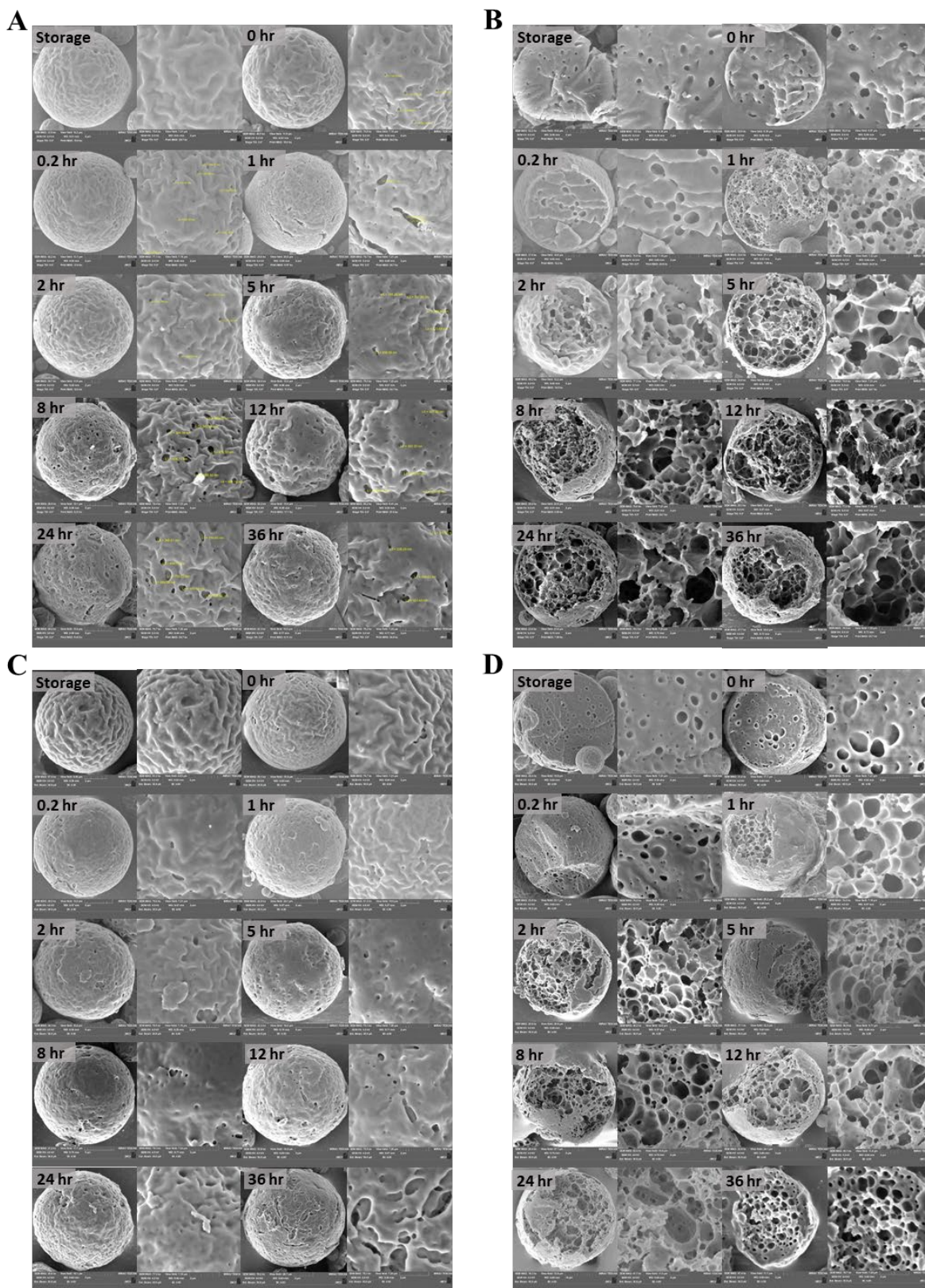


Figure S2-5. External morphology (A, C) and internal structure (B, D) of Ratio<sub>ALL</sub> 2 (A, B) and 8 microspheres (C, D) from storage and after 0, 0.2, 1, 2, 5, 8, 12, 24, and 36 hours of incubation in the continuous monitoring system. Left image shows full microsphere. Right shows high magnification (field view = 7.2  $\mu\text{m}$ ).

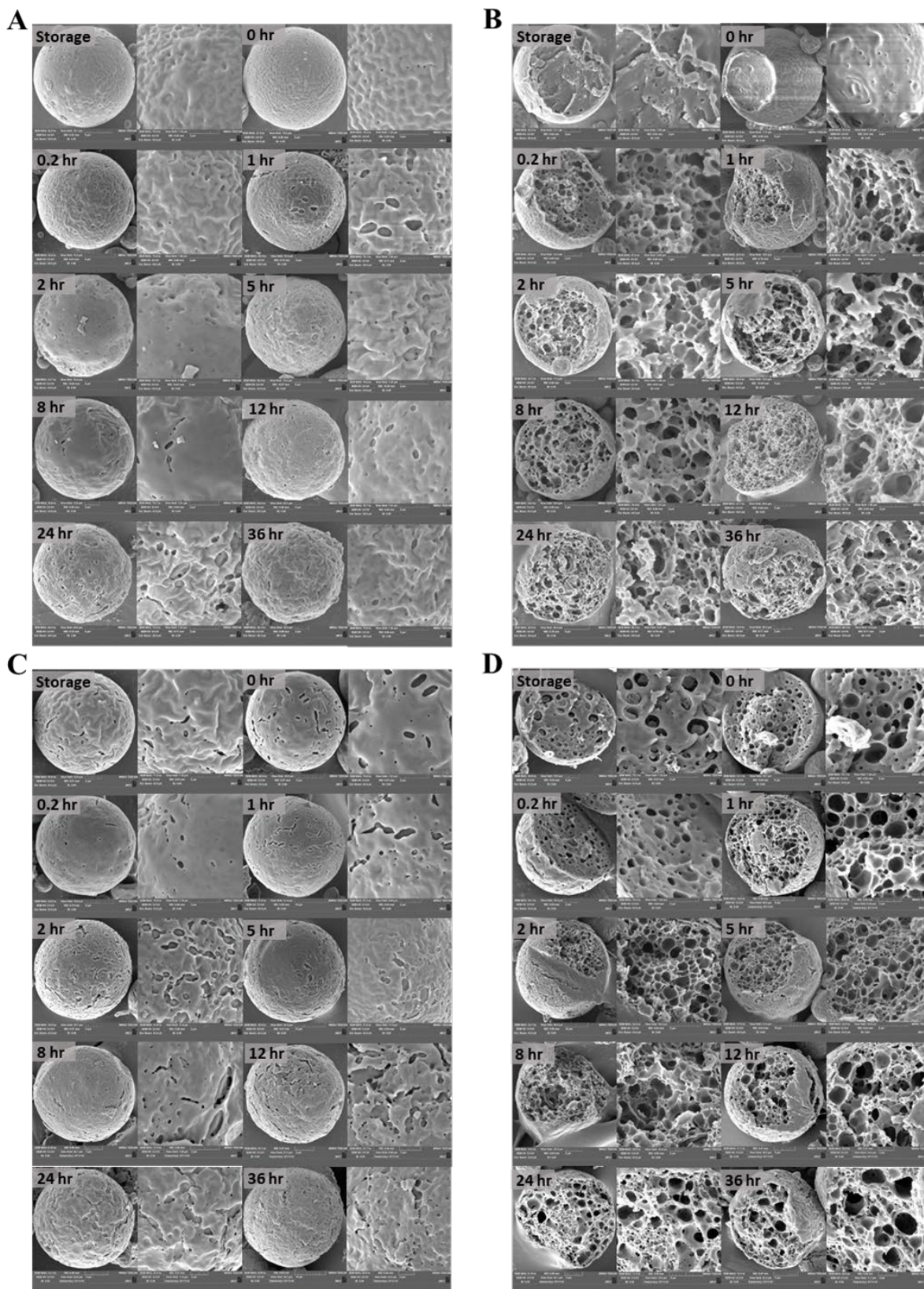


Figure S2-6. External morphology (A, C) and internal structure (B, D) of  $S_{nozzle}$  0.6 (A, B) and 1.2 mm microspheres (C, D) from storage and after 0, 0.2, 1, 2, 5, 8, 12, 24, and 36 hours of incubation in the continuous monitoring system. Left image shows full microsphere. Right shows high magnification (field view =  $7.2 \mu\text{m}$ ).

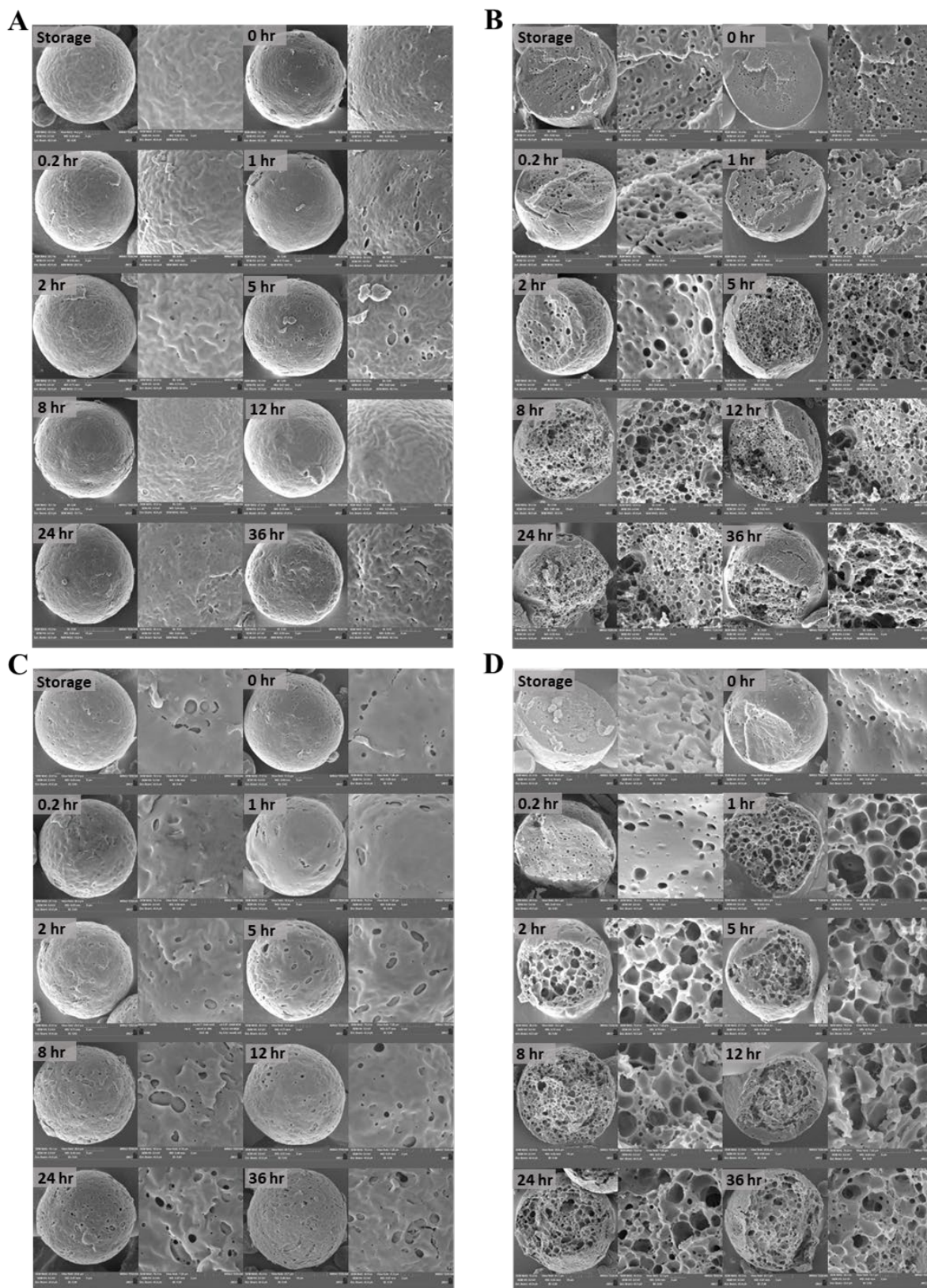


Figure S2-7. External morphology (A, C) and internal structure (B, D) of  $C_{feed}$  30% (A, B) and  $T_{feed}$  13°C microspheres (C, D) from storage and after 0, 0.2, 1, 2, 5, 8, 12, 24, and 36 hours of incubation in the continuous monitoring system. Left image shows full microsphere. Right shows high magnification (field view = 7.2  $\mu\text{m}$ ).

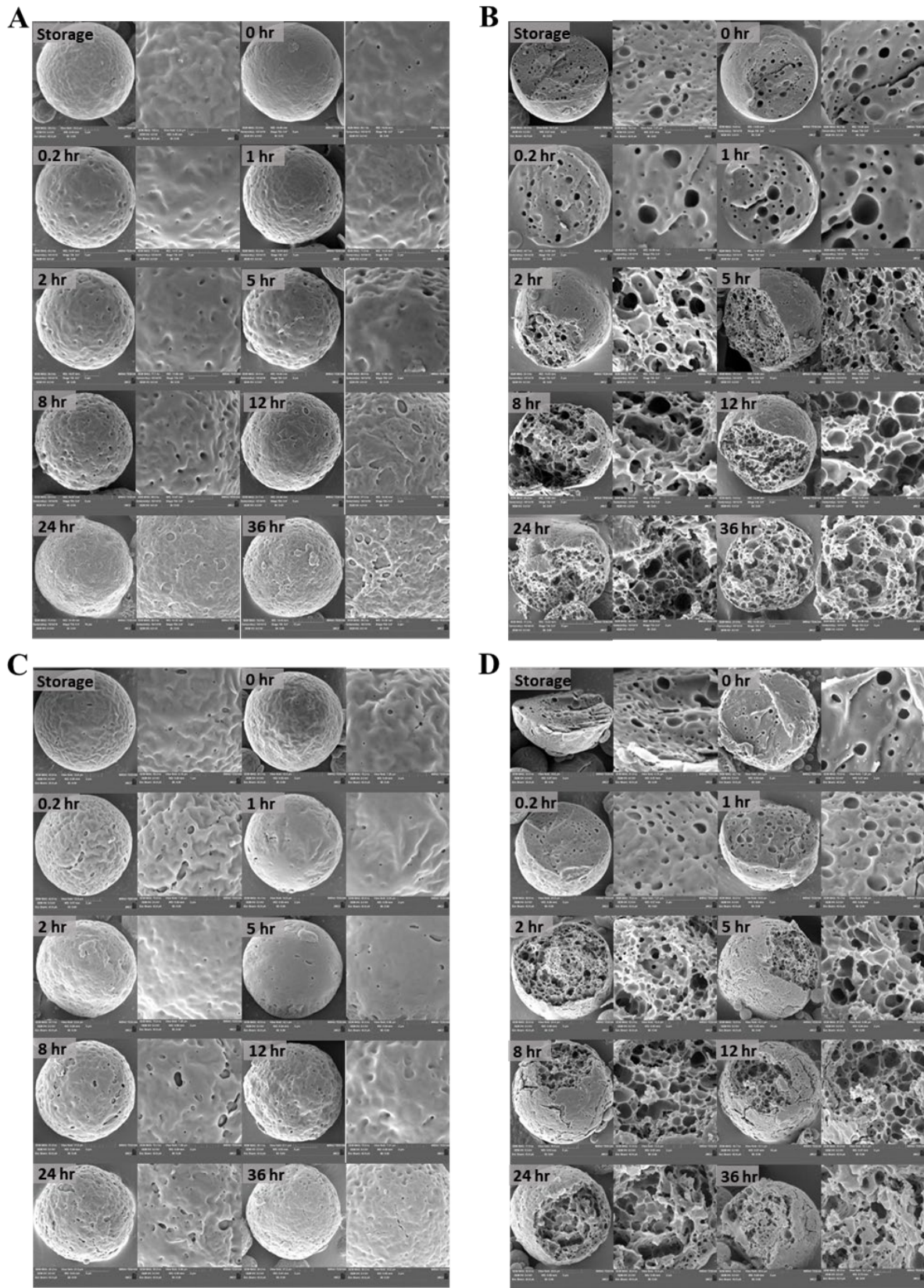


Figure S2-8. External morphology (A, C) and internal structure (B, D) of  $T_{feed}$  25°C (A, B) and 37°C microspheres (C, D) from storage and after 0, 0.2, 1, 2, 5, 8, 12, 24, and 36 hours of incubation in the continuous monitoring system. Left image shows full microsphere. Right shows high magnification (field view = 7.2  $\mu$ m).

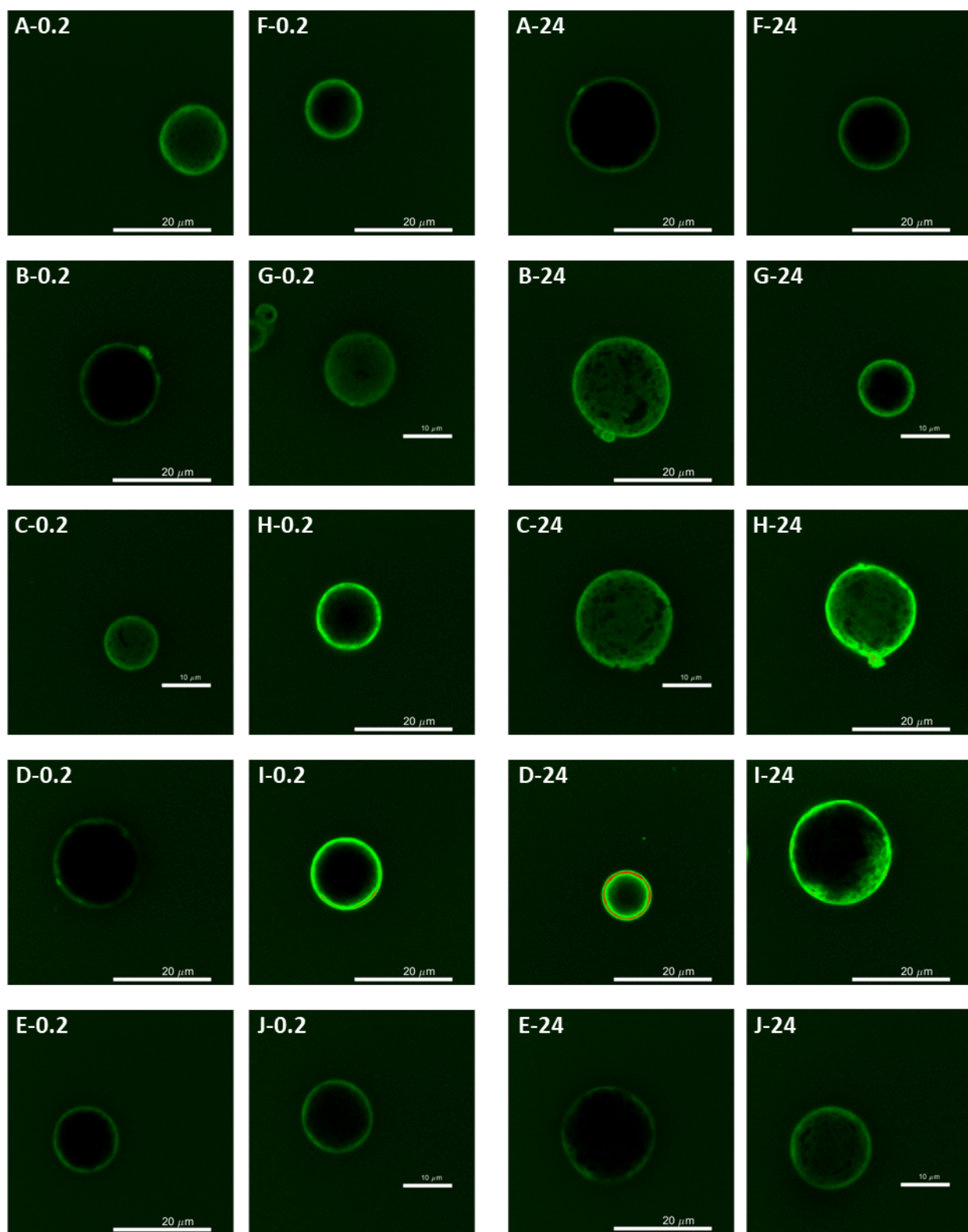


Figure S2-9. Confocal images of dye penetration of bodipy-dextran in  $T_{inlet}$  50°C (A),  $C_{feed}$  30% (B),  $AF_{nozzle}$  13.0 (C) and 16.0 (D) L/min,  $Ratio_{A/L}$  2.0 (E) and 8.0 (F),  $S_{nozzle}$  0.6 (G) and 1.2 mm (H), and  $T_{feed}$  25°C (I) and 37°C (J) after 30 min incubation at 37°C with 0.2 hr (left) and 24 hr (right) of pre-incubation in the continuous monitoring

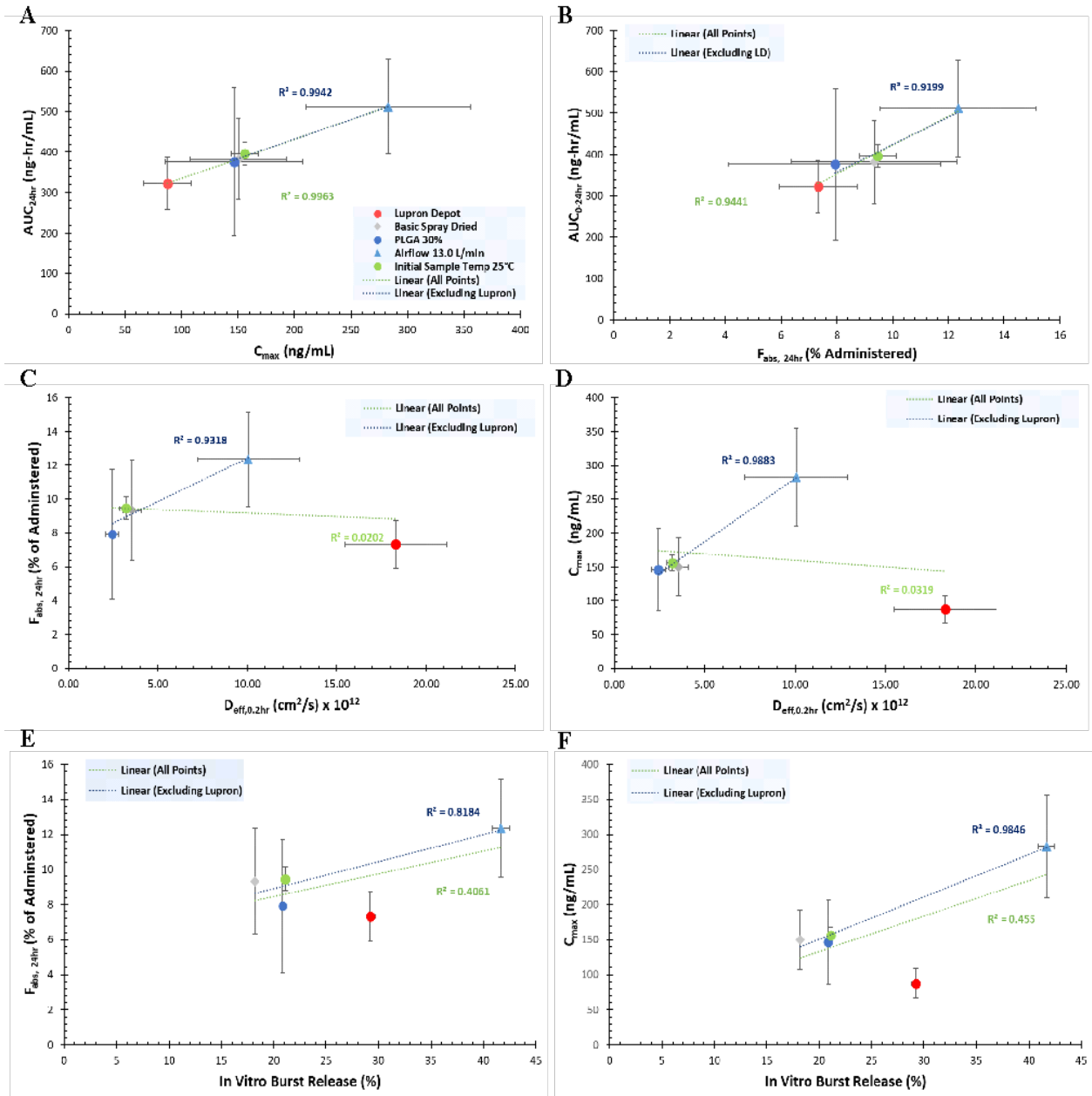


Figure S2-10.  $C_{max}$  heavily influences  $AUC_{0-24hr}$  (A). Pharmacokinetic parameters are highly correlated in first 24 hr (A, B).  $C_{max}$  (D, F) and the fraction absorbed at 24 hr (C, E) are compared to other calculated parameters from in vitro testing: effective diffusion coefficients at 0.2 hr (C, D) and cumulative fraction released at the end of the initial burst in the continuous monitoring system (E, F). Correlations are determined for all spray-dried formulations without (blue) or with (green) including Lupron Depot<sup>®</sup>. Error bars show  $\pm SE$ .

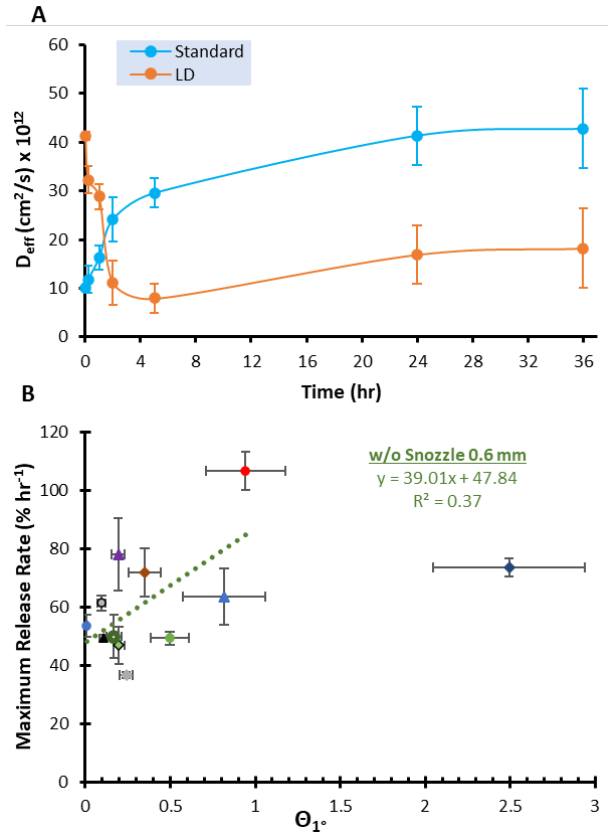


Figure S2-11. Effective Diffusion coefficients of unconjugated bodipy from 30 minutes incubation at 37°C after different periods of pre-incubation in the continuous monitoring system. Error bars show  $\pm SE$  ( $n=5-10$ ) (A). Maximum rate compared to dimensionless times (B).

## **Chapter 3 Optimization of a Coaxial Electropray System for Etonogestrel-loaded Core-Shell Poly(D,L-lactide) Microparticles (ENG csMPs) and Effect of Shell Composition**

### **3.1 Introduction**

With trends in recent years, there have been significant interest that long-acting contraceptives because the reversibility, increased efficacy, and cost-effectiveness makes them attractive [1]. Implants such as Nexplanon<sup>®</sup>, which require administration from trained health care professional, are less desirable in areas with low healthcare access. Other shorter duration products such as pills, intravaginal rings or transdermal have high failure rates due to poor compliance and incorrect application [2]. For these reasons, long-acting injectable contraceptive can be especially appealing. Currently on the market, the only injectable contraceptive is Depo-Provera. Depo-Provera releases a progestin-like steroid—medroxyprogesterone acetate—for 3-month due to its slow intra-muscular adsorption rate. The release of Depo-Provera is dissolution-controlled and, consequently, has high initial medroxyprogesterone plasma levels. In addition, it suffers from a delayed return to fertility has a high inter-patient variability [3,4].

In previous work, core-shell microparticles of controlled size and shell thickness, which contained a third-generation progesterone—etonogestrel—were produced by coaxial electropray. The drug-rich core is surrounded by a medium molecular weight PLA and was able to achieve a drug loading of over 50% w/w with an encapsulation efficiency greater than 90% as well as

pharmacokinetics that could make it suitable for 3 months of sustained contraceptive release [5]. However, this formulation was difficult to characterize due to low yields (10~15%). In addition, a significant fraction of encapsulated drug was released *in vitro* in the first month (40-60%), preventing the formulation from achieving the desired six months of release. The present work focused on addressing these issues and improving the release kinetics for 6 months both *in vitro* and eventually *in vivo* without reducing the high encapsulation efficiency. The approach investigated modifications to the electrospray system and the effect of using alternative polymers in the shell layer.

## **3.2 Materials and Methods**

### **3.2.1 Materials**

Poly(D,L-lactide) (PLA) polymer (Resomer® R205S, inherent viscosity: 0.55–0.75 dL/g, ester terminated; Resomer® R203S, inherent viscosity: 0.25–0.35 dL/g, ester terminated), polyvinyl alcohol (PVA) (M<sub>w</sub> 13,000-23,000, 87-89% hydrolyzed), polycaprolactone (PCL) (average M<sub>n</sub> 45,000) as well as all other chemicals were purchased from Sigma-Aldrich, Inc (St. Louis, MO, USA). Micronized etonogestrel with purity more than 99.9% was purchased from Industriale Chimica S.R.L (Saronno, Italy). HPLC and LCMS grade solvents were purchased from Fisher Scientific (Hampton, NH, USA).

### **3.2.2 Preparation of ENG-core-shell microparticles by coaxial electrospray**

ENG-loaded cs-MPs were prepared using a coaxial needle (Ramé-hart instrument, Succasunna, NJ, USA) with a 15-gauge outer needle and 25-gauge inner needle. The core solution was comprised of PLA (10% w/v) and ENG (30% w/v) in chloroform, while the shell solution was PLA (15% w/v) in chloroform\ethyl acetate (1:1 v/v). GASTIGHT® syringes (Hamilton®)

containing these solutions were driven using two syringe pumps (Fisher Scientific) at a flow rate of 0.5 mL/hr. A high voltage to the needle (14-17 kV) and a ring electrode (10 kV) were placed 20 mm from the needle via two voltage generators (range: 0–30 kV, Gamma High Voltage Research, Ormond Beach, FL, USA). The particles were sprayed into a grounded aluminum container (10”x3”, round) containing 0.25% PVA with or without 5% NaCl and a magnetic stirrer (Fisher Scientific). The spray bath was transferred to a beaker and placed under an overhead stirrer at 600 rpm for 2 hours to evaporate residual organic solvents. After drying, aggregates were removed using a 125 µm sieve, and particles were collected using a 20 µm sieve and 3 µm nylon vacuum filter (Millipore Sigma) after thoroughly rinsing away spray bath additives with distilled water. Collected particles were lyophilized for 48 hours and then stored at room temperature with desiccant. Voltages for different formulations were optimized to produce an approximate particle size of 20-30 µm by examination of particles under a bright field microscope after spraying onto glass microscope slides.

### ***3.2.3 Determination of ENG drug loading and encapsulation efficiency***

ENG drug loading was determined by ultraviolet absorbance at 245 nm measured by ultra-high performance liquid chromatography (UPLC) (Acquity, Waters Corp., Milford, MA, USA) equipped with a UV detector. Approximately 5 mg of ENG-cs-MPs were dissolved in 25 mL of acetonitrile and vigorous vortexing. 25 mL of water was added followed by additional vortexing before further dilution by 50% v/v acetonitrile in water. The final solution was centrifuged at 20,000 x g for 10 min, and 10 µL were injected into a Waters ACQUITY BEH C18 column (1.7 µm, 100 mm × 2.1 mm id) at 50°C with a mobile phase of a mixture of acetonitrile and water (55:45 v/v) containing 0.1% formic acid. The flow rate was set at 0.3 mL/min.

### ***3.2.4 In Vitro Release Studies***

Approximately 3 mg of ENG-cs-MPs were placed into a nylon mesh bag with a pore size of 1  $\mu\text{m}$  (NMO1FMC, Midwest Filter, LLC, St. Charles, IL, USA). The bag was submerged initially into 200 mL of PBS (phosphate buffered saline, pH 7.4) with 0.05 % (w/v) sodium azide and agitated in an incubator (MaxQ™ 6000, Thermo Fisher Scientific, Waltham, MA, USA) at 80 rpm at 37 °C. At 1, 3, 7 days and every week thereafter, 0.5 mL of media was collected, the outside of the bags was rinsed with distilled water and the release media was completely replaced. After 14 days, the bags were transferred to a smaller glass bottle and 50 mL of release media to maintain a quantifiable concentration. Release media were centrifuged, and 100  $\mu\text{L}$  of the upper layer were taken and stored at 4°C in Waters 300  $\mu\text{L}$  polypropylene UPLC vials until quantification. ENG concentrations in release media were determined by UPLC after the addition of equal volumes of acetonitrile and vortexing.

### ***3.2.5 Characterization of thermal properties and etonogestrel solid-state***

Glass transition ( $T_g$ ), melting and recrystallization enthalpies and temperatures were determined by a modulated Q2000 differential scanning calorimeter (DSC) (TA Instruments, New Castle, DE, USA). 2-5 mg were sealed into Tzero® aluminum DSC pans. Samples were heated under a nitrogen atmosphere from -20°C to 250°C at 10°C/min to characterize recrystallization and melting events of ENG. Samples were then cooled at 15°C/min to -20°C and heated again to 100°C at 15°C/min to determine the glass transition temperature of PLA. Results were analyzed in TA TRIOS software (TA Instruments). Drug crystallinity was calculated by:

$$\% \text{ Relative Crystallinity} = \frac{\Delta H_m - \Delta H_R}{\Delta H_{m,ENG} * DL} \quad (3-1)$$

where  $\Delta H_m$  is the melting enthalpy measured for ENG in microparticles,  $\Delta H_R$  is the enthalpy of recrystallization events for microparticles, and  $\Delta H_{m,ENG}$  is the melting enthalpy of pure etonogestrel.

### 3.3 Results and Discussion

#### 3.3.1 Yields and performance of new system design

The coaxial electro spray method for producing core-shell microparticles was constructed as shown in Figure 3-1. The design was similar to previous work [5] with the addition of a copper ring electrode attached to a secondary voltage source and 5% sodium chloride to the spray bath. The original design suffered from poor yields (10~15%) and Taylor cone instability, which led to needle blockages, polymer aggregation, and cone multi-jets. Beside polymer aggregates forming

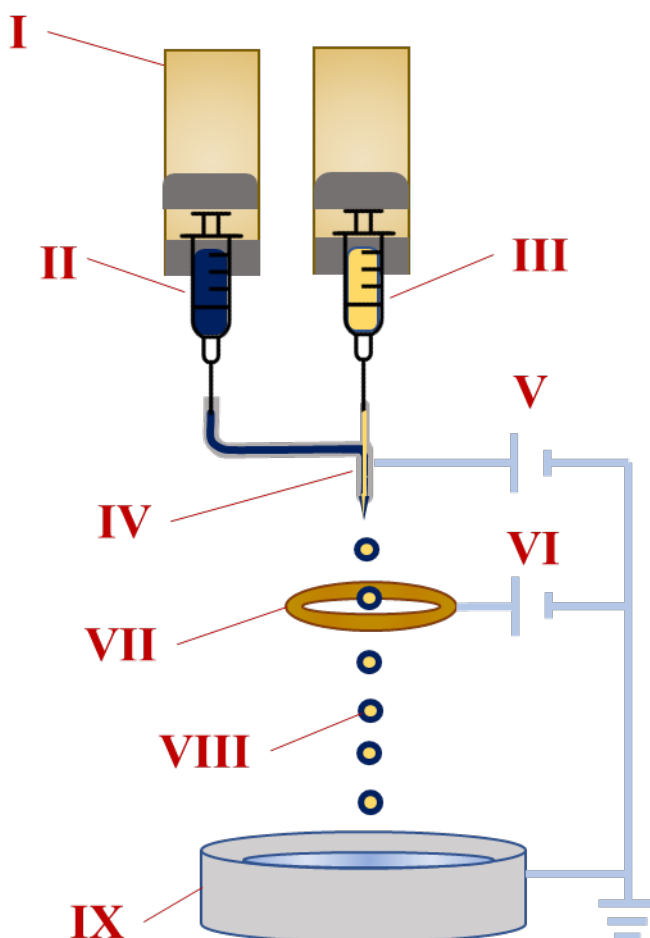


Figure 3-1. Diagram of coaxial electro spray system. Syringe pumps (I) control the flow rate of outer, shell solution (II) and inner core solution (III) through a coaxial needle (IV). The coaxial needle is connected to voltage source (V). Core-shell micro-droplets (VIII) can be focused through a copper ring electrode (VII) connected to voltage source (VI) and collected into aluminum vessel (IX) containing the spray bath solution, which is connected to the common ground.

in the spray bath, a significant source of loss was accumulation of particles on the side and outside of the grounded aluminum collection vessel. As shown in Figure S3-1 the ring-shaped electrode led to a reduced spray area evidenced by the greater accumulation of particles onto black paper in the absence of the collection vessel. The intermediate electrode focuses the electric field [6], which charged particles would be expected to travel along, and can prevent Taylor cone instabilities [6–9]. While on paper the ring electrode appeared to be beneficial, yields after collection using the aluminum pan containing 0.25% PVA were not significantly different from the previous configuration. It was suspected that the solution was not sufficiently grounded since it was poorly conductive compared to the high-walled metal container. To direct charged particles into the solution, 5% w/v NaCl was added to increase the conductivity of the spray bath. The combination of the ring electrode and salt led to yields consistently over 25% with the standard formulation having a yield of  $35.6 \pm 2.5\%$ .

### ***3.3.2 In vitro release of standard formulation***

In order to achieve the desired near zero-order rates for a consistent 6 months of drug release, proper engulfment and encapsulation of the drug core are essential. Other works have primarily relied on thermodynamically stable structures driven by low interfacial tension between immiscible organic shell solution and aqueous core solutions relative to the interfacial tension between aqueous core and surrounding air [9–12]. Because the hydrophobic nature of both the polymer and drug and their limited solubility in many solvents, chloroform is used as a primary solvent. While similar solvents would be expected to have low interfacial tension and prevent separation of inner and outer solutions, the miscibility of the solutions could lead to the rapid diffusion of ENG from core to shell in the drying droplet.

Based on previously developed formulations [5], ethyl acetate, which has a lower solubility for ENG than chloroform, was used as a shell cosolvent to prevent drug migration. In addition, 10% polymer in the core may help retard diffusion from the core by increasing its viscosity. Overall, these changes improved the encapsulation efficiency [5], but the standard without the ring electrode and electrolyte solution released greater than 50% of the loaded ENG in the first month

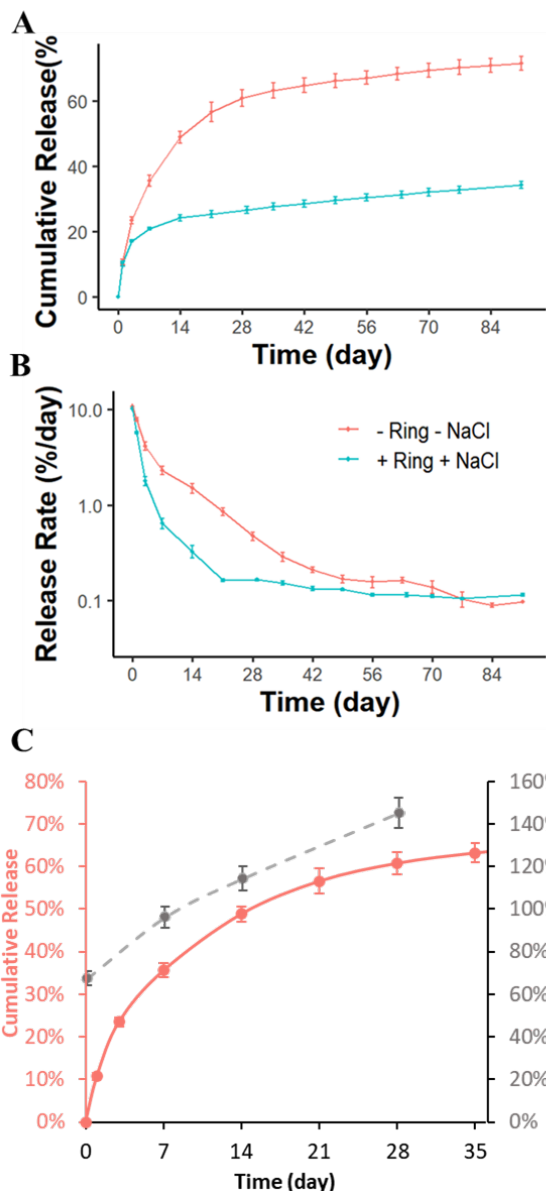


Figure 3-2. Cumulative release (A) and release kinetics (B) of cs-MPs made with and without system modifications. Relative crystallinity over the course of the first month for particles made without system modifications (C). ( $n = 3$ , mean  $\pm$  SEM)

(Figure 3-2A), suggesting incomplete engulfment of the core within the shell. Rates eventually plateaued to  $\sim 0.2\%/day$  at 42 days and remained at that level for the next two months of release (Figure 3-2B), which could be related to the depletion of more superficial drug reservoirs. The ring-stabilized formulation showed a significant reduction in this rapid release phase and released only  $\sim 22\%$  before the rates plateaued to a similar level as the ringless formulation at 21 days.

Based on these results, the Taylor cone instability during spraying appeared to have translated to incomplete/poor engulfment of the core within the shell, which could be reduced by the introduction of electrolytes in the collection solution and a ring electrode. The poorly encapsulated core allowed for the highly

amorphous drug phases to diffuse out rapidly in early time points. DSC thermographs of both formulations show exothermic events at 70 to 75°C and 90 to 95°C. Melts followed by rapid quenches of pure etonogestrel and physical mixtures with PLA confirm these to correspond to the recrystallization from amorphous solid dispersion of the drug in the polymer and separate amorphous drug phases, respectively (Figure S2). The net enthalpy of all etonogestrel melting and recrystallization events in the first heating cycle was used to calculate the relative crystallinity of etonogestrel in particles through (3-1). The initial crystallinity for the ringless formulation was 61.9±3.4%. As the release continued, the crystallinity continued to increase and reached 100% at the end of the first month (Figure 3-2C) when rates began to plateau. The coincidence of increased crystallinity and constant release rates suggests that the amorphous phase may provide an increased driving force for those superficial drug reservoirs from incomplete core engulfment.

### 3.3.3 Effect of PLA molecular weight in shell on release

Five new shell compositions using R203S (7.5, 15, 30, 50, and 100% w/w) were made with the total polymer concentration of the shell solution constant at 15% w/v. As expected, all five formulations showed larger amounts of release in the first 3 days during the rapid release phase.

Interestingly, all rates plateaued at similar times around 7 days of release. High concentrations of

Table 3-1. Compositions and yields of PLA blend formulations

Formulation	Core in CF		Shell in CF/EA (1:1)		Measured Drug Loading %	Encapsulation Efficiency %	Yield %
	R205S (% w/v)	ENG (% w/v)	R205S (% w/v)	R203S (% w/v)			
-Ring -NaCl Standard (+Ring +NaCl)			15	0	54.2 ± 1.0	98.5 ± 1.8	12.5
<b>7.5:92.5</b>	10	30	13.875	1.125	45.2 ± 0.3	84.6 ± 0.6	20.1
<b>15:85</b>			12.75	2.25	43.9 ± 0.5	84.7 ± 0.9	39.9
<b>30:70</b>			10.5	4.5	48.2 ± 0.6	89.8 ± 1.1	25.8
<b>50:50</b>			7.5	7.5	45.7 ± 0.6	88.0 ± 1.2	40.0
<b>R203S</b>			0	15	38.3 ± 1.2	73.1 ± 2.3	45.2

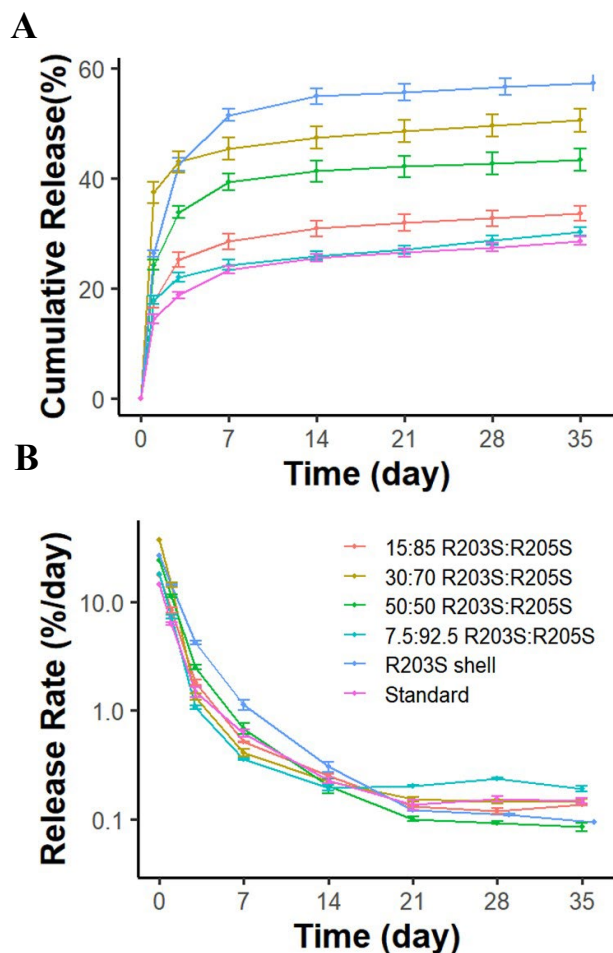


Figure 3-3. Cumulative release (A) and release kinetics (B) of cs-MPs made with varying blends of Resomer® R203S and R205S. (n = 3, mean ± SEM)

R203S (50% and 100%) showed high rapid phase release, but long-term rates (day 21 – 35) were lower than pure R205S, which may be related to depletion of more superficial drug domains, or faster loss and/or recrystallization of amorphous drug. Additionally, the diffusion path length could have been increased due to swelling of the more hydrophilic, lower molecular weight R203S. It is this behavior that could also explain the rapid release of the 30% R203S. At lower percentages, R205S could be expected to preferentially precipitate on the surface of the particle due to its lower solubility. R205S would then act as a barrier

to water uptake and prevent the subsequent increased void volume caused by R203S swelling. At 30%, the R205S barrier may be only partial and the amount of R203S would not be enough to swell homogenously, leading to increased void space and faster release.

### 3.3.4 Alternative polymers in shell and the effect on release

In addition to using a lower molecular weight PLA, the inclusion of other polymers in the shell was also investigated to determine the extent the release could be modified. Two polymers--polyethylene glycol (PEG) and polycaprolactone (PCL)—that both had a molecular weight average of 45kDa were tested.

Table 3-2. Compositions and yields when using alternative polymer in shell of csMPs

Formulation	Core in CF		Shell in CF/EA (1:1)			Measured Drug Loading %	Encapsulation Efficiency %	Yield %
	R205S	ENG	R205S	Second Polymer	Poly. Conc (%)			
3.3% PEG			14.5	PEG-45kDa	0.5	51.0 ± 0.5	97.3 ± 1.0	43.4
13% PEG	10	30	13	PEG-45kDa	2	47.4 ± 0.7	89.6 ± 1.3	32.1
100% PCL			0	PCL 45kDa	15	48.2 ± 0.7	92.2 ± 1.2	42.8
30% PCL			10.5	PCL 45kDa	4.5	51.2 ± 0.9	97.9 ± 1.7	38.9

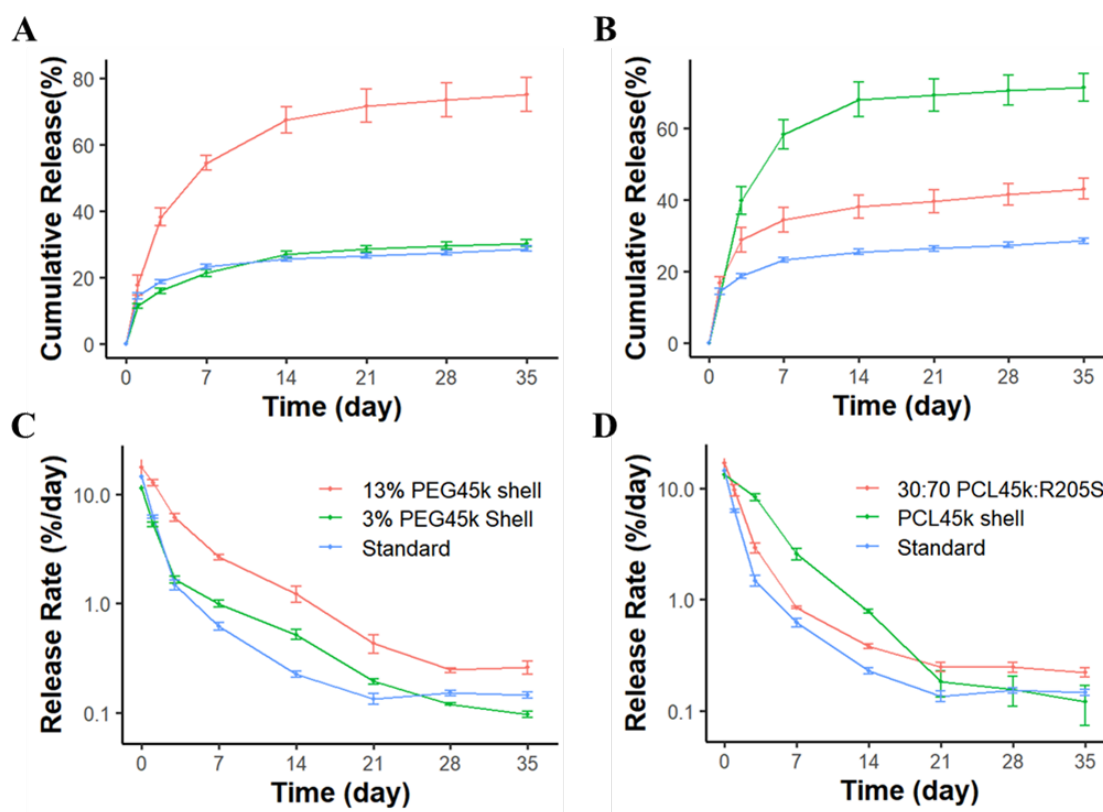


Figure 3-4. Cumulative release (A, B) and release kinetics (C, D) of cs-MPs with shells containing PEG 45kDa (A, C) or PCL 45kDa (B, D).

PEG, which is a water-soluble polymer, was used to help enhance the permeability of the shell. This would serve as an alternative to reducing the thickness by lowering the polymer concentration, which could lead to renewed Taylor cone instability or poor core encapsulation. During the solvent evaporation step or early stages of release, the PEG in the shell could be expected to leach out and reduce the overall mass of the shell. The permeability of the shell would

then be enhanced either by voids left in the polymer if the PEG leaches rapidly or by the thinning of the shell if it is sufficiently slow to allow remodeling of the remaining polymer.

In line with expectations, the high molecular weight PEG maintained the encapsulation efficiency and drug loading as shown in Table 3-2. The PEG also appeared to enhance the permeability of the shell. With a 3% PEG shell, rates from day 3 to 7 stayed at around 1%/day, which may correspond to the period where PEG was leaching out of the shell (Figure 3-4B). After this, the rates were similar to the standard formulation. If the PEG content is quadrupled to 13%, the initial release in the first 2 week is tripled to  $67.4\pm 3.9\%$ . Because the high concentration, the extraction of PEG into release media likely more rapidly as there was less PLA to act as a barrier. The extracted PEG would then leave voids which increase the release until the PLA could remodel and heal. The long-term rates remained high around  $0.31\pm 0.7\%$ /day at the end of the first month, which would be consistent with thinner or more permeable shell.

PCL was also expected to enhance the permeability. The semi-crystalline nature leads PCL to degrade slower and have reduced permeability compared to amorphous poly(D,L-lactic acid)s. A low molecular weight PCL, which has a lower solubility than a low molecular weight PLA, could have better encapsulation of the core but increased overall permeability. To test this hypothesis, a blend of the R205S PLA and PCL as well as PCL alone was investigated. Unlike the pure R203S shell, the PCL shell showed a high encapsulation efficiency and no loss of drug loading; the same was true for the 30/70 blend with R205S (Table 3-2). Similar to R203S, PCL increased the initial release in the first week to two weeks. Shown in Figure 3-4B and D, the 30% PCL blend released less in the first week ( $38.1\pm 3.2\%$ ) compared to the same ratio of R203S ( $47.4\pm 2.1\%$ ) but maintained a slightly higher long-term rate than both the R203S 30/70 blend and the standard R205S shells at  $0.22\pm 0.02\%$ . A pure PCL shell, on the other hand, release significantly

more than a pure R203S in the first two weeks ( $68.1\pm 4.9\%$  vs.  $54.8\pm 1.5\%$ ), but like the R203S was similar in the long-term. The better performance of R203S alone may be related to the homogeneous swelling that could occur mentioned earlier while PCL alone would have an overall higher diffusion than R205S but would not swell significantly to compensate.

### **3.4 Conclusion**

The major sources of loss in the present electrospray process were found to be the accumulation of sprayed core-shell droplets outside the collection vessel as well as the aggregation of soft, incompletely dried particles inside the collection solution. The addition of an intermediate ring electrode and inclusion of sodium chloride in the collection solution was capable of focusing the electric field and directing particles into solution, which doubled to tripled yields. In addition, the initial drug release in the first week was reduced by greater than 50% due to the increased Taylor cone stability and subsequent improved engulfment of the core within the shell. Changing the shell composition to lower molecular weight polymer were capable of increasing this initial release and increasing the long-term rates and could be adjusted by the ratio of medium molecular weight PLA to other polymers such as a low molecular weight PLA, PEG, or low molecular weight PCL. Overall, the particles showed tunability without significant changes in drug loading.

### 3.5 References

- [1] M.L. Kavanaugh, J. Jerman, Contraceptive method use in the United States: trends and characteristics between 2008, 2012 and 2014, *Contraception*. 97 (2018).  
<https://doi.org/10.1016/j.contraception.2017.10.003>.
- [2] B. Winner, J.F. Peipert, Q. Zhao, C. Buckel, T. Madden, J.E. Allsworth, G.M. Secura, Effectiveness of Long-Acting Reversible Contraception, *New England Journal of Medicine*. 366 (2012). <https://doi.org/10.1056/nejmoa1110855>.
- [3] L.M. Wren, Depo Provera: still controversial., *International Health News / National Council for International Health*. 9 (1988).
- [4] E.B. McDaniel, T. Pardthaisong, Depot-medroxyprogesterone acetate as a contraceptive agent: Return of fertility after discontinuation of use, *Contraception*. 8 (1973).  
[https://doi.org/10.1016/0010-7824\(73\)90163-7](https://doi.org/10.1016/0010-7824(73)90163-7).
- [5] J. Tang, R. Schutzman, C.A. Rodríguez, J. Lahann, N. Rodríguez-Hornedo, M.R. Prausnitz, S.P. Schwendeman, Coaxial electrospray of uniform polylactide core-shell microparticles for long-acting contraceptive, *Journal of Controlled Release*. 341 (2022).  
<https://doi.org/10.1016/j.jconrel.2021.12.017>.
- [6] Y. Kuwahata, H. Takehara, T. Ichiki, Comprehensive study on electrospray deposition in the single Taylor cone-jet mode by changing the spatial electric potential using a ring-shaped ternary electrode, *AIP Adv.* 10 (2020). <https://doi.org/10.1063/1.5142317>.
- [7] J. Xie, J.C.M. Marijnissen, C.H. Wang, Microparticles developed by electrohydrodynamic atomization for the local delivery of anticancer drug to treat C6 glioma in vitro, *Biomaterials*. 27 (2006). <https://doi.org/10.1016/j.biomaterials.2006.01.034>.

- [8] J. Xie, C.H. Wang, Electrospray in the dripping mode for cell microencapsulation, *J Colloid Interface Sci.* 312 (2007). <https://doi.org/10.1016/j.jcis.2007.04.023>.
- [9] T. Si, L. Zhang, G. Li, C.J. Roberts, X. Yin, R. Xu, Experimental design and instability analysis of coaxial electrospray process for microencapsulation of drugs and imaging agents, *J Biomed Opt.* 18 (2013). <https://doi.org/10.1117/1.jbo.18.7.075003>.
- [10] S. Zhang, C. Campagne, F. Salaün, Influence of solvent selection in the electro spraying process of polycaprolactone, *Applied Sciences (Switzerland)*. 9 (2019). <https://doi.org/10.3390/app9030402>.
- [11] L. Zhang, J. Huang, T. Si, R.X. Xu, Coaxial electrospray of microparticles and nanoparticles for biomedical applications, *Expert Rev Med Devices*. 9 (2012) 595–612. <https://doi.org/10.1586/erd.12.58>.
- [12] J. Xie, W.J. Ng, L.Y. Lee, C.H. Wang, Encapsulation of protein drugs in biodegradable microparticles by co-axial electrospray, *J Colloid Interface Sci.* 317 (2008) 469–476. <https://doi.org/10.1016/j.jcis.2007.09.082>.

### 3.6 Supplementary Materials

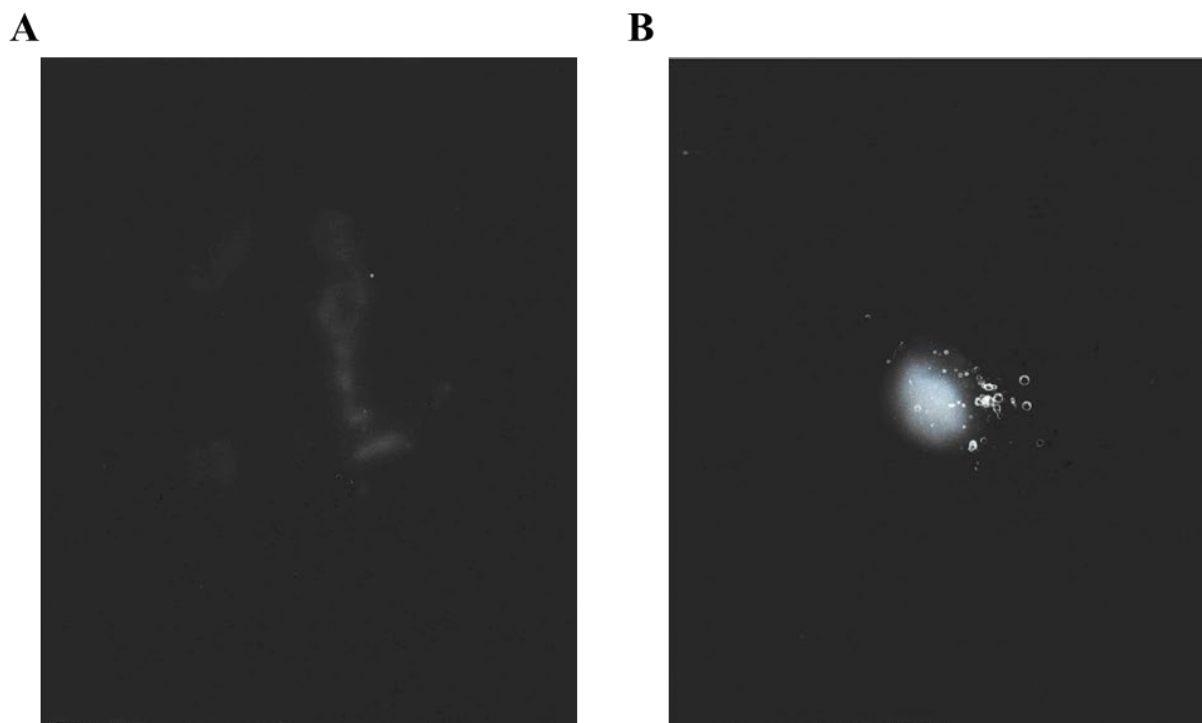


*Figure S3-1. Accumulation of microparticles on black paper after 20 minutes of spraying without (A) and with (B) the ring electrode.*

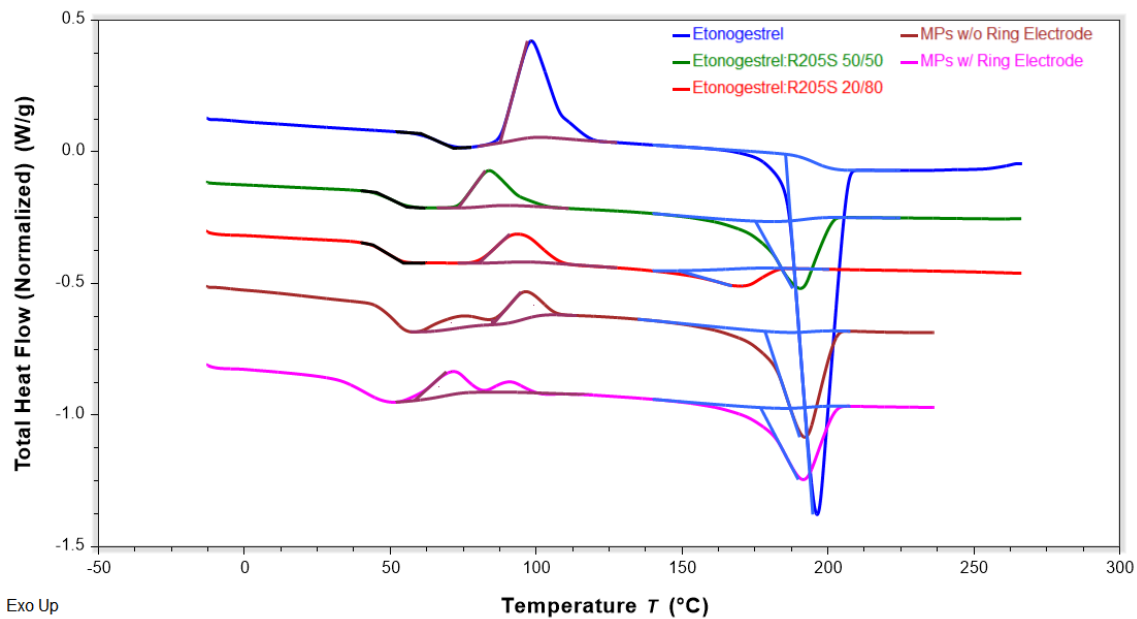


Figure S3-2. DSC thermographs of pure etonogestrel, physical mixes with Resomer<sup>®</sup> R205S PLA, and electrospayed microparticles made with and without the ring electrode.

## **Chapter 4 Improving the Long-term ENG Release Kinetics of Injectable csMPs by Controlling Particle Morphology and Drug Crystallinity**

### **4.1 Introduction**

As discussed in Chapter 3, the solid-state of etonogestrel appeared to strongly affect the release rates *in vitro*. The release rates decreased as the crystallinity of ENG inside the csMPs increased. This can be explained by the corresponding decrease in drug solubility and decrease in the driving force for diffusion. Previous studies with risperidone [1] and naltrexone [2] have demonstrated relationships in PLGAs between drug crystallinity and release. The primary conclusion was that residual solvents resulted in the reduced crystallinity and various drug solvates. Residual solvents in PLGAs and PLAs can act as plasticizers as well and reduce the glass transition temperature of PLGA [3] and accelerated degradation [1]. Overall, in a similar way, high residual solvents have been associated with increased initial release rates [4] because the corresponding decrease in the resistance to diffusion. The crystallinity was increased in the risperidone and naltrexone formulations by introducing longer drying stages and a secondary extraction of residual solvents with 25% ethanol for 4 hours [2]. The temperature and extent of exposure to ethanol through parameters such as ethanol concentration and length of treatment was correlated with different degrees of extraction for solvents like benzyl alcohol [1]. The purpose of

this study was to investigate extraction of residual and changes in crystallinity by different methods and extents of ethanol as well as the morphology of the particles.

## **4.2 Materials and Methods**

### ***4.2.1 Materials***

Poly(D,L-lactide) (PLA) polymer (Resomer® R205S, inherent viscosity: 0.55–0.75 dL/g, ester terminated), polyvinyl alcohol (PVA) (Mw 13,000-23,000, 87-89% hydrolyzed) as well as all other chemicals unless otherwise specified were purchased from Sigma-Aldrich, Inc (St. Louis, MO, USA). Micronized etonogestrel with purity more than 99.9% was purchased from Industriale Chimica S.R.L (Saronno, Italy). HPLC and LCMS grade solvents were purchased from Fisher Scientific (Hampton, NH, USA).

### ***4.2.2 Preparation of ENG-core-shell microparticles by coaxial electrospray***

ENG-loaded cs-MPs were prepared using a coaxial needle (Ramé-hart instrument, Succasunna, NJ, USA) with a 15 gauge outer needle and 25 gauge inner needle. The core solution was comprised of PLA (10% w/v) and ENG (30% w/v) in chloroform while the shell solution was PLA (15% w/v) in chloroform\ethyl acetate (1:1 v/v). GASTIGHT® syringes (Hamilton®) containing these solution were driven using two syringe pumps (Fisher Scientific) at a flowrate of 0.5 mL/hr. A high voltage to the needle (14-17 kV) and a ring electrode (10 kV) placed 20 mm from the needle via two voltage generators (range: 0–30 kV, Gamma High Voltage Research, Ormond Beach, FL, USA). The particles were sprayed into a grounded aluminum container (10”x3”, round) containing 0.25% PVA and 5% NaCl and a magnetic stirrer (Fisher Scientific) with or without ethanol and/or surfactants. The spray bath was transferred to a beaker and placed under an overhead stirrer at 600 rpm for 2 hours to evaporate residual organic solvents. After

drying, aggregates were removed using a 125- $\mu\text{m}$  sieve and particles were collected using a 20  $\mu\text{m}$  sieve and 3  $\mu\text{m}$  nylon vacuum filter (Millipore Sigma) after thoroughly rinsing away spray bath additives with distilled water. Collected particles were lyophilized for 48 hours and then stored at room temperature with desiccant. Voltages for different formulations were optimized to produce an approximate particle size of 20-30  $\mu\text{m}$  by examination of particles under bright field microscope after spraying onto glass microscope slides.

#### ***4.2.3 Ethanol treatment of csMPs during solvent evaporation (Drying)***

csMPs were sprayed into collection media without ethanol. After electro spraying of particles was completed, the collection media was divided into equal two parts. Both were placed under overhead stirrer at 600 rpm. To one part, ethanol was slowly introduced until the solution was the desired concentration of ethanol. The same collection procedure was followed as 4.3.2.

#### ***4.2.4 Resuspension of csMPs with ethanolic solution (Rinse)***

75 mg of csMPs that were collected from media without ethanol and lyophilized were resuspended in 15 mL of 25% v/v ethanol in water. After vortexing for 30 sec, the suspension was centrifuged at 3,200 x g for 10 min and the supernatant was discarded. This resuspension and separation process was repeated twice. Particles were then resuspended with 1 mL water and lyophilized for 48 hours.

#### ***4.2.5 Incubation of csMPs with ethanol vapor (Vapor)***

75 mg of csMPs that were collected from media without ethanol and lyophilized were placed onto a 5x5 cm tray and spread out using a spatula. A chamber with a closed vial of ethanol was pre-equilibrated to the desired temperature. The vial was opened, and the chamber was sealed for 4 hours prior to particle incubation to allow the ethanol vapor to equilibrate. The

tray with particles was placed into chamber for 24 hours. After incubation, the tray was placed under vacuum for 48 hours to remove residual ethanol vapor.

#### ***4.2.6 Determination of ENG drug loading and encapsulation efficiency***

ENG drug loading was determined by ultraviolet absorbance at 245 nm measured by ultra-high performance liquid chromatography (UPLC) (Acquity, Waters Corp., Milford, MA, USA) equipped with a UV detector. Approximately 5 mg of ENG-cs-MPs were dissolved in 25 mL of acetonitrile and vigorous vortexing. 25 mL of water was added followed by additional vortexing before further dilution by 50% v/v acetonitrile in water. The final solution was centrifuged at 20,000 x g for 10 min and 10 µL were injected into a Waters ACQUITY BEH C18 column (1.7 µm, 100 mm × 2.1 mm id) at 50°C with a mobile phase of mixture of acetonitrile and water (55:45 v/v) containing 0.1% formic acid. The flow rate was set at 0.3 mL/min.

#### ***4.2.7 Scanning electron microscopy (SEM)***

The morphology of particles was examined using a Tescan MIRA3 FEG electron microscope (TESCAN Brno, s.r.o., Kohoutovice, Czech Republic). Gold was sputtered onto particles for 60 s at 40 W under vacuum after mounting onto brass studs via double-sided tape.

#### ***4.2.8 In Vitro Release Studies***

Approximately 3 mg of ENG-cs-MPs were placed into a nylon mesh bag with a pore size of 1 µm (NMO1FMC, Midwest Filter, LLC, St. Charles, IL, USA). The bag was submerged initially into 200 mL of PBS (phosphate buffered saline, pH 7.4) with 0.05 % (w/v) sodium azide and agitated in an incubator (MaxQ™ 6000, Thermo Fisher Scientific, Waltham, MA, USA) at 80 rpm at 37 °C. At 1, 3, 7 days and every week thereafter, 0.5 mL of media was collected, the outside

of the bags were rinsed with distilled water and the release media was completely replaced. After 14 days, the bags were transferred to a smaller glass bottle and 50 mL of release media to maintain a quantifiable concentration. Release media were centrifuged and 100  $\mu$ L of the upper layer were taken and stored at 4°C in Waters 300  $\mu$ L polypropylene UPLC vials until quantification. ENG concentrations in release media were determined by UPLC after addition of equal volumes of acetonitrile and vortexing.

#### ***4.2.9 Residual Solvent Quantification***

Gas chromatography by a ThermoSci Trace 1310 gas chromatographer with a flame ionization detector was used to determine residual chloroform, ethyl acetate and ethanol in ENG-cs-MPs. Approximately 10 mg of microparticles were dissolved in 1 mL of DMSO. Measurements were performed in triplicate with a nitrogen carrier at 25 mL/min. Solvents were detected with air flow at 350 mL/min, hydrogen flow at 35 mL/min at 240°C, and inlet flow at 2 mL/min. Samples were agitated for 20 min at 80°C before injecting 1 mL of the headspace with a split flow of 40 mL/min, split ratio of 20 and the headspace needle at 140°C. The column was initially set at 40°C for 15 min, then ramped to 240°C at 10°C/min, and held at 240°C for 2 min. The detection limit (signal-to-noise ratio = 3) was 2.3, 6.7, and 0.6 ppm for ethanol, chloroform, and ethyl acetate, which corresponded to 0.021, 0.06, and 0.0055% w/w in csMPs.

#### ***4.2.10 Characterization of thermal properties and etonogestrel solid-state***

Glass transition ( $T_g$ ), melting and recrystallization enthalpies and temperatures were determined by a modulated Q2000 differential scanning calorimeter (DSC) (TA Instruments, New Castle, DE, USA). 2-5 mg were sealed into Tzero<sup>®</sup> aluminum DSC pans. Samples were heated under a nitrogen atmosphere from -20°C to 250°C at 10°C/min to characterize recrystallization

and melting events of ENG. Samples were then cooled at 15°C/min to -20°C and heated again to 100°C at 15°C/min to determine the glass transition temperature of PLA. Results were analyzed in TA TRIOS software (TA Instruments). Drug crystallinity was calculated by:

$$\% \text{ Relative Crystallinity} = \frac{\Delta H_m - \Delta H_R}{\Delta H_{m,ENG} * DL} \quad (4-1)$$

where  $\Delta H_m$  is the melting enthalpy measured for ENG in microparticles,  $\Delta H_R$  is the enthalpy of recrystallization events for microparticles and  $\Delta H_{m,ENG}$  is the melting enthalpy of pure etonogestrel.

### 4.3 Results and Discussion

More soluble amorphous ENG has been linked to faster drug release in csMPs [5]. As ethanol has been used during the encapsulation and drying of risperidone- [1] and naltrexone- [2] PLGA microspheres, the use of ethanol in the preparation of csMPs encapsulating ENG was investigated. Ethanol was introduced through four different routes: (1) the collector media during spraying; (2) the collector media during the typical drying step; (3) an ethanolic solution used to rinse particles after the first lyophilization; and (4) ethanol vapor in a sealed chamber after the first lyophilization. These are referred to as ethanol spraying, drying, rinsing, and vapor treatments, respectively. The extent of exposure was controlled primarily through the concentration of ethanol that was used in the process except for vapor treatments, which utilized temperature to control the vapor pressure of ethanol in the chamber, while all other things remained equal such as the length of the treatment.

#### 4.3.1 Encapsulation efficiency and yield of ethanol treatments

The drug loading and encapsulation efficiency was measured to determine the effect of ethanol exposure. Ethanol has the potential to extract ENG from csMPs during treatment since

Table 4-1. Yields and loading of various ethanol-treated formulations

Treatment					Measured Drug Loading	Encapsulation Efficiency	Yield/ Recovery
Exposure Type	Step in Production	Temperature	Conc (%)	Time (hr)			
Vapor	Post-production	4°C	-	24	50.4 ± 0.2	97.6 ± 0.4	-
Vapor	Post-production	25°C	-	24	44.3 ± 1.7	81.3 ± 3.2	-
Solution (2x Rinse)	Post-production	25°C	25	Immediate	45.4 ± 0.3	86.7 ± 0.6	82.0 (Recovery)
Collector Media	Drying/Solvent Evaporation	25°C	10	2	51.5 ± 0.2	99.6 ± 0.4	38.3
Collector Media	Drying/Solvent Evaporation	25°C	25	2	46.1 ± 0.5	89.1 ± 0.9	22.5
Collector Media	Spraying	25°C	25	4	45.7 ± 0.2	85.3 ± 0.3	15.1
Collector Media	Spraying	25°C	40	4	44.9 ± 0.6	83.5 ± 1.0	30.5

the solubility of ENG in ethanol is approximately 50 times greater than water [6]. As shown in Table 4-1, the treatment of csMPs did not affect the encapsulation of ENG in csMPs. The drug loadings of all treatments were similar to untreated particles (46.1±0.2%, Table 3-1). Because ENG was confined to the core, exposure appeared to be insufficient to extract ENG and produce a decrease in encapsulation efficiency. In addition, ethanol in the drying step lead to an apparent increase in drug loading and perfect encapsulation efficiency. The ethanol improved dispersion of particles that had aggregated during the spraying as evident by the increase of the yield from 28.2% to 38.3%. The previously lost fraction may have been responsible for the increase in drug loading. The low temperature vapor treatment demonstrated that the removal of a significant fraction of residual solvent could have also contributed to the improved encapsulation as both showed treatments showed a near complete removal of solvents.

#### 4.3.2 Ethanol treatments effects on residual solvents and crystallinity

The residual solvents of formulations treated by these various methods are shown in Figure 4-1A through 4-1C. The amount of residual chloroform trended with the extent of exposure

between different treatments. Without treatment, the standard formulation showed  $1.44 \pm 0.08\%$  and  $0.023 \pm 0.001\%$  for chloroform and ethyl acetate, respectively. The drying treatment with 10% ethanol, where ethanol was added during the 2-hour solvent extraction phase, showed a modest decrease in chloroform and ethyl acetate to  $0.85 \pm 0.01\%$  and  $0.0067 \pm 0.0001\%$  w/w. Increasing the concentration to 25% ethanol led to a near-complete removal of chloroform, and complete removal of ethyl acetate within the detection limit. However, rising with 25% ethanol two times only showed reduced chloroform to the same extent that the 10% drying treatment was able.

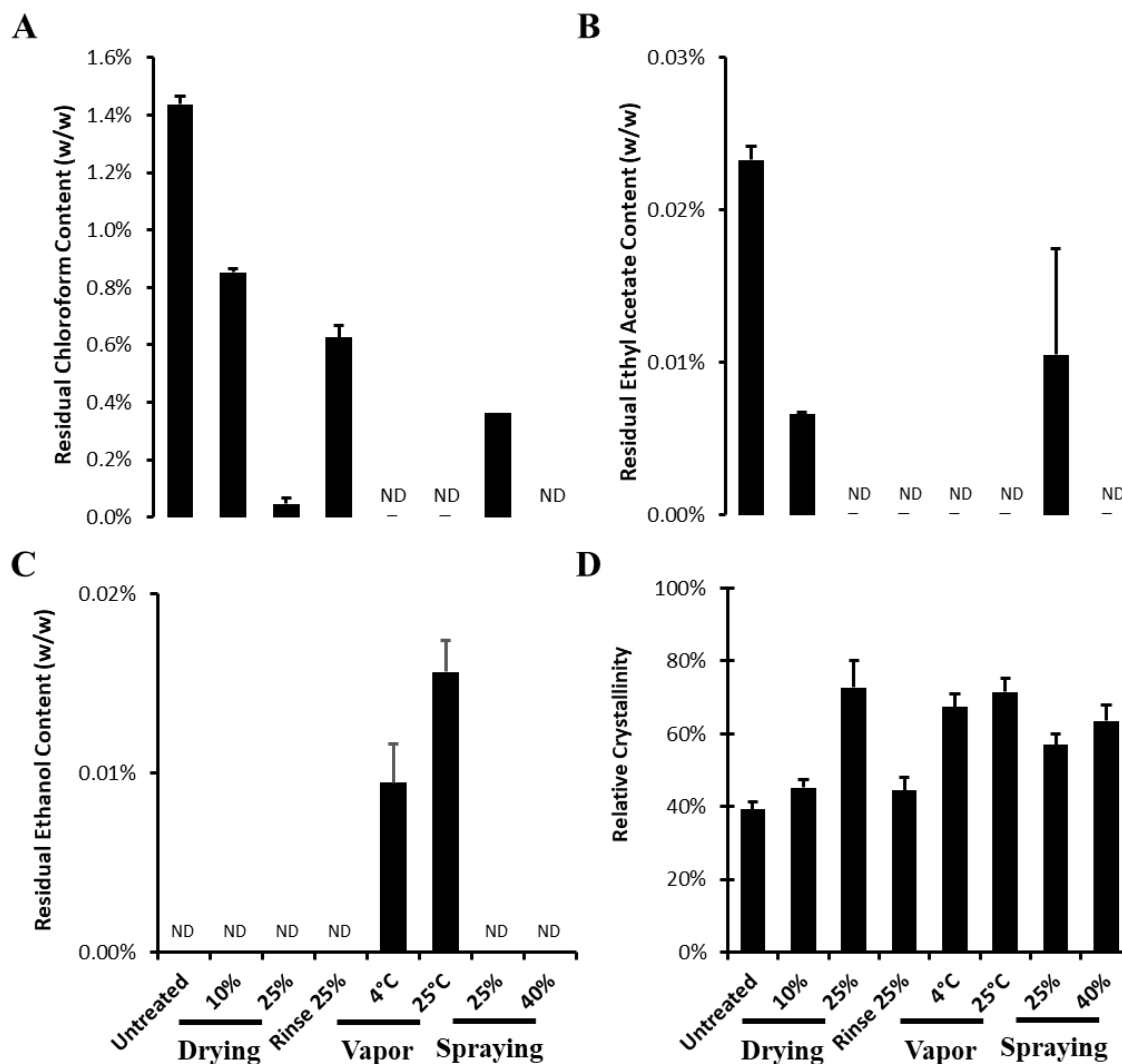


Figure 4-1. Residual chloroform (A), ethanol and ethyl acetate (B) of lyophilized microparticles after spraying into ethanol or after post-spray treatments with ethanol (drying, vapor, or rinsing) and their effect on etonogestrel crystallinity (C). (n=3, mean  $\pm$  SEM) ND = not detected.

Interestingly, only brief exposure to ethanol was capable of completely extracting the residual ethyl acetate from the newly formed csMPs.

The initial extraction of ethyl acetate was expected to be faster than that of chloroform. Ethyl acetate is only present in the particle shell feed solution and therefore could be expected to be easier to extract than chloroform, which is also present in the core feed. In addition, despite its higher boiling point than chloroform, ethyl acetate is 10 times more soluble in water [7,8]. It can be seen in Figure 4-1 that the amount of solvent extracted relative to the untreated particles was always greater for ethyl acetate compared to chloroform. Even in the absence of water, exposure to ethanol through vapor for one day completely removed the original solvents. The vapor may have had a significant plasticization effect, which was evident by the aggregation of particles after exposure (not shown), that facilitated the mass transfer of the solvents. The low partial pressure of chloroform and ethyl acetate in the incubation chamber and the lowered resistance to mass transport allowed the extraction of these residual solvents while ethanol also appeared to penetrate the polymer significantly enough to leave residual ethanol. During drying under vacuum, extraction of ethanol near the particle surface may have reduced ethanol diffusion and created a barrier to extraction. The concentration of residual ethanol increased with higher temperatures and demonstrated that vapor pressure can increase the overall ethanol exposure. Interestingly, although, by adding ethanol during spraying, particles would be exposed to ethanol throughout spraying as well as drying (additional 1~3 hours), the 25% spraying condition showed more residual solvents than only adding ethanol up to 25% after spraying (25% drying). By increasing the concentration to 40%, all residual solvents could be removed with only modest losses of drug encapsulation efficiency (Table 4-1).

As expected, the extent of the solvent removal correlated with the relative crystallinity of ENG in particles (Figure 4-1C). Untreated particles had a relative crystallinity of  $39.2 \pm 1.8\%$ . The 10% drying and 25% rinse treatments, which showed similar residual solvent levels, also had similar crystallinities at  $45.2 \pm 2.3\%$  and  $44.4 \pm 3.7\%$ , respectively. The highest crystallinity attainable was around 70% with the 25°C vapor condition achieving a crystallinity of  $71.6 \pm 3.6\%$ . No recrystallization events were observed for vapor treated particles. The inability of achieving complete crystallinity might be related to metastable states. Additionally, reduction in the enthalpy of the first recrystallization event occurred preferentially to the second recrystallization. This less stable amorphous phase converted with less aggressive treatments such as rinsing while the enthalpy of the more stable did not decrease significantly unless treated with 40% spraying or vapor. Although solid-state conversion may be expected upon heating during DSC, the possibility of a non-detectable metastable supersaturation of drug in the polymer cannot be excluded, since these fractions may be soluble in the polymer at the temperatures required for conversion of amorphous to crystalline.

#### ***4.3.3 Release from ethanol-treated csMPs***

The release for each treatment was tested over one month to determine the effect of changes in residual solvents and crystallinity. All treatments and levels had very distinct rapid release and long-term release phases (Figure 4-2). The 25% drying condition showed a slight reduction in the initial week compared to the untreated particles but reached a similar level at day 14. The release rate remained 1.5 times as fast ( $0.302 \pm 0.009\%/day$  vs.  $0.200 \pm 0.005\%/day$ ) for the remainder of the month. In contrast, 10% showed no significant difference in either phase compared to the untreated particles. Rinsing with 25% ethanol did not appear to show a very strong rapid release phase but showed an overall faster and more steady release rate, which was  $0.46 \pm 0.025/day$  at day

35. The behavior of vapor was similar to that of the rinsed condition, but more accelerated. For 25°C vapor treated particles, the release rate was nearly constant for the entire release period and

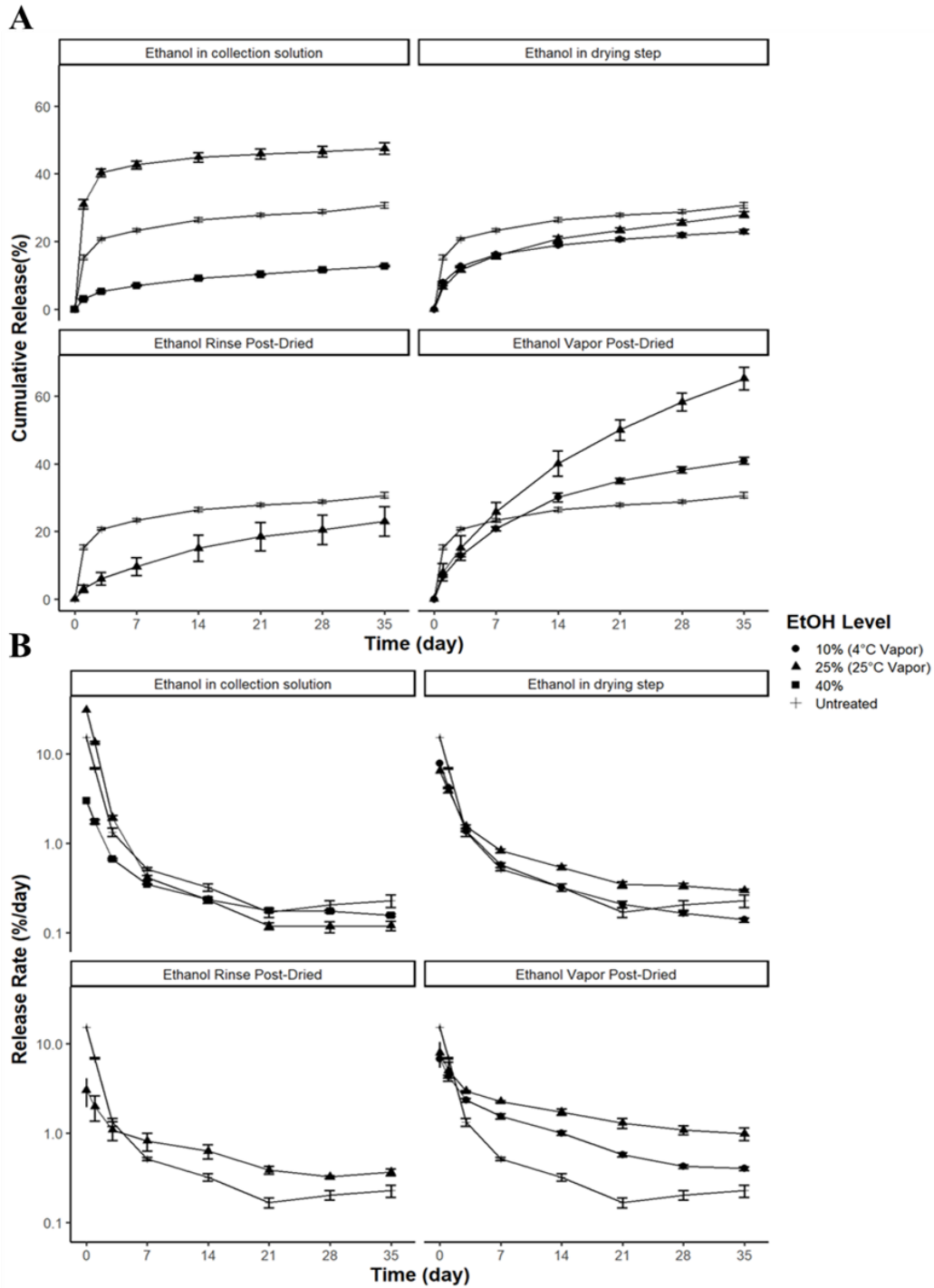


Figure 4-2. Cumulative release (A) and release rates (B) of csMPs after treatment with ethanol during spraying (lower left), during drying (upper left), and after lyophilizing through rinsing (upper right) or exposure to ethanol vapor (lower right). Marker shape denote the concentration of ethanol in solution for all conditions except treatment with vapor, which is the incubation temperature (see legend).

was at  $0.7 \pm 0.1\%$ /day on day 35, which lead to over 50% drug release in one month. While vapor treatment at  $4^\circ\text{C}$  was very similar to the higher temperature in the release amounts and rates that were reached at the end of release, the behavior appeared to be less linear and more first-order as the rates showed a log-linear decay. Overall, reducing residual solvents and increasing crystallinity did lead to some reduction in the initial week of release, but residual ethanol, especially in the vapor treated particles, may have led to long-term acceleration. In contrast to this, ethanol spraying conditions show drastic differences in the rapid release. At 25% ethanol in the spray bath, drug release jumped to over 40% in the first 3 days. On the other hand, increasing to 40% caused the 14-day release to drop only  $9.1 \pm 0.3\%$ . Release rates plateaued after this period with both formulations reaching levels less than the untreated group.

#### 4.3.4 Morphology of csMPs sprayed in ethanolic solutions

To better understand the differences between particles sprayed into various levels of ethanol, the morphology of the csMPs was examined under SEM. While under bright-field microscope untreated standard csMPs appear circular and were considered to be spherical, closer investigation with SEM revealed that they were disc shaped (Figure 4-3A). The diameter was

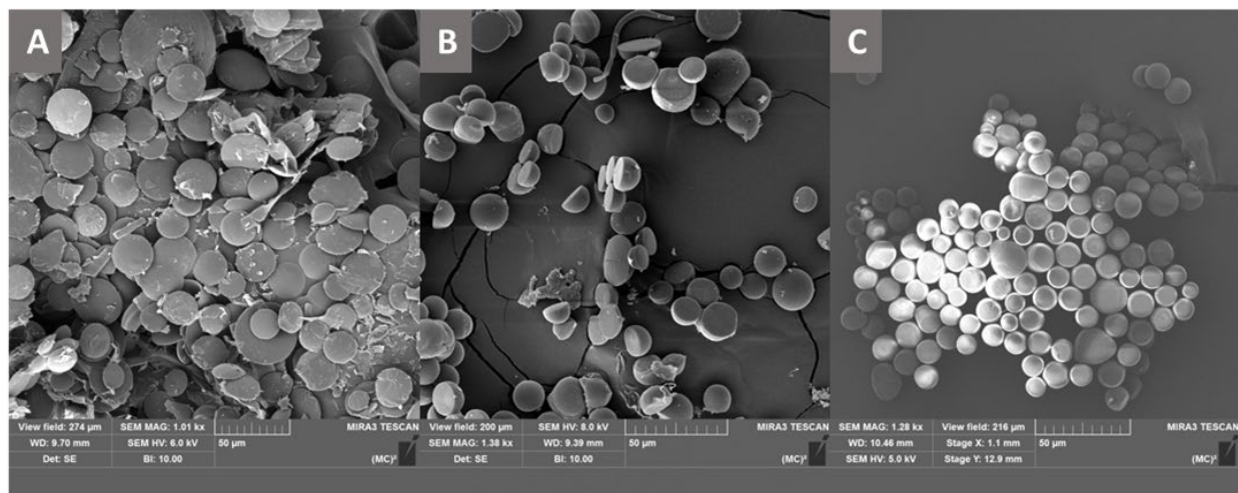


Figure 4-3. Morphology of core-shell particles without surface tension modifiers (A), 25% Ethanol (B) and 40% Ethanol (C).

around 20-30  $\mu\text{m}$  which is consistent with calculations from bright-field images ( $24.7 \pm 0.2 \mu\text{m}$ ), but the disc showed a thickness of around 2-3  $\mu\text{m}$ . would lead to a significantly higher surface area to volume and consequently faster release. For example, if the disc is represented a cylinder, the surface-volume ratio of a disc with a diameter of 25  $\mu\text{m}$  and thickness of 3  $\mu\text{m}$  would be 0.83. On the other hand, 14  $\mu\text{m}$  sphere, which would be the same volume, would have a surface-volume ratio of 0.43, making the disc 1.9 times greater. Adding 25% ethanol to the collection solution created particles that were hemispherical (Figure 4-3B). The surface area would still be less than the disc-shaped, but these hemispherical microparticles have a large fraction released in the first three days. Higher magnification (Figure S4-1) reveal that the flat surface of the hemisphere is porous, which explains the rapid initial release. Healing of the medium MW PLA is expected to be slower than the PLGA in Chapter 2 and therefore the rate plateau on day 3 could be related to this delayed healing. When the concentration of ethanol in the collection solution is increased to 40%, the particles are undamaged spheres (Figure 4-3C). Initially, the rates of the untreated particles are on average 2 times higher than the 40% ethanol condition, while, after 14 days, they are closer to unity. It is possible that disc-shaped particles undergo remodeling, which is drive by surface tension of the polymer similar to pore healing.

#### ***4.3.5 Effect of spraying into various surfactant solutions on morphology***

The change in morphology was suspected to be the result of the collector solution surface tension. The embryonic microparticles still have a significant fraction of solvents before entering the solution and would be highly deformable. Incomplete drying of particles has led to unsmooth particle surfaces and polymer films on filter collectors [9]. In this case, to enter into solution, the particle must displace the solution and will therefore experience an impact force related to the solution surface tension since this is the energy required to increase the surface. According to

Table 4-2. Yields and loading of formulations after using different surfactants in collection media and with or without addition of ethanol during solvent evaporation step

Treatment			Measured Drug Loading %	Encapsulation Efficiency %	Yield %
Surfactant	Conc (μM)	Post-Spray Treatment			
Tween 80	40	-	52.0 ± 0.7	97.4 ± 1.3	45.0
Tween 80	40	25% Drying	50.7 ± 0.6	81.3 ± 3.2	40.6
Span 80	80	-	51.3 ± 0.4	95.0 ± 0.8	35.3
Span 80	80	25% Drying	49.3 ± 0.4	91.4 ± 0.7	25.2
Pluronic L121	10	-	51.8 ± 0.5	97.5 ± 0.9	69.1
Pluronic L121	10	25% Drying	47.7 ± 1.6	89.7 ± 3.0	60.7
Triton X-100	40	-	51.3 ± 0.7	97.4 ± 1.3	45.4
Triton X-100	40	25% Drying	50.2 ± 0.4	95.5 ± 0.8	41.5

literature, the surface tension of 25 and 40% v/v ethanol solution at 25°C would be approximately 38 and 32 mN/m, respectively, compared to 72 mN/m for water without ethanol [10–12]. It has been shown that electrospraying PLGA into methanol and ethanol created particles with concave and disc-like morphologies, but additional of surfactants like Tween 80 and oleic acid created particles with more spherical shapes [13]. Low concentrations of Tween 80 and polyethylene glycol have also been shown to prevent aggregation of PLA nanoparticles, which may be beneficial for increasing yields [14]. A major portion of material loss for spraying into ethanol solutions was aggregation, which reduced the yield for the formulation with 25% ethanol to only 15% (Table 4-1).

To determine the role of surface tension in the collection media and whether aggregation could be prevented, the addition of Tween 80, Span 80, Pluronic L121 and Triton X-100 was tested at concentrations slightly above their critical micellar concentration (CMC) found in literature to ensure the solution surface was saturated with surfactant. All surfactants selected were non-ionic but differ in their HLB values, water solubility, and equilibrium surface tension. All showed increased yields that were over 40% with the exception of span 80. Encapsulation efficiency and

drug loading were similar to that of the standard formulations, so no drug was lost due to increased solubilization (Table 4-2). Interestingly, addition of Pluronic L121 showed no particle aggregation and yield reached 69.1%. Use of surfactants in collection vehicles while electrospraying and nanoprecipitation were able to improve the dispersion of nanoparticles and reduce their particle size in previous studies [13,15,16]. The Pluronic L121 has a very low HLB and may be better suited to improve dispersion of the very hydrophobic PLA. The addition of Pluronic L121 at this concentration also led to increased solution opacity, which is a sign of micelle formation. While

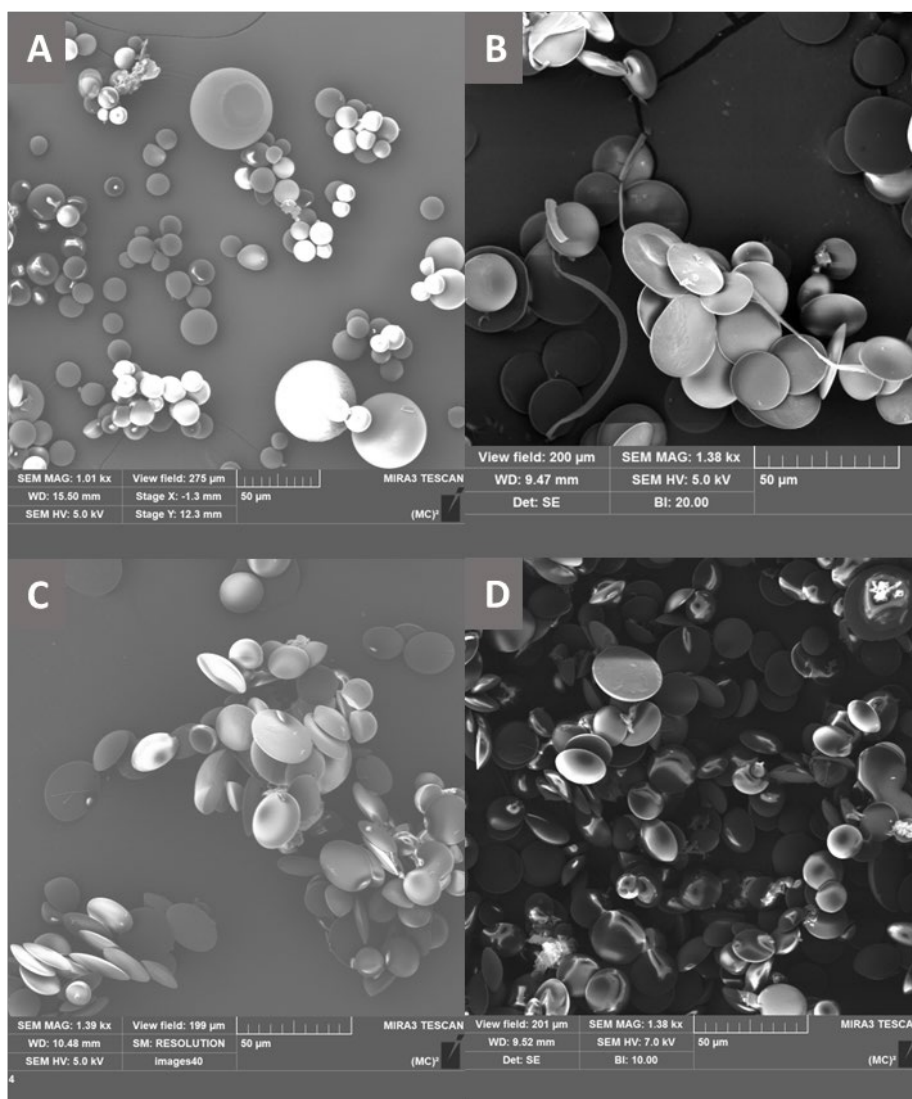


Figure 4-4. Morphology of core-shell particles with 250  $\mu\text{M}$  Triton X-100 (A), 40  $\mu\text{M}$  Tween 80 (B), 80  $\mu\text{M}$  Span 80 (C), and 10  $\mu\text{M}$  Pluronic L121 (D).

the other surfactant concentrations used were above their CMC, the concentration of micelles or their size may not have been sufficient to improve the dispersion of the particles.

Using 250  $\mu\text{M}$  Triton X-100 was able to successfully replicate the results of 40% ethanol results and spraying into this solution produced particles that were spherical (Figure 4-4A). When dissolved at the CMC, Triton X-100 has been found to have a surface tension of 31.4 mN/m [17], which is similar to that of 40% v/v ethanol. On the other hand, Pluronic L121 and Span 80 only showed a slight increase in the disc thickness (Figure 4-4C, D). At the concentrations tested, Pluronic L121 and Span 80 are expected to have a surface tension of approximately 35 [18,19] and 30 mN/m [20] respectively. While, based on the surface tension alone, Pluronic L121 may be expected to produce hemispheres or Span 80 to produce spheres, the low HLB value and subsequent low/negligible water solubility would prevent proper saturation of the solution surface with surfactant. This may impact the dynamic surface tension of the solution as it is highly agitated. Use of Tween 80, which is water-soluble, only reduces the surface tension of aqueous solutions to 38 mN/m [20,21]. The surface tension also increases to around 42 mN/m higher at the sodium chloride concentration used [21]. Solutions with Tween 80 also exhibit a much slower surface tension decay [21] compared to those with Triton X-100 [22] according to dynamic surface tension measures. Flat microparticles are consistent with the surface tensions mentioned.

#### ***4.3.6 Release kinetics of particles spraying into surfactant solutions***

Spraying into surfactant solutions produced particles with in vitro release profiles as shown in Figure 4-5 that are consistent with their morphologies. While there was some variability in the exact extent of the rapid phase, Pluronic L121, Tween 80, and Span 80 in the collection bath produced csMPs that displayed release kinetics very similar to that of disc-shaped untreated particles. Use of Span and Tween resulted in almost super-imposable release between those

prepared without surfactants. Pluronic, on the other hand, showed a slightly higher rapid phase and released  $35.4 \pm 1.7\%$  by two weeks compared to  $28.2 \pm 0.5\%$  and  $26.6 \pm 0.5\%$  for Tween 80 and Span 80, respectively. Long-term release rates at the end of the study were also slightly higher at

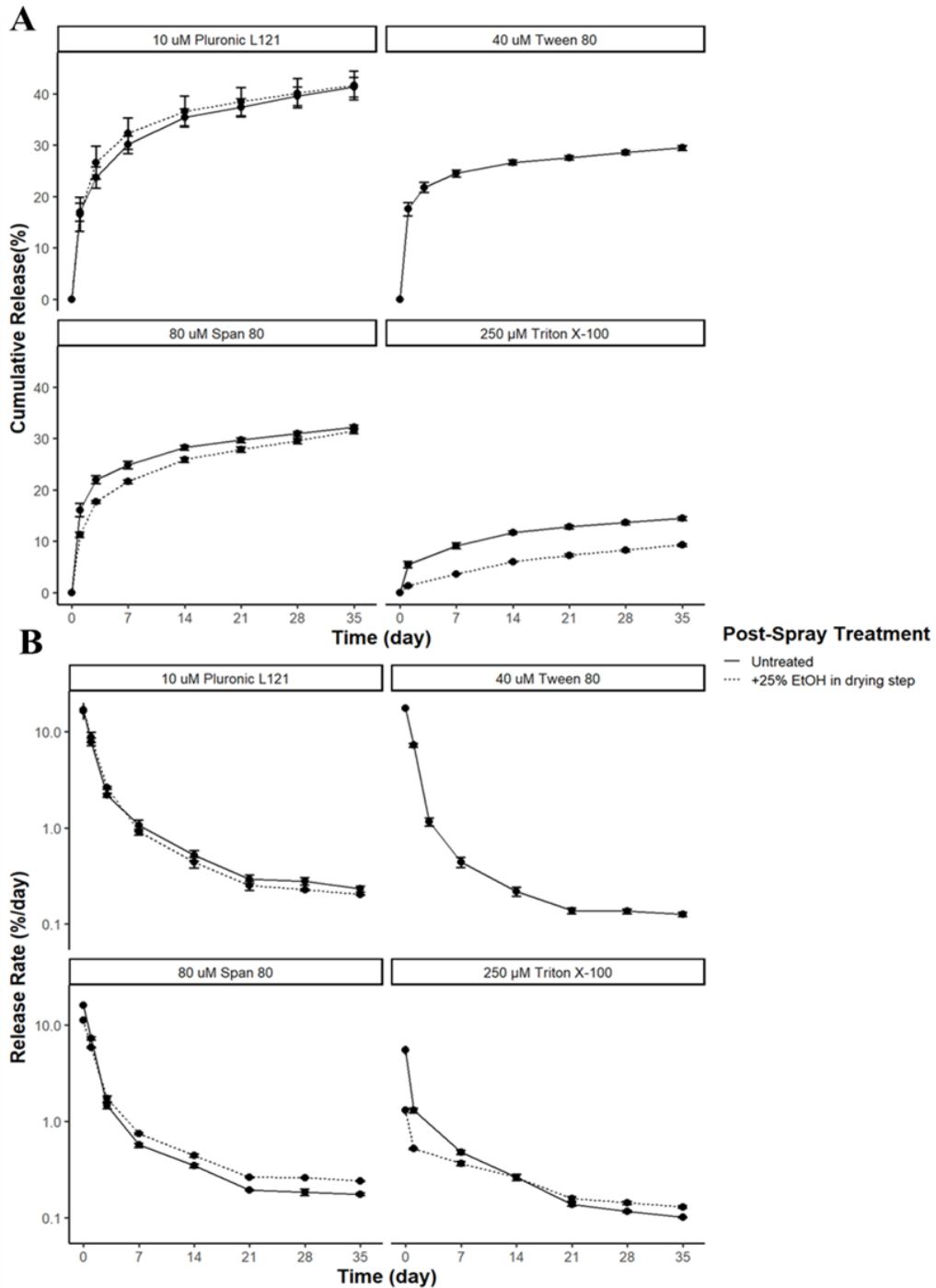


Figure 4-5. Cumulative release (A) and release kinetics (B) of cs-MPs after inclusion of Pluronic L121 (upper left), Tween 80 (upper right), Span 80 (lower left), or Triton X-100 (lower right) in the spraying bath with (solid) and without (dotted) drying in 25% ethanol.

0.23±0.02 %/day compared to 0.175±0.005 %/day and 0.127±0.007 %/day, respectively, but overall, all were similar to untreated csMPs. In contrast, csMPs prepared with Triton X-100 showed a reduction in the rapid phase similar to those prepared with 40% ethanol in the collector solution, with a 14-day release of 11.7±0.4%. The release rate was also reduced and was 0.101±0.002 %/day at the end of the release period.

Since the surfactants like Triton X-100 showed a change a morphology similar to ethanol, 25% ethanol was added during the drying to determine whether the effects of surfactants in the collection media and treatments with ethanol were additive. The use of 25% ethanol in the drying solution with Pluronic L121 in the collection media did not show a significant difference compared to csMPs produced with Pluronic L121 without ethanol. On the other hand, Span 80 showed a slight reduction in the initial release when csMPs were treated with ethanol compared to untreated particles, which was similar to previous results for 25% ethanol drying conditions without surfactants. The reduction in the release was more significant in the Triton group, and the rapid phase was nearly eliminated from the particles. The 14-day release was cut in half to 6.0±0.1%. The reduction may be related to the extraction of residual solvents. All untreated surfactant formulations showed higher residual chloroform and ethyl acetate than the untreated standard formulation (Figure S4-2A, C). After treatment of the csMPs with ethanol, no residual solvents were detected in formulation (Figure S4-2B, D). Additionally, the relative crystallinity for all formulations were high (>60%) (Figure S4-2E) and similar to crystallinity seen by spraying into 25% ethanol (Figure 4-1C). There were no significant differences between the crystallinity of untreated and ethanol-treated particles when spraying into surfactant solutions (Figure S4-2F). The results imply that, when the drug-filled core is properly encapsulated, the rapid release period is related to plasticization or increased void volume from residual solvents rather than an increased

driving force from amorphous drug. The combination of low residual solvents and proper morphology eliminated extraneous release in the first two weeks.

#### **4.4 Conclusion**

Ethanol treatments and inclusion of ethanol in different steps in the production of csMPs was successful in removing residual solvents and increasing the crystallinity of encapsulated ENG without strongly affecting the drug loading. The overall extent of the exposure was related to the total amount of residual solvents extracted and the change in crystallinity. Addition of ethanol to the collection solution during the solvent evaporation step shows a reduction in the initial release, but ethanol vapor significantly increased release likely owing to increased residual ethanol from the treatment and the resulting polymer plasticization as well as the increased osmotic activity.

The morphology of typical formulations before optimization was disc shaped. The sphericity of particles was increased by including ethanol in the collection solution during spraying, and virtually perfect spheres were achieved with 40% ethanol. The disc-shaped morphology and subsequent transformation appeared to be related to incomplete drying of the particles in the air. These soft particles collapsed upon impact with the collection solution. Reduction of surface tension via ethanol or strong surfactants such as Triton X-100 reduced the interfacial forces on impact to a degree that it was not significant enough to deform particles. These spherical particles also showed large reductions in the initial release, likely by increasing the diffusion barrier to the steroid. In addition, after removal of residual solvents by ethanol treatment, formulations prepared with Triton X-100 had no rapid release phase and achieved the ideal *in vitro* release profile. Hence, these approaches have yielded highly useful formulations for future pharmacokinetic testing.

## 4.5 References

- [1] M.E. Rickey, J.M. Ramstack, D.H. Lewis, J. Mesens, Preparation of extended shelf-life biodegradable, biocompatible microparticles containing a biologically active agent, US5792477A, 1997.
- [2] H.G. Brittain, D.A. Dickason, J.M. Hotz, S.L. Lyons, J.M. Ramstack, S.G. Wright, Polymorphic forms of naltrexone, US10328070B1, 2004.
- [3] S.G. Wright, T. Christensen, T. Yeoh, M.E. Rickey, J.M. Hotz, R. Kumar, H.R. Costantino, Polymer-based sustained release device, US8431685B2, 2005.
- [4] A. Beig, R. Ackermann, Y. Wang, R. Schutzman, S.P. Schwendeman, Minimizing the initial burst of octreotide acetate from glucose star PLGA microspheres prepared by the solvent evaporation method, *Int J Pharm.* 624 (2022) 121842.  
<https://doi.org/https://doi.org/10.1016/j.ijpharm.2022.121842>.
- [5] J. Tang, R. Schutzman, C.A. Rodríguez, J. Lahann, N. Rodríguez-Hornedo, M.R. Prausnitz, S.P. Schwendeman, Coaxial electrospray of uniform polylactide core-shell microparticles for long-acting contraceptive, *Journal of Controlled Release.* 341 (2022).  
<https://doi.org/10.1016/j.jconrel.2021.12.017>.
- [6] X.F. Chen, X.F. Gong, J. Xu, P. Li, H.P. Wang, L.F. Ning, Measurement and Correlation of the Solubility of Etonogestrel in Ten Pure and Binary Mixed Solvent Systems at Temperatures from 273.15 to 323.15 K, *J Chem Eng Data.* 65 (2020) 3190–3202.  
<https://doi.org/10.1021/acs.jced.0c00201>.
- [7] A.P. Altshuller, H.E. Everson, The Solubility of Ethyl Acetate in Water, *J Am Chem Soc.* 75 (1953). <https://doi.org/10.1021/ja01103a501>.

- [8] D. Mackay, A. Bobra, W.Y. Shiu, S.H. Yalkowsky, Relationships between aqueous solubility and octanol-water partition coefficients, *Chemosphere*. 9 (1980).  
[https://doi.org/10.1016/0045-6535\(80\)90122-8](https://doi.org/10.1016/0045-6535(80)90122-8).
- [9] J. Xie, J.C.M. Marijnissen, C.H. Wang, Microparticles developed by electrohydrodynamic atomization for the local delivery of anticancer drug to treat C6 glioma in vitro, *Biomaterials*. 27 (2006).  
<https://doi.org/10.1016/j.biomaterials.2006.01.034>.
- [10] D.H. Rasmussen, Dynamic surface tension and classical nucleation theory, *J Chem Phys*. 85 (1986). <https://doi.org/10.1063/1.451123>.
- [11] M. Sharma, P.K. Roy, J. Barman, K. Khare, Mobility of Aqueous and Binary Mixture Drops on Lubricating Fluid-Coated Slippery Surfaces, *Langmuir*. 35 (2019).  
<https://doi.org/10.1021/acs.langmuir.9b00483>.
- [12] G. Vazquez, E. Alvarez, J.M. Navaza, Surface Tension of Alcohol + Water from 20 to 50 °C, *J Chem Eng Data*. 40 (1995). <https://doi.org/10.1021/jc00019a016>.
- [13] A.R. Faramarzi, J. Barzin, H. Mobedi, Effect of solution and apparatus parameters on the morphology and size of electrosprayed PLGA microparticles, *Fibers and Polymers*. 17 (2016). <https://doi.org/10.1007/s12221-016-6685-3>.
- [14] H. Valo, L. Peltonen, S. Vehviläinen, M. Karjalainen, R. Kostianen, T. Laaksonen, J. Hirvonen, Electrospray encapsulation of hydrophilic and hydrophobic drugs in poly(L-lactic acid) nanoparticles, *Small*. 5 (2009). <https://doi.org/10.1002/sml.200801907>.
- [15] A.D. Duong, G. Ruan, K. Mahajan, J.O. Winter, B.E. Wyslouzil, Scalable, semicontinuous production of micelles encapsulating nanoparticles via electrospray, *Langmuir*. 30 (2014). <https://doi.org/10.1021/la404679r>.

- [16] A.Í.S. Morais, E.G. Vieira, S. Afewerki, R.B. Sousa, L.M.C. Honorio, A.N.C.O. Cambrussi, J.A. Santos, R.D.S. Bezerra, J.A.O. Furtini, E.C. Silva-Filho, T.J. Webster, A.O. Lobo, Fabrication of polymeric microparticles by electrospray: The impact of experimental parameters, *J Funct Biomater.* 11 (2020).  
<https://doi.org/10.3390/jfb11010004>.
- [17] Y. Zhu, G. Xu, X. Xin, H. Zhang, X. Shi, Surface tension and dilational viscoelasticity of water in the presence of surfactants tyloxapol and triton X-100 with cetyl trimethylammonium bromide at 25 °C, *J Chem Eng Data.* 54 (2009).  
<https://doi.org/10.1021/jc800788f>.
- [18] P. Alexandridis, T. Alan Hatton, Poly(ethylene oxide)poly(propylene oxide)poly(ethylene oxide) block copolymer surfactants in aqueous solutions and at interfaces: thermodynamics, structure, dynamics, and modeling, *Colloids Surf A Physicochem Eng Asp.* 96 (1995). [https://doi.org/10.1016/0927-7757\(94\)03028-X](https://doi.org/10.1016/0927-7757(94)03028-X).
- [19] A.R. Goddard, E.A. Apebende, J.C. Lentz, K. Carmichael, V. Taresco, D.J. Irvine, S.M. Howdle, Synthesis of water-soluble surfactants using catalysed condensation polymerisation in green reaction media, *Polym Chem.* 12 (2021).  
<https://doi.org/10.1039/d1py00415h>.
- [20] S.C. Kothekar, A.M. Ware, J.T. Waghmare, S.A. Momin, Comparative analysis of the properties of Tween-20, Tween-60, Tween-80, Arlacel-60, and Arlacel-80, *J Dispers Sci Technol.* 28 (2007). <https://doi.org/10.1080/01932690601108045>.
- [21] M.J. Qazi, S.J. Schlegel, E.H.G. Backus, M. Bonn, D. Bonn, N. Shahidzadeh, Dynamic Surface Tension of Surfactants in the Presence of High Salt Concentrations, *Langmuir.* 36 (2020). <https://doi.org/10.1021/acs.langmuir.0c01211>.

- [22] G. Geeraerts, P. Joos, Dynamic surface tensions of micellar Triton X-100 solutions, *Colloids Surf A Physicochem Eng Asp.* 90 (1994). [https://doi.org/10.1016/0927-7757\(94\)02924-5](https://doi.org/10.1016/0927-7757(94)02924-5).

## 4.6 Supplementary Material

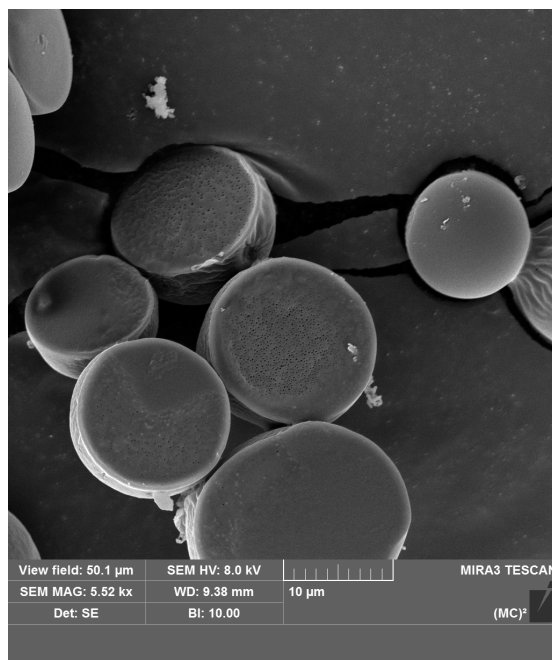


*Figure S4-1. Higher magnification of 25% ethanol collector solution particles without surfactants.*

## **Chapter 5 Pharmacokinetics and In Vitro-In Vivo Correlation of disc-shaped csMPs**

### **5.1 Introduction**

One major challenge in the development of long-acting controlled-release formulations can be the time to determine the effect of formulation or process changes. In vivo studies especially of significant length are costly. The release and absorption *in vivo* are typically faster than *in vitro* so *in vitro* release cannot necessarily be direct surrogate for *in vivo* [1–3]. Therefore *in vitro-in vivo* correlations (IVIVCs) become a critical tool to expediate development and inform early-stage decisions. For the csMPs developed through electrospray, there was significant variation in the initial with different shell compositions (Chapter 3) and ethanol treatments to remove residual solvents (Chapter 4) but long-term rates were more consistent and did not change significantly after the first month for the remainder of the desired 6 month period. The initial period in the first two months are critical for understanding the release long-term and the translation to *in vivo* absorption. The following work focused on developing an IVIVC covering the first two months of *in vivo* absorption for previously developed disk-shaped ENG-csMPs.

### **5.2 Materials and Methods**

#### **5.2.1 Materials**

Poly(D,L-lactide) (PLA) polymer (Resomer® R205S, inherent viscosity: 0.55–0.75 dL/g, ester terminated; Resomer® R203S, inherent viscosity: 0.25–0.35 dL/g, ester terminated), polyvinyl alcohol (PVA) (M<sub>w</sub> 13,000-23,000, 87-89% hydrolyzed), polycaprolactone (PCL) (average M<sub>n</sub> 45,000) as well as all other chemicals were purchased from Sigma-Aldrich, Inc (St. Louis, MO, USA). Micronized etonogestrel with purity more than 99.9% was purchased from Industriale Chimica S.R.L (Saronno, Italy). HPLC and LCMS grade solvents were purchased from Fisher Scientific (Hampton, NH, USA).

### ***5.2.2 Preparation of ENG-core-shell microparticles by coaxial electrospray***

ENG-loaded cs-MPs were prepared using a coaxial needle (Ramé-hart instrument, Succasunna, NJ, USA) with a 15-gauge outer needle and 25-gauge inner needle. The core solution was comprised of PLA (10% w/v) and ENG (30% w/v) in chloroform, while the shell solution was PLA (15% w/v) in chloroform/ethyl acetate (1:1 v/v). GASTIGHT® syringes (Hamilton®) containing these solutions were driven using two syringe pumps (Fisher Scientific) at a flow rate of 0.5 mL/hr. A high voltage to the needle (14-17 kV) and a ring electrode (10 kV) were placed 20 mm from the needle via two voltage generators (range: 0–30 kV, Gamma High Voltage Research, Ormond Beach, FL, USA). The particles were sprayed into a grounded aluminum container (10”x3”, round) containing 0.25% PVA with or without 5% NaCl and a magnetic stirrer (Fisher Scientific). The spray bath was transferred to a beaker and placed under an overhead stirrer at 600 rpm for 2 hours to evaporate residual organic solvents. After drying, aggregates were removed using a 125 µm sieve, and particles were collected using a 20 µm sieve and 3 µm nylon vacuum filter (Millipore Sigma) after thoroughly rinsing away spray bath additives with distilled water. Collected particles were lyophilized for 48 hours and then stored at room temperature with desiccant. Voltages for different formulations were optimized to produce an approximate particle

size of 20-30  $\mu\text{m}$  by examination of particles under a bright field microscope after spraying onto glass microscope slides.

### ***5.2.3 Determination of ENG drug loading and encapsulation efficiency***

ENG drug loading was determined by ultraviolet absorbance at 245 nm measured by ultra-high performance liquid chromatography (UPLC) (Acquity, Waters Corp., Milford, MA, USA) equipped with a UV detector. Approximately 5 mg of ENG-cs-MPs were dissolved in 25 mL of acetonitrile and vigorous vortexing. 25 mL of water was added followed by additional vortexing before further dilution by 50% v/v acetonitrile in water. The final solution was centrifuged at 20,000  $\times$  g for 10 min, and 10  $\mu\text{L}$  were injected into a Waters ACQUITY BEH C18 column (1.7  $\mu\text{m}$ , 100 mm  $\times$  2.1 mm id) at 50°C with a mobile phase of a mixture of acetonitrile and water (55:45 v/v) containing 0.1% formic acid. The flow rate was set at 0.3 mL/min.

### ***5.2.4 In Vitro Release Studies***

Approximately 3 mg of ENG-cs-MPs were placed into a nylon mesh bag with a pore size of 1  $\mu\text{m}$  (NMO1FMC, Midwest Filter, LLC, St. Charles, IL, USA). The bag was submerged initially into 200 mL of PBS (phosphate buffered saline, pH 7.4) with 0.05 % (w/v) sodium azide and agitated in an incubator (MaxQ™ 6000, Thermo Fisher Scientific, Waltham, MA, USA) at 80 rpm at 37 °C. At 1, 3, 7 days and every week thereafter, 0.5 mL of media was collected, the outside of the bags was rinsed with distilled water and the release media was completely replaced. After 14 days, the bags were transferred to a smaller glass bottle and 50 mL of release media to maintain a quantifiable concentration. Release media were centrifuged, and 100  $\mu\text{L}$  of the upper layer were taken and stored at 4°C in Waters 300  $\mu\text{L}$  polypropylene UPLC vials until quantification. ENG

concentrations in release media were determined by UPLC after the addition of equal volumes of acetonitrile and vortexing.

### **5.2.5 Characterization of thermal properties and etonogestrel solid-state**

Glass transition ( $T_g$ ), melting and recrystallization enthalpies and temperatures were determined by a modulated Q2000 differential scanning calorimeter (DSC) (TA Instruments, New Castle, DE, USA). 2-5 mg were sealed into Tzero<sup>®</sup> aluminum DSC pans. Samples were heated under a nitrogen atmosphere from -20°C to 250°C at 10°C/min to characterize recrystallization and melting events of ENG. Samples were then cooled at 15°C/min to -20°C and heated again to 100°C at 15°C/min to determine the glass transition temperature of PLA. Results were analyzed in TA TRIOS software (TA Instruments). Drug crystallinity was calculated by:

$$\% \text{ Relative Crystallinity} = \frac{\Delta H_m - \Delta H_R}{\Delta H_{m,ENG*DL}} \quad (5-1)$$

where  $\Delta H_m$  is the melting enthalpy measured for ENG in microparticles,  $\Delta H_R$  is the enthalpy of recrystallization.

### **5.2.6 Pharmacokinetic (PK) assessment of ENG-cs-MPs in rats**

PK evaluation of ENG-cs-MPs was conducted in adult male Sprague-Dawley rats (8 weeks old, 300–350 g) in accordance with the terms of Animal Care and Use Committee of University of Michigan. ENG-cs-MPs were weighed and suspended in sterile PBS with 3% (w/v) carboxymethyl cellulose then subcutaneously administered into rats at the ENG dose of 15 mg/kg. The exact administered dose was corrected by the residual drug amount in vials, needles and syringes. Blood samples (0.5 mL) were drawn from the jugular vein into BD Microtainer<sup>®</sup> tube with serum separator additives (Franklin Lakes, NJ, USA) at 2 hours, days 1, 3, 7, and then once

a week thereafter. Serum was separated by centrifuging blood samples at 10,000 g for 1.5 min, and stored at  $-80^{\circ}\text{C}$  before HPLC-QTOF-MS/MS analysis.

### **5.2.7 Quantification of ENG in rat serum**

A quantification method on high performance liquid chromatography quadrupole time-of-flight tandem mass spectrometry (HPLC-QTOF-MS/MS) was developed to measure the ENG concentrations in rat serum. An eight-point calibration curve was made by spiking 100  $\mu\text{L}$  of rat serum with 10  $\mu\text{L}$  ENG working solution corresponding to final concentration of 50, 100, 200, 500, 1000, 2000, 5000 and 10,000  $\text{pg/mL}$ , respectively, and 10  $\mu\text{L}$  of internal standard (500  $\text{ng/mL}$  ENG-d6 in a mixture of acetonitrile and distilled water at ratio of 1,1, v/v). The above mixtures were vortexed for 20 s and loaded onto the preconditioned Oasis HLB cartridge (1  $\text{cm}^3$ , 30 mg). Cartridges were first washed with 1 mL water and 1 mL 5% (v/v) methanol in water and subsequently eluted with 1 mL 10% (v/v) methanol in acetonitrile to collect ENG and internal standard fraction.

The collected elution was evaporated under nitrogen stream until dryness, and then reconstituted with 80  $\mu\text{L}$  50% (v/v) acetonitrile in water. 20  $\mu\text{L}$  1 M hydroxylamine hydrochloride solution was further added to derivatize both ENG and the internal standard at  $60^{\circ}\text{C}$  for 20 min. After centrifugation, 70  $\mu\text{L}$  upper layer was transferred into HPLC vials for further analysis. Derivatized ENG and ENG-d7 were separated on an Agilent C18 column (100  $\text{mm} \times 3.0 \text{ mm i.d.}$ , 2.7  $\mu\text{m}$  particle size, Waldbroen, Germany) at room temperature and a gradient elution of solvent A (acetonitrile containing 0.1% (v/v) formic acid) and solvent B (water containing 0.1% (v/v) formic acid) at flow rate of 0.5  $\text{mL/min}$  as follows: 0–0.5 min (30% A), 0.5–1 min (30–60% A), 1–3 min (60% A), 3–3.5 min (60–90% A), 3.5–4.5 min (90% A), followed by recovery with initial conditions for 2 min. The injection volume was 30  $\mu\text{L}$ .

The mass spectra of derivatized ENG and ENG-d6 were acquired by Sciex X500R QTOF system (Sciex Applied Biosystems, Framingham, MA, USA) in the positive ion mode under spray voltage of 5500 V and collision energy of 10 V. The mass spectra peaks of derivatized ENG and ENG-d6 on the extracted ion chromatograms (EICs) were used for quantification, which were obtained by extracting from total ion chromatogram (TIC) at molecular weight of 340.22 and 346.25 with a width of 0.05 Da.

### 5.2.8 Pharmacokinetic analysis and *in vitro-in vivo* correlations

$T_{max}$  and  $C_{max}$  was determined for serum concentrations over time in MATLAB. Absorption kinetics were calculated in MATLAB for each animal using a previously published point-area deconvolution technique [4] and 2-compartment pharmacokinetic model for ENG [5]. Interpolated absorption curves were compared to *in vitro* release. For time point, T, in the *in vitro* release curve, the *in vivo* time,  $\tau$ , to the same mean fraction absorbed as the mean fraction released was determined such that:

$$F_{abs}(\tau) = F_R(T) \quad (5-2)$$

where  $F_{abs}$  and  $F_R$  are the mean fraction absorbed *in vivo* and mean fraction released *in vitro*, respectively. These times were modeled as have a power law relationship to establish a power law-based time scaling:

$$\tau = aT^k \quad (5-3)$$

These were log-transformed and regressed linearly with the interpolated *in vivo* times. The fitted pre-exponential term,  $a$ , and exponential term,  $k$ , were used to determine the predicted equivalent *in vivo* time,  $\hat{\tau}$ , for each of the true *in vitro* times. The fraction absorbed at  $\hat{\tau}$  was interpolated from

the calculated mean absorption curves and linear regressed with the mean fraction release at the corresponding time,  $T$ , such that:

$$F_{abs}(\hat{t}) = b_1 F_R(T) + b_0 \quad (5-4)$$

## 5.3 Results and Discussion

### 5.3.1 Pharmacokinetic Profile and Noncompartmental parameters

After subcutaneous administration of the 15 mg/kg in rats, a majority of formulations showed the peak serum concentrations immediately (Figure 5-1). The  $C_{max}$  were similar amongst the different groups around 30 ng/mL (Figure S5-1A). Treatment with 25% ethanol in the drying

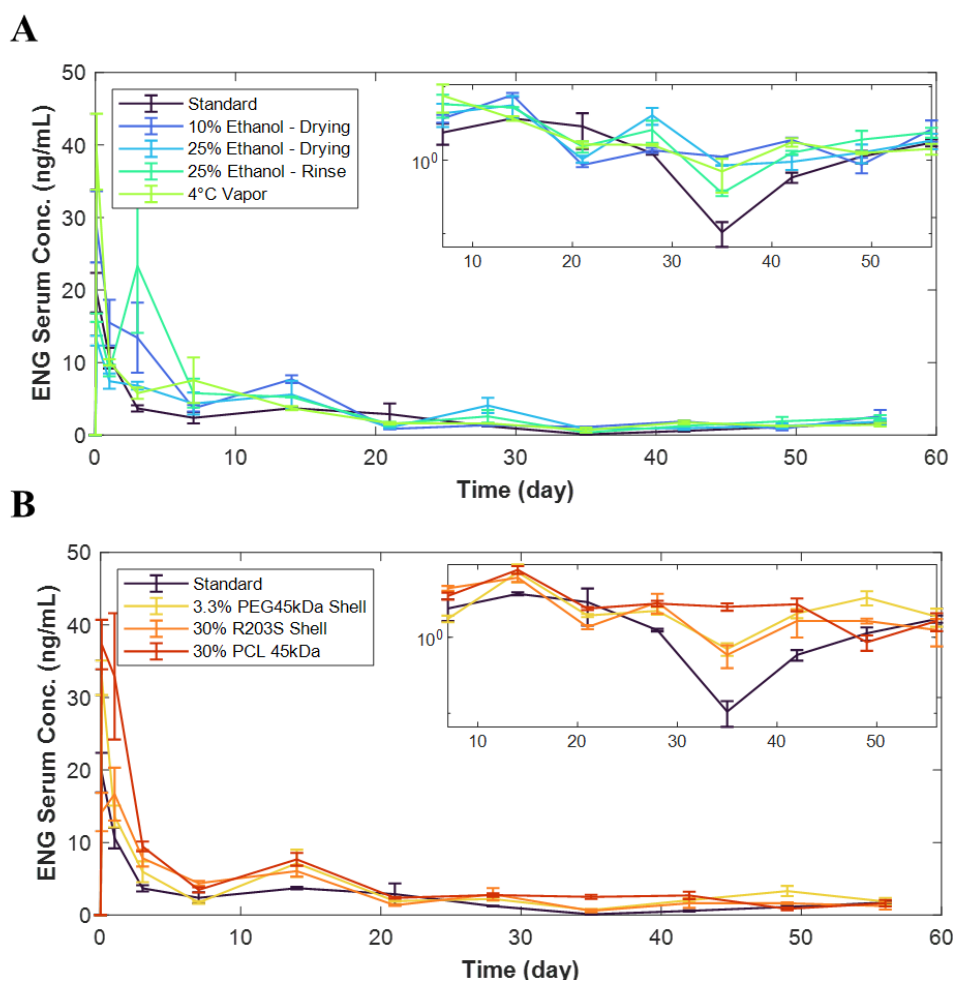


Figure 5-1. Pharmacokinetic profiles in rats of ethanol-treated (A) microparticles and microparticles with varying shell compositions (B) after 15 mg/kg ENG dose ( $n=3$ ). Inset displays log-linear plot of same data. Error bars show  $\pm$  SEM.

step or 4°C vapor after drying as well as the additional of PEG in the shell all had their peak serum concentrations on the first time point at 2 hours. The 25% ethanol drying also had the lowest  $C_{max}$  at  $13.0 \pm 0.8$  ng/mL. The 30% PCL shell showed the highest  $C_{max}$  at  $41.4 \pm 7.1$  ng/mL. Although the  $t_{max}$  of some formulations like the 25% ethanol rinse treatment were greater than day 1, the  $AUC_{0-1 \text{ day}}$  mirrors the  $C_{max}$  data (Figure S5-1C). All the  $AUC_{0-56 \text{ days}}$  were within error of each other around 4000 ng/mL-hr. PCL showed a slightly higher  $AUC_{0-56 \text{ days}}$  (Figure S5-1), which could be expected since it showed higher long-term rates *in vitro* compared to other formulations (Chapter 3). The results of the  $C_{max}$  and other parameters were fairly consistent with the rank order of the rapid phase release seen *in vitro* (Figure S5-1).

### 5.3.2 Absorption Kinetics

Serum concentrations over time were deconvoluted using a point-area technique previously used in the calculation absorption curves for exenatide microsphere formulations [4]. A unit-dose impulse response used in the deconvolution was calculated from intravenous injection of an etonogestrel solution given at 25 mg/kg (Figure S5-2). The results are shown in Figure 5-2.

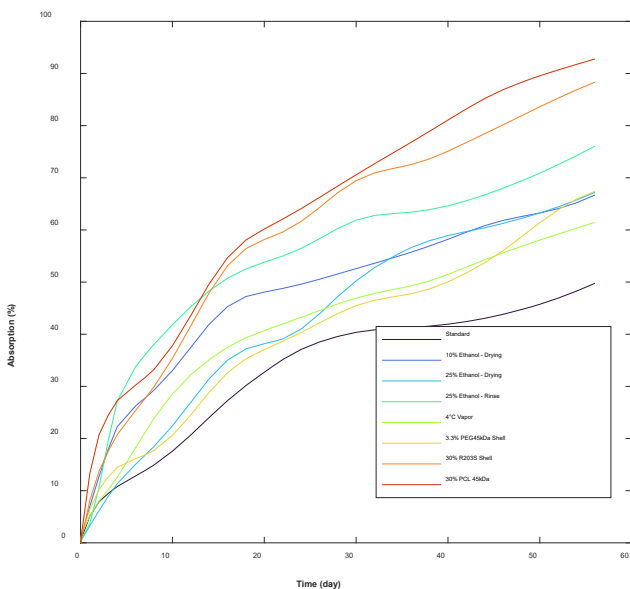


Figure 5-2. Mean absorption kinetics of individually deconvoluted pharmacokinetics profiles.

Overall, the transition between a rapid release phase and the long-term release are not as clear as those seen for the *in vitro* release (Chapter 3 and Chapter 4). Some slowing of the absorption rates appears to occur around 2 weeks based on the absorption kinetics of 10% ethanol in the drying step or the 25% ethanol rinse. The relative absorption vs the release *in vitro*

follows expectations with some exceptions such as 25% ethanol drying displaying a higher fraction absorbed than the standard formulation (Figure 5-2).

### 5.3.3 Unscaled *in vitro-in vivo* correlation

The initial *in vitro-in vivo* correlation (IVIVC) compared the *in vitro* release to the *in vivo* absorption at the same time for all formulations aggregated together. The IVIVC shown in Figure 5-3 had a relatively poor correlation ( $R^2=0.6$ ). The initial relationship is weak since no consideration of the effect of the *in vivo* environment on drug release. Previous studies with PLGA microspheres have shown that the *in vivo* absorption is faster than the release *in vitro* for both water-soluble drugs and peptides [3,6,7] as well as small molecules [1,3,6]. To properly compare the absorption and release, time-scaling is necessary to correct for the faster apparent release *in vivo*. Commonly, linear time-scaling is applied especially in the case of absorption for oral modified release dosage forms and has been for microsphere formulations [3]. Nonlinear scaling

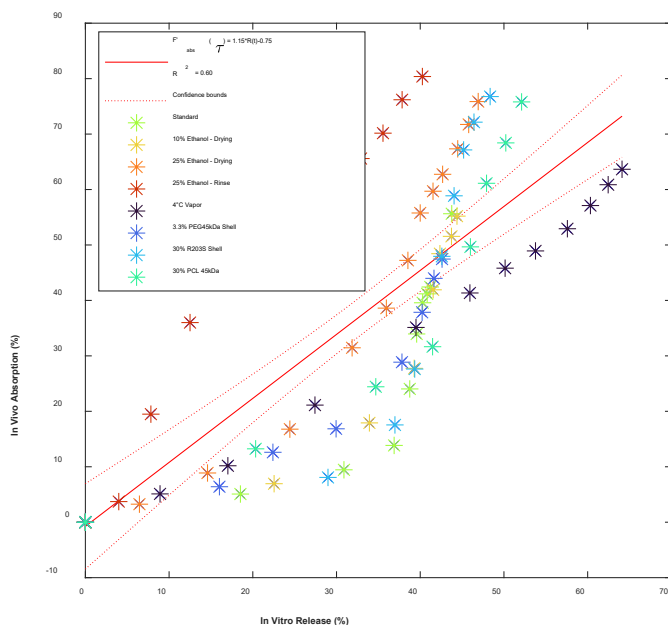


Figure 5-3. Unscaled time-by-time *in vivo-in vitro* correlation. Data points show mean values for absorption and release at a given time.

has also been investigated [8–11] such as an  $E_{max}$  model [10] or piece-wise linear models [8], which may relate to differences in release phase behavior *in vivo* and *in vitro*. More importantly in the FDA guidance for extended-release oral dosage forms nonlinear correlations are still considered to be acceptable [12].

### 5.3.4 Power-based time scaling and scaled IVIVC

Based on plotting of *in vitro* and *in vivo* times to a given amount, a simple linear relationship was deemed inappropriate. As shown in Figure 5-4A, the *in vitro* and *in vivo* times displayed a clear nonlinear behavior. Log transform of these times created a linear relationship with fairly consistent slopes, but different formulations were shifted (not shown). For this reason, a power law relationship was used to link the two times. Power laws between the fraction released and time have commonly used to describe *in vitro* release from polymer matrices and hydrogels [11,13,14]. Use of different powers between *in vivo* and *in vitro* has also been performed with success in other work [11]. Therefore, equation (5-3) was used to establish the relationship

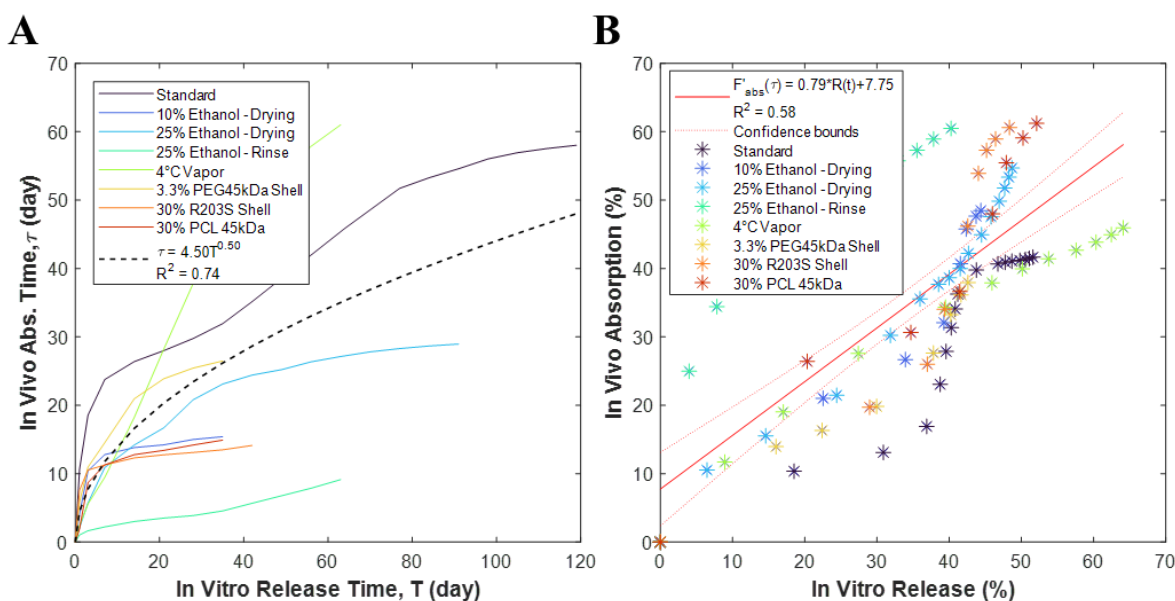


Figure 5-4. Power law fit of *in vivo/in vitro* times to a given fraction absorbed/released (A). Power-scaled *in vitro-in vivo* correlation (B).

between *in vivo* and *in vitro* times. Figure 5-4A also displays the fitted power law model. The exponential term showed a square root relationship between times. This model had an overall moderate correlation for the times ( $R^2=0.74$ ). The model was used to predict the corresponding *in vivo* time for each *in vitro* time, and these fitted times were used to evaluate a linear IVIVC (Figure 5-4B). The correlation for the new scaled relationship appeared to perform worse than unscaled time-by-time IVIVC. Closer examination of the fit showed that poor correlation is primarily the result of a single high leverage group—the 25% ethanol rinse treatment. Removal of this group from the IVIVC did not show a change in the power law scaling, but significantly improved the absorption-release correlation (Figure S5-2).

### ***5.3.5 Mixed effects of linearized power law scaling***

To investigate the differences between the ethanol rinse treatment and the other formulations, mixed effects modeling was used. For this, all formulations except the ethanol rinse treatment were grouped together while the ethanol rinse treatment was considered as a separate group. Random effects for the pre-exponential and exponential terms that was dependent on the group. While the full model appears to increase the overall IVIVC based on the adjusted correlation coefficient, the regressed power law model does not seem to properly describe the data with the random effects skewing the model toward the 4°C ethanol vapor treatment for the large group of formulations (Figure S5-4).

It is relevant to see the potential of reducing the model. Since the full model shows similar pre-exponential terms for both groups, removing the random effects for this variable was examined first. Similar to the full model, 25% ethanol rinse group times are not well defined by reducing the model by the pre-exponential term random effect. The random effects for the other formulations, however, seem to be more, but the overall correlation is lower than the full model (Figure S5-5).

On the other hand, if the model is reduced by the random effect of the exponential term, the times of both the 25% ethanol rinse treatment and the group of all other formulations appear to be well explained by the power law scaling (Figure 5-5A, B). This scaling showed the same power of 0.5 that was seen without the use of a mixed effects model. The model showed the these two “types”

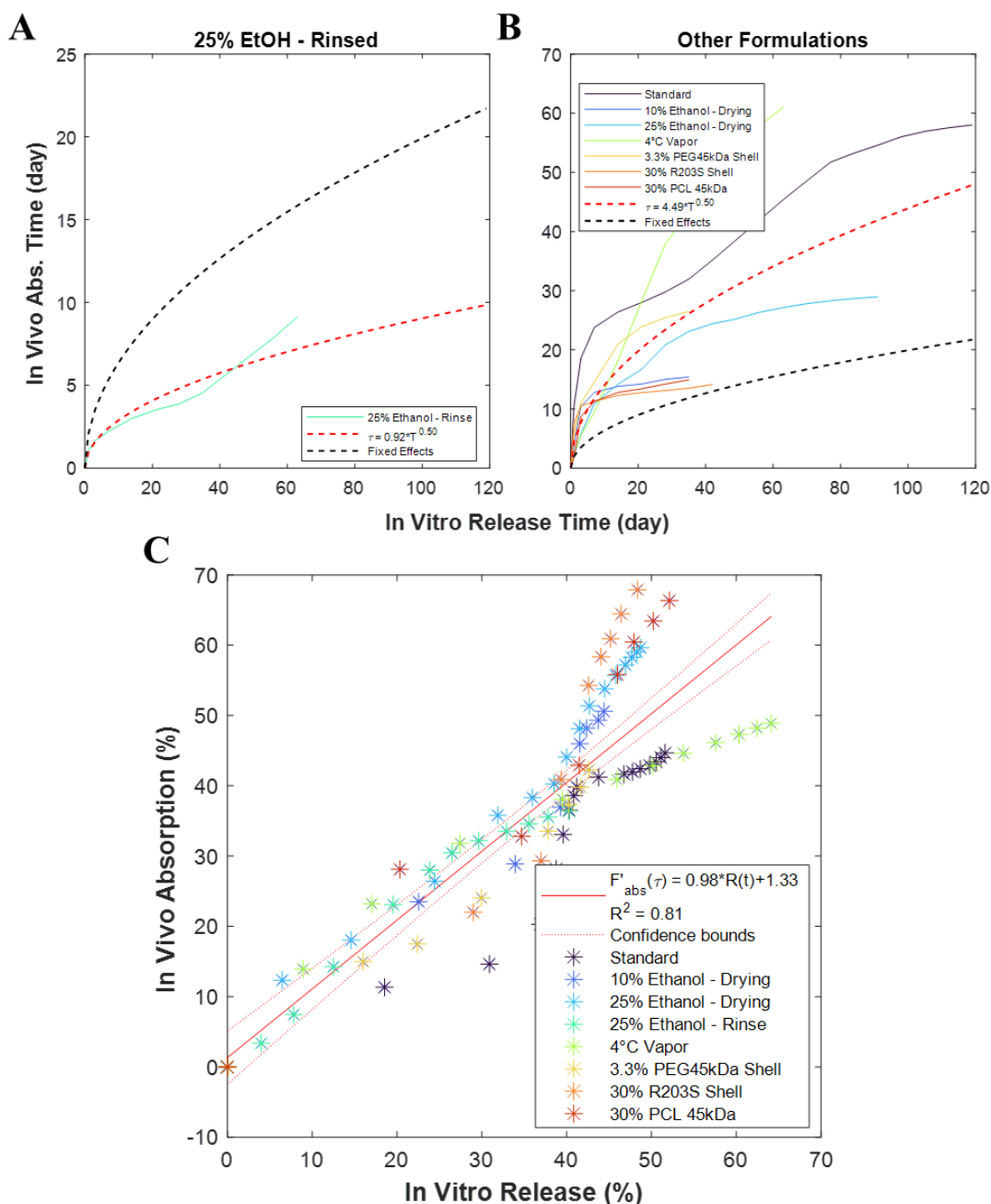


Figure 5-5. Mixed effects power law model of in vivo/in vitro times to a given fraction absorbed/released reduced by the random effect of the exponential term for the 25% ethanol rinse treatment (A) and all other formulation (B). Power-scaled in vitro-in vivo correlation (C)

of formulations only differed by a pre-exponential that was four times lower for the rinse treatment. Essentially, the rates were increased *in vivo* relative to *in vitro* to a greater extent for this treatment than for all other formulations. If this scaling is used to link the absorption and release data, the correlation remains high with a  $R^2$  of 0.81 (Figure 5-5C). The correlation also displays a 1:1 ratio between the amount released *in vitro* and the amount absorbed *in vivo*. The values shown for the absorption are not normalized by the bioavailability since release was not expected to have concluded by the end of the study. A previous study found that subcutaneous injection of etonogestrel-PLA microparticles had an estimated bioavailability of 87% [5], so a slope of 0.96 for the correlation is unexpected. Normalization of the absorption by bioavailability may improve the correlation between the data.

### ***5.3.6 Predictive capabilities of IVIVC***

While the model is internally consistent and capable of explaining the variability of the absorption, the predictive properties of this type of IVIVC is of greater importance. The accuracy of predictions was assessed through a leave-one-out analysis. For the analysis, one formulation is designated as the “out” group and the remaining formulations are used to fit the model described in Figure 5-5. This model was then used to predict the absorption curves of the out group through its *in vitro* release. The predicted absorption curve could then be compared to the actual absorption through  $f_2$  similarity. Additionally, the predicted absorption was convoluted with the pharmacokinetic model to create a predicted serum concentration over time. The  $C_{max}$  and  $C_{ss}$  (mean concentration for last 5 time points) of the predicted interval were calculated for the predicted curve and compared to the actual pharmacokinetic parameters through simple hypothesis testing to determine if there were any statistically significant differences. Finally, the overall

predictions for the entire serum concentrations were used to calculate the median symmetric ratio accuracy [15]. This process was repeated for each formulation.

Overall, the predicted absorption data showed a high level of similarity to the actual *in vivo* absorption (Figure S5-6). The  $f_2$  values for a majority of the formulations was over 50 (Table 5-1), which meets the FDA criteria for sameness [12]. The vapor treatment and standard formulation scored slightly below this threshold, but still demonstrated high similarity. The 25% rinse treatment had a very poor prediction, which further contrasts it with other formulations. The poor performance is consistent with expectations. Since no other formulations were included in its group, the exclusion of the rinse treatment when fitting would essentially remove the random effects altogether and leave the model shown in Figure S5-2.

After convolution with the pharmacokinetic model, the predicted serum concentrations do appear to mirror the actual values and shows diverging behaviors for different formulations (Figure S5-7). As shown in Table 5-1, the IVIVC was capable of predicting the serum concentrations with high ratio accuracy (>75%) for five out of eight of the formulations. Interestingly, two of the poor performers were different from those seen with the absorption predictions. The 25% ethanol in the drying step treatment may have shown some difficulty in predicting its pulsatile-like multi-peak

Table 5-1. Predicted values, similarity, and accuracies from leave-one-out analysis of mixed effects power law scaled IVIVC. NS refers to “not statistically significant”, \*  $p < 0.05$ , \*\*  $p < 0.01$ , and \*\*\*  $p < 0.001$ .

Formulation	Cmax (ng/mL)			Css (ng/mL)			Absorption $f_2$ similarity	Serum Conc. Ratio Accuracy (%)
	Actual	Predicted	P-value	Actual	Predicted	P-value		
Standard	19.6 ± 3.4	13.6	NS	1.4 ± 0.7	3.7	**	47.4	76.1
10% EtOH-Drying	31.4 ± 3.5	16.1	***	3.1 ± 0.8	1.1	*	67.3	97.5
25% EtOH-Drying	13.0 ± 0.8	8.4	***	3.4 ± 1.2	1.6	NS	82.2	57.6
25% EtOH-Rinse	27.1 ± 8.3	4.4	**	1.4 ± 0.3	3.5	***	29.1	28.4
4°C Vapor	39.1 ± 6.4	10.9	***	3.6 ± 1.1	5.6	NS	44.4	80.6
3.3% PEG	32.7 ± 2.9	12.0	***	2.9 ± 0.5	1.5	**	55.0	84.9
30% R203S	16.7 ± 4.5	19.7	NS	3.7 ± 0.4	1.4	***	50.8	83.5
30% PCL	41.4 ± 7.1	15.4	***	4.1 ± 0.2	2.3	***	59.8	66.8

pharmacokinetic profile. For the 30% PCL shell formulation, the low performance appears to primarily correspond to the underpredict of high initial serum concentrations (Figure S5-7). Again, the ethanol rinse treatment performed very poorly for similar reasons as the absorption predictions.

While the curves have overall high accuracies and similarities, the model did not perform as well in the prediction of singular values such as the  $C_{\max}$  or  $C_{ss}$ . Hypothesis testing showed that the predicted  $C_{\max}$  were statistically different from the actual mean values for all formulations and treatments except for the standard formulation and the 30% R203S shell formulation. In general, the model underpredicted the  $C_{\max}$  by greater than 50% in many cases (Table 5-1). Similarly, the  $C_{ss}$  at the end of the predicted interval was statistically different for all except 25% ethanol in the drying step and the 4°C vapor treatment. While there were more cases of overprediction such as the standard, the model also tended to underpredicted the  $C_{ss}$  by nearly 50%. The poor performance on these more exact measures of concentration may be related to the introduction of more variance that would be in the true pharmacokinetic model and one of the major limitations of IVIVC modeling [8,11,16]. This variability could be minimized by intravenous bolus and pharmacokinetic profiling of subjects prior to injection with the formulation to be tested, but this approach would be impractical for lower-species studies.

## 5.4 Conclusions

The pharmacokinetics and noncompartmental parameters ( $C_{\max}$ , AUC, etc.) followed the rank order of the *in vitro* release of csMPs. *In vivo* absorption was faster than *in vitro* release and unscaled IVIVCs between the fraction absorbed and fraction released had a poor correlation. Linearized power law time scaling was used to properly link the absorption and release, but the initial correlation was poor because the 25% ethanol rinse treatment had different time scale compared to other formulations. This formulation *in vitro* had little apparent rapid release, high

variability, and relatively high release rates. Mixed effects modeling showed that while this formulation shared the same exponent for the power time scaling as other formulations it differed in the pre-exponential term. Overall, the release could explain 81% of the variability in the absorption with this minor adjustment. Additionally, the model showed high overall predictive capabilities for absorption and serum concentrations with the exception of the 25% rinse treatment, but specific predicted values like  $C_{\max}$  were significantly underpredicted. The study points to the common issue of IVIVC development, which is the high inter-subject variability for pharmacokinetics and error propagation when convoluting on top of a prediction. More investigation into formulations that behave similar to the 25% ethanol rinse treatment is warranted.

## 5.5 References

- [1] A.C. Doty, D.G. Weinstein, K. Hirota, K.F. Olsen, R. Ackermann, Y. Wang, S. Choi, S.P. Schwendeman, Mechanisms of in vivo release of triamcinolone acetonide from PLGA microspheres, *Journal of Controlled Release*. 256 (2017) 19–25. <https://doi.org/10.1016/j.jconrel.2017.03.031>.
- [2] J. v Andhariya, R. Jog, J. Shen, S. Choi, Y. Wang, Y. Zou, D.J. Burgess, Development of Level A in vitro-in vivo correlations for peptide loaded PLGA microspheres, *J Control Release*. 308 (2019) 1–13. <https://doi.org/10.1016/j.jconrel.2019.07.013>.
- [3] J. v Andhariya, R. Jog, J. Shen, S. Choi, Y. Wang, Y. Zou, D.J. Burgess, In vitro-in vivo correlation of parenteral PLGA microspheres: Effect of variable burst release, *J Control Release*. 314 (2019) 25–37. <https://doi.org/10.1016/j.jconrel.2019.10.014>.
- [4] A. Beig, R. Ackermann, Y. Wang, R. Schutzman, S.P. Schwendeman, Minimizing the initial burst of octreotide acetate from glucose star PLGA microspheres prepared by the solvent evaporation method, *Int J Pharm*. 624 (2022) 121842. <https://doi.org/https://doi.org/10.1016/j.ijpharm.2022.121842>.
- [5] J. Tang, R. Schutzman, C.A. Rodríguez, J. Lahann, N. Rodríguez-Hornedo, M.R. Prausnitz, S.P. Schwendeman, Coaxial electrospray of uniform polylactide core-shell microparticles for long-acting contraceptive, *Journal of Controlled Release*. 341 (2022). <https://doi.org/10.1016/j.jconrel.2021.12.017>.
- [6] A.C. Doty, K. Hirota, K.F. Olsen, N. Sakamoto, R. Ackermann, M.R. Feng, Y. Wang, S. Choi, W. Qu, A. Schwendeman, S.P. Schwendeman, Validation of a cage implant system for assessing in vivo performance of long-acting release microspheres, *Biomaterials*. 109 (2016). <https://doi.org/10.1016/j.biomaterials.2016.07.041>.

- [7] I. Tomic, M. Mueller-Zsigmondy, A. Vidis-Millward, J.M. Cardot, In vivo release of peptide-loaded PLGA microspheres assessed through deconvolution coupled with mechanistic approach, *Eur J Pharm Biopharm.* 125 (2018) 21–27.  
<https://doi.org/10.1016/j.ejpb.2017.12.007>.
- [8] J.M. Cardot, B.M. Davit, In vitro-in vivo correlations: Tricks and traps, *AAPS Journal.* 14 (2012). <https://doi.org/10.1208/s12248-012-9359-0>.
- [9] P.H. Hemmingsen, A.M. Haahr, C. Gunnergaard, J.M. Cardot, Development of a new type of prolonged release hydrocodone formulation based on egalets<sup>®</sup> sup<sup>®</sup> spii<sup>®</sup> sup<sup>®</sup> adprem technology using in vivo-in vitro correlation, *Pharmaceutics.* 3 (2011).  
<https://doi.org/10.3390/pharmaceutics3010073>.
- [10] M.E.F. Mohamed, S. Trueman, A.A. Othman, J.H. Han, T.R. Ju, P. Marroum, Development of In Vitro–In Vivo Correlation for Upadacitinib Extended-Release Tablet Formulation, *AAPS Journal.* 21 (2019). <https://doi.org/10.1208/s12248-019-0378-y>.
- [11] J. Kytariolos, A. Dokoumetzidis, P. Macheras, Power law IVIVC: An application of fractional kinetics for drug release and absorption, *European Journal of Pharmaceutical Sciences.* 41 (2010). <https://doi.org/10.1016/j.ejps.2010.06.015>.
- [12] F.T. Análisis, P. Costa, J.M. Sousa Lobo, T. Data, P. Quetiapine, M.R. Tablets, B. Grintjes, A.M. Gmt, F.F.B.R.P. L, J. Pharm, L. Summary, The Mendeley Support Team, H.A. Andreetta, P. Blends, F. Dosage, U. Sampling, E. Costa, A. Arancibia, J. Aïache, S. Feature, Q.G.D. Lisci, Q.F.B. María, E. Girard, G.D.N. Materiales, R.E. N, D. Ph, P.D. Prasad, N.U. Lakshmi, D.A. Kumar, M. Jhansee, M. Kumar, P. Product, N. Seroquel, S. Xr, C. Qu, C.N. Recommendations, C.D. Release, M. Release, S. Oral, D. Forms, M.E. Addendum, S. de Seguridad, P.H. Service, H. Services, N.R. Tebes, M. Towers,

- Guidance for Industry: Extended Release Oral Dosage Forms: Development, Evaluation, and Application of In Vitro/In Vivo Correlations, Food and Drug Administration. 24 (2010).
- [13] E. Kaunisto, M. Marucci, P. Borgquist, A. Axelsson, Mechanistic modelling of drug release from polymer-coated and swelling and dissolving polymer matrix systems, *Int J Pharm.* 418 (2011). <https://doi.org/10.1016/j.ijpharm.2011.01.021>.
- [14] N.A. Peppas, B. Narasimhan, Mathematical models in drug delivery: how modeling has shaped the way we design new drug delivery systems, *J Control Release.* 190 (2014) 75–81. <https://doi.org/10.1016/j.jconrel.2014.06.041>.
- [15] S.K. Morley, T. v. Brito, D.T. Welling, Measures of Model Performance Based On the Log Accuracy Ratio, *Space Weather.* 16 (2018). <https://doi.org/10.1002/2017SW001669>.
- [16] A. Dunne, C. Gaynor, J. Davis, Deconvolution based approach for level A in vivo/in vitro correlation modelling: Statistical considerations, *Clin Res Regul Aff.* 22 (2005). <https://doi.org/10.1081/CRP-54957>.

## 5.6 Supplementary Materials

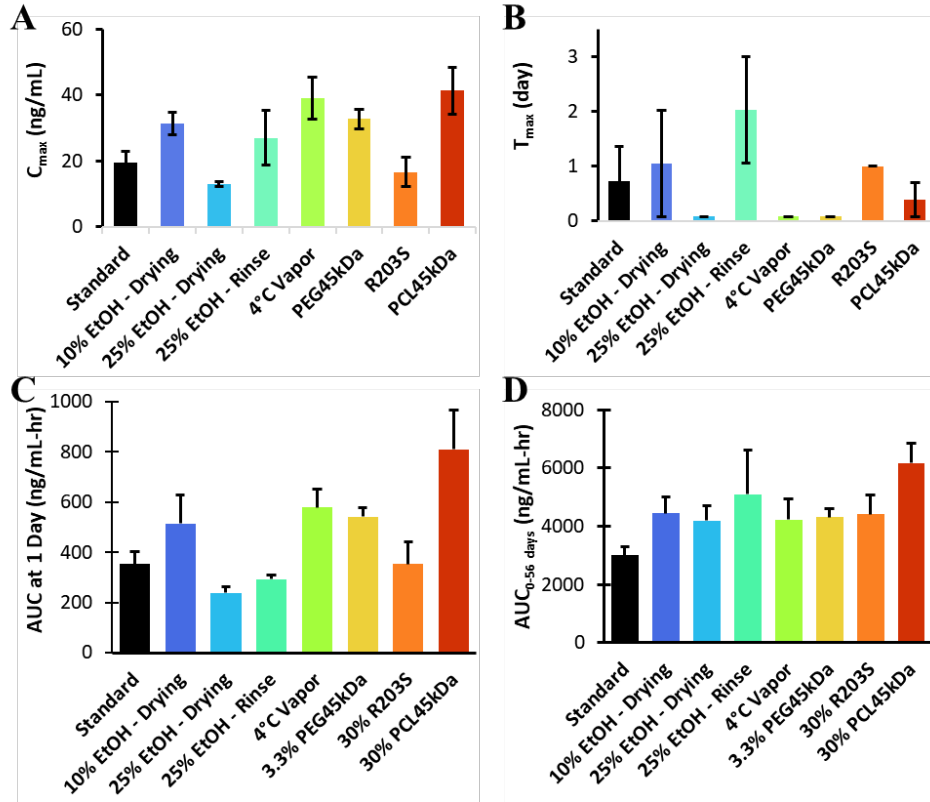


Figure S5-1. Noncompartmental parameters of studied formulations:  $C_{max}$  (A),  $T_{max}$  (B),  $AUC_{0-1 \text{ day}}$  (C), and  $AUC_{0-56 \text{ days}}$  (D). Error bars show  $\pm$  SEM.

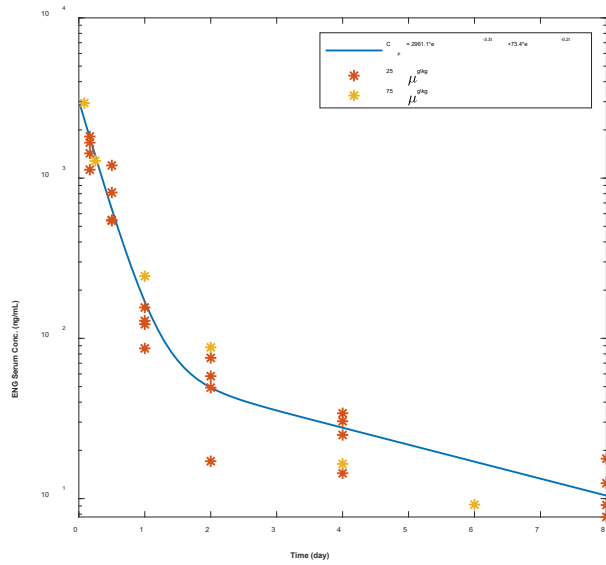


Figure S5-3. Two-compartment model fit of intravenous injection for 25 µg/kg (n=3) and 75 µg/kg (n=1). Pre-exponential coefficients show ng/mL per mg dose. Higher dose is normalized to 25 µg/kg for plot.

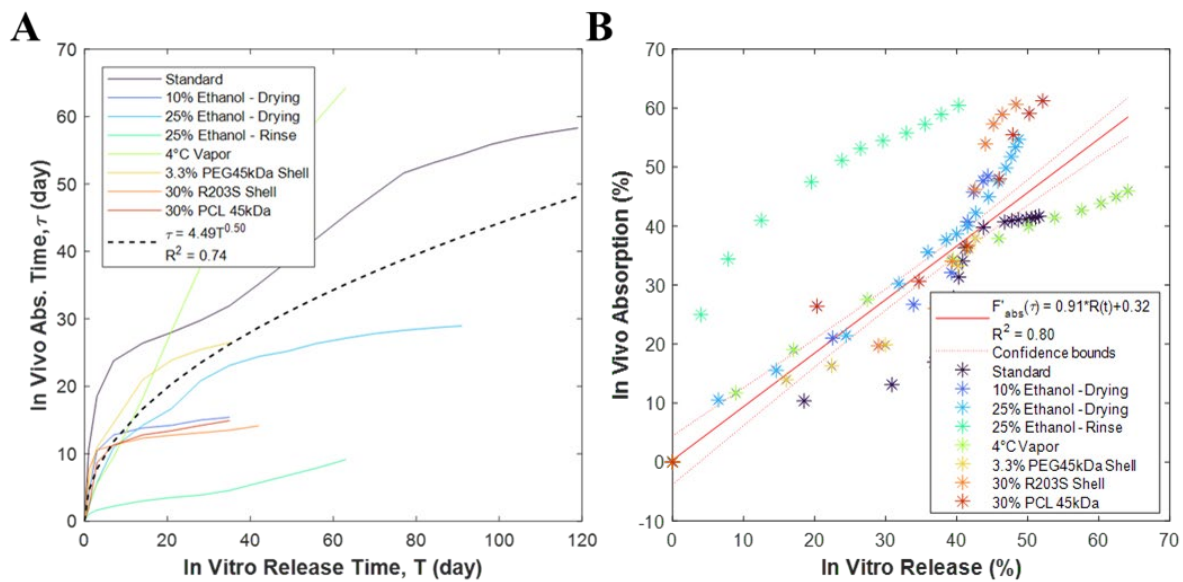


Figure S5-2. Power law fit of in vivo/in vitro times to a given fraction absorbed/released excluding 25% Ethanol-Rinsed (A). Power-scaled in vitro-in vivo correlation (B).

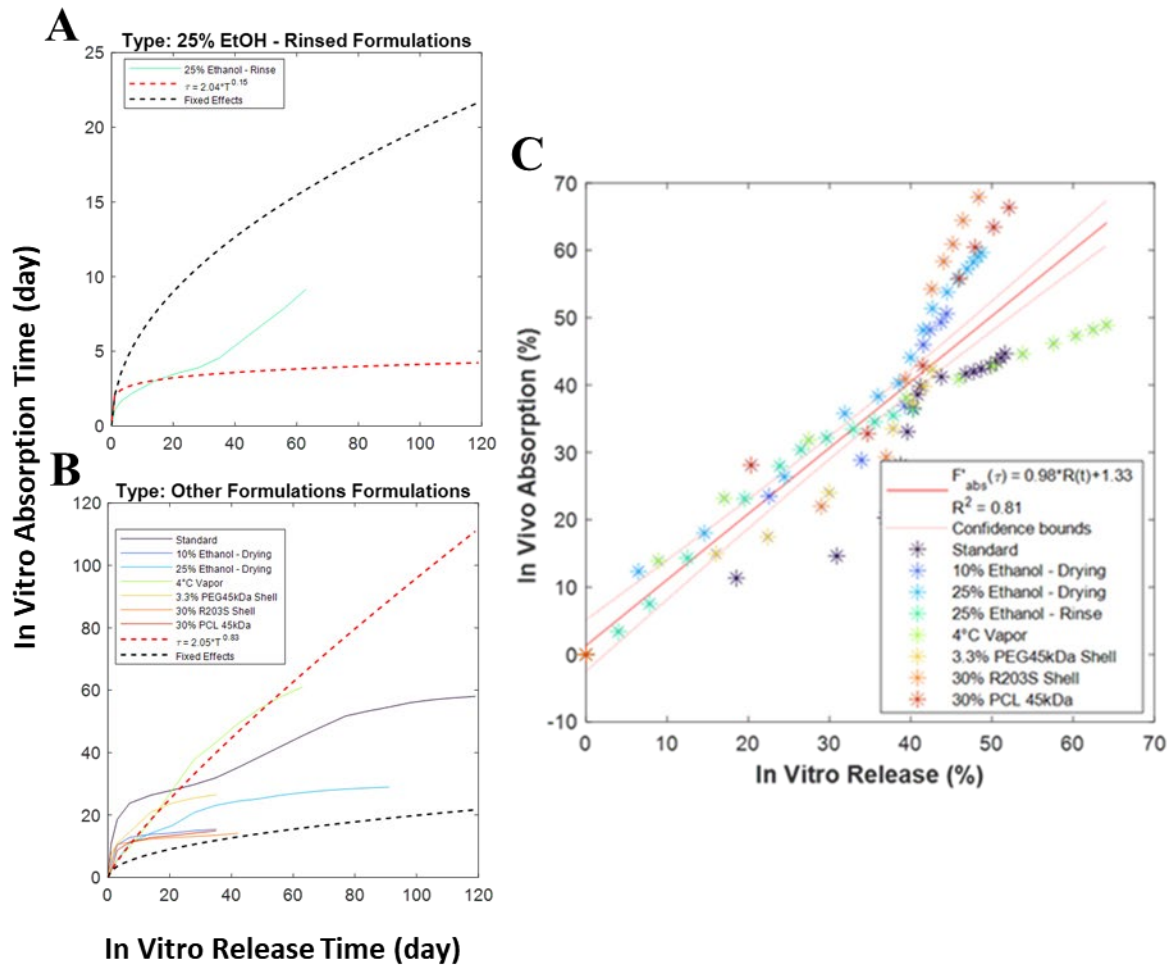


Figure S5-4. Full mixed effects power law model of in vivo/in vitro times to a given fraction absorbed/released for the 25% ethanol rinse treatment (A) and all other formulation (B). Power-scaled in vitro-in vivo correlation (C).

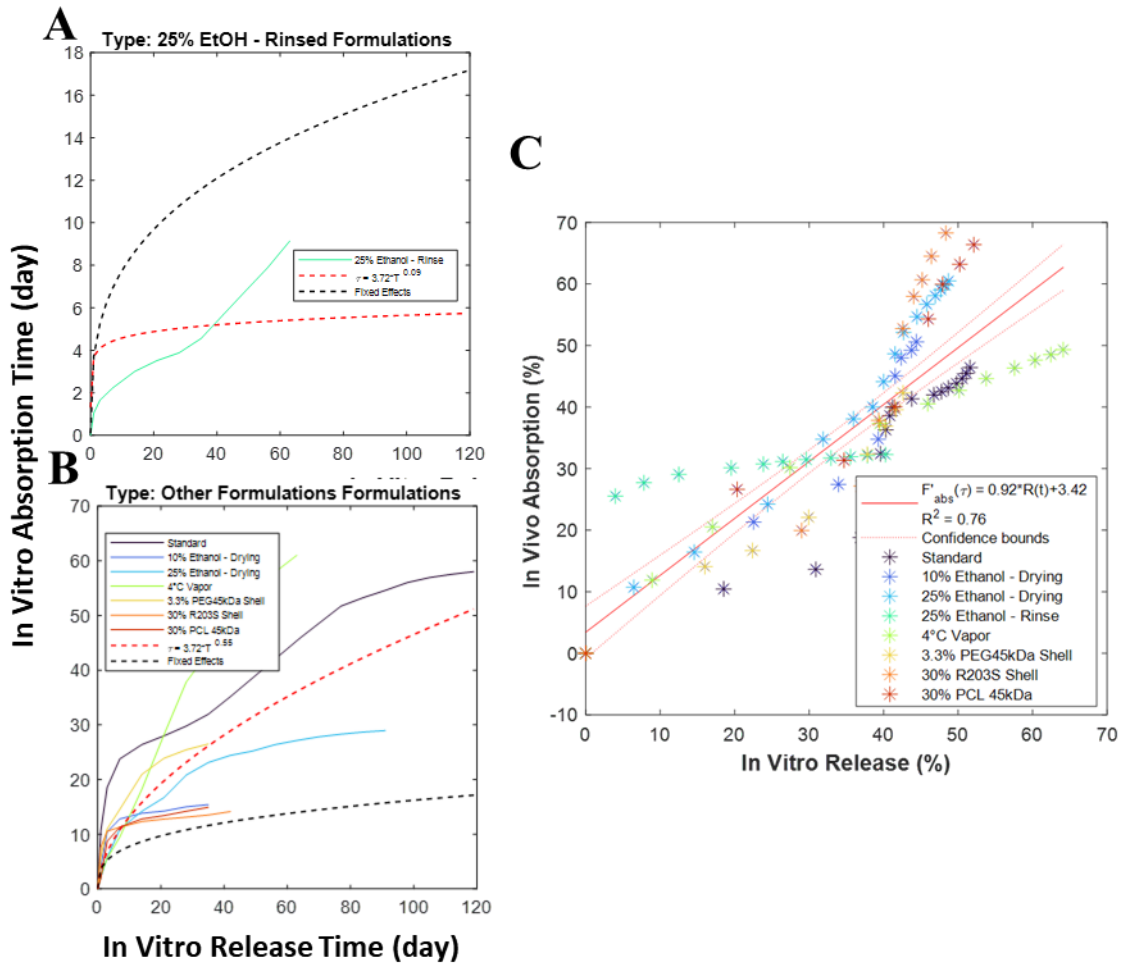


Figure S5-5. Pre-exponential term-reduced mixed effects power law model of in vivo/in vitro times to a given fraction absorbed/released for the 25% ethanol rinse treatment (A) and all other formulation (B). Power-scaled in vitro-in vivo correlation (C).

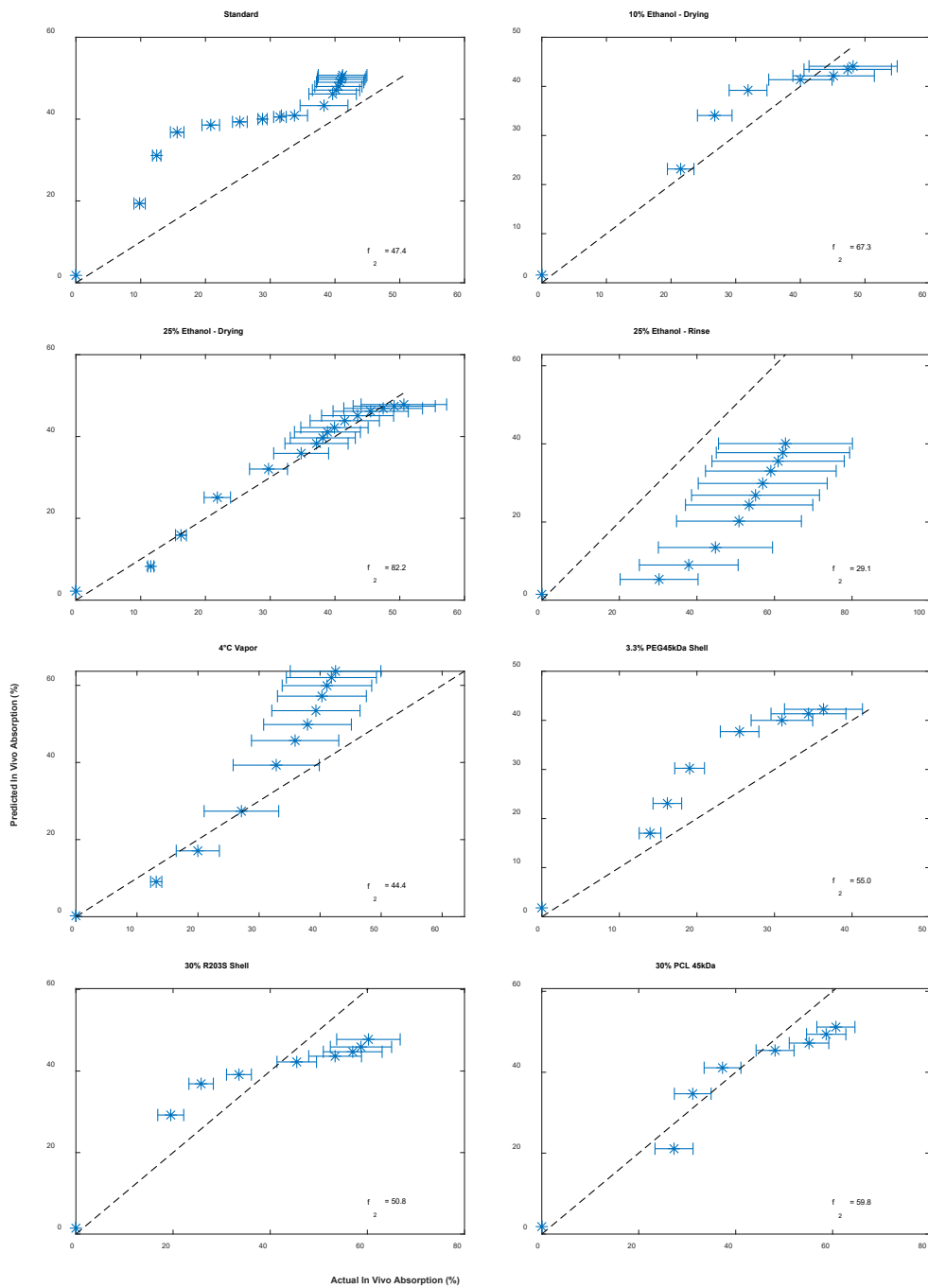


Figure S5-6. Predicted absorption from leave-one-out analysis of mixed effects power law scaled IVIVC compared to actual in vivo absorption. Error bars show  $\pm$ SEM.  $f_2$  refers to the  $f_2$  similarity of the actual absorption over time to the predicted absorption over time.



## Chapter 6 Conclusions, Significance and Future Directions

The work presented in this thesis has demonstrated the potential of atomization techniques as an alternative to traditional encapsulation techniques like coacervation and solvent evaporation. Not only this but it has also examined different mechanisms of early release periods in two different formulations—a peptide in PLGA and a steroidal hormone in PLA produced by spray drying and coaxial electrospray, respectively. While qualitative analysis of the initial burst and healing in PLGA has been performed prior to this work, the correlations between diffusivity and peptide release—*in vitro* and *in vivo*—in this very early stage have not been investigated to this extent previously. It was found that the extent of the burst release was related to the polymer diffusivity for spray-dried, and the relationship held *in vivo*. In addition, the work was able to successfully optimize a core-shell microparticle made through electrospraying for 6-month release and completely eliminated the initial rapid and extraneous release from the particle. Performance was validated *in vivo*, and correlations established to help guide future development.

In Chapter 2, the initial burst of leuprolide acetate from spray-dried microspheres with significant variations in release but not composition or size were characterized. The diffusivity and morphology were examined throughout the first 24 hours of release. Dimensionless diffusion time of a bodipy-dextran probe was directly proportional to the extent of the initial burst measured in a continuous monitoring. The timing of healing in these microspheres as well as the commercial product, Lupron Depot<sup>®</sup>, was confirmed by these measurements and imaging of the particle surface

through SEM. SEM also showed extensive swelling of some spray-dried particles that had high matrix diffusivity and release. The continuous monitoring release was also validated in vivo and displayed better correlation to 24-hour fraction absorbed than traditional sample-and-separate release methods.

In Chapter 3, previous work for a high drug loading, high encapsulation efficiency long-acting contraceptive microparticle through coaxial electrospray was further developed and optimized. System modifications (addition of ring electrode, sodium chloride-containing collection solution) improved yield of etonogestrel core-shell microparticles (csMPs) from 15% to 30-40% and reduced the initial release from 60% to 25%. Varying the shell composition was also shown to modulate the release rates and initial release. Increasing the permeability by adding lower molecular weight polymer or water-soluble polyethylene glycol increased release rates and initial release in the first two weeks.

In Chapter 4, ethanol treatments were evaluated for their ability to remove residual solvents and increase ENG crystallinity. These treatments demonstrate that the total amount of solvent extracted and changes in etonogestrel solid-state was related to the extent of exposure of ethanol. Several methods such as addition of ethanol to the collection solution and vapor treatment were capable of successfully removing all residual solvents used during spraying. In addition, ethanol in the collection solution during spraying increased the sphericity of particle in a concentration-dependent manner from disc-shaped particles when no ethanol was used. The morphology was demonstrated to be dependent on the surface tension of the solution and a strong surfactant was able to produce spherical particles as well. These spherical particles had little to no rapid release in the initial 2 weeks.

In Chapter 5, several disc-shaped particles that had undergone different ethanol treatments and selected ones with different shell compositions were evaluated *in vivo* to determine the relationship to *in vitro* release. An IVIVC was established by linking *in vitro* release times to *in vivo* times through a power law scaling. One treatment—rinsing with 25% ethanol—reduced the correlation and was determined to require a smaller pre-exponential term for the time-scaling through mixed effects modeling. The model had high predictive capabilities for the overall absorption and serum concentrations for all formulations except for the rinse treatment, but poorly predicted  $C_{\max}$  and  $C_{ss}$ .

Future studies will study the spherical particles produced by methods outlined in Chapter 5. The use of Triton X-100 in the collection solution during spraying followed by 25% ethanol while drying had no residual solvents and excellent release kinetics, but the high toxicity of Triton X-100 may make quantification of residual surfactant or assessment of safety necessary. The performance of spherical particles should also be determined *in vivo* and, if necessary, the IVIVC expanded to accommodate their release kinetics.

The work outlined here can provide framework for developing IVIVCs for polymer-based diffusion-controlled formulations. This applies to both the early stages such as the initial burst of matrices that may be long-term erosion-controlled and matrices that erosion time are sufficiently longer than the characteristic diffusion time for the encapsulated drugs such as the core-shell PLA microparticles developed here. The adjustments utilized for the electrospray to increase particle yields are relatively simple in implementation and can hopefully add to adoption of this platform for future formulation development.